Fakultät für Chemie

Lehrstuhl für Biotechnologie

In vitro reconstitution of the Atg1-kinase complex: Revealing the molecular mechanism of autophagy initiation

Marco Giuseppe Perna

Vollständiger Abdruck der von der Fakultät für Chemie
der Technischen Universität München zur Erlangung des akademischen Grades eines
Doktors der Naturwissenschaften (Dr. rer. nat.)
genehmigten Dissertation.

Vorsitzender: Univ.-Prof. Dr. Tobias A. M. Gulder
Prüfer der Dissertation: 1. Univ.-Prof. Dr. Johannes Buchner
2. Univ.-Prof. Dr. Sevil Weinkauf

Die Dissertation wurde am 23. Juni 2014 bei der Technischen Universität München
eingereicht und durch die Fakultät für Chemie
am 16. September 2014 angenommen.

Contents

List of Figures

List of Tables

Abbreviations

AAA	ATPases Associated with various cellular Activities
AIEX	Anion exchange chromatography
AIM	Atg8-interaction motif
ALP	Alkaline phosphatase
AMP	Adenosin monophosphate
Atg	Autophagy related gene
$Atg1^{PC}$	Atg1-kinase complex
$Atg1^{monoPC}$	Monomeric Atg1-kinase complex
$Atg17^{TC}$	Atg17-Atg31-Atg29 complex
$Atg17^{monoTC}$	$Atg17^{1-320}$-Atg31-Atg29 complex
ATP	Adenosin triphosphate
CATCHR	Complexes associated with tethering containing helical rods
CCTP	Coiled-coil homodimer tethering proteins
CMA	Chaperone mediated autophagy
COG	Conserved oligomeric Golgi
COP	Coat protein
CORVET	Class C core vacuole/endosome tethering
CP	Core particle
Cvt	cytoplasm to vacuole
DLS	Dynamic light scattering
DTT	Dithiothreitol
EE	Early endosome
ER	Endoplasmic reticulum
ERES	ER exit sites
ERGIC	ER-Golgi intermediate compartment
ESI	Electron spray ionization
FRAP	Fluorescence recovery after photobleaching
FRET	Förster resonance energy transfer
GAP	GTPase-activating protein
GDP	Guanosin diphosphate
GEF	Guanosin nucleotide exchange factor
GTP	Guanosin triphosphate
GUV	Giant unilamellar vesicle
HOPS	Homotypic fusion and vacuole protein sorting
IDP	Intrinsically disordered protein
IP	Immunoprecipitation
LB	Luria-Bertani
LC	Liquid chromatography
LE	Late endosome
LUV	Large unilamellar vesicle
MLV	Mulitlamellar vesicle

MS	Mass spectrometry
MS/MS	Tandem mass spectrometry
MSTC	Multi subunit tethering complexes
MVB	Multi-vesicular body
NSF	N-ethylmaleimide-sensitive factor
ORF	Open reading frame
PAGE	Polyarcylamide gel electrophoresis
PAS	Pre-autophagosome structure
PCR	Polymerase chain reaction
PE	Phosphatidylethanolamine
PI	Phosphatidylinositol
PI3P	Phosphatidylinositol-3-phosphate
$PI(4,5)P_2$	Phosphatidylinositol-4,5-bisphosphate
PKA	Proteinkinase A
PL	Proteoliposome
PM	Plasma membrane
PO	Palmitoyl-oleoyl
R_H	Hydrodynamic radius
RP	Regulatory particle
SDS	Sodium dodecyl sulfate
SLIC	Seamless ligation independent cloning
SNAP	Soluble NSF attachment protein
SNARE	Soluble NSF attachment protein receptor
SPR	Surface plasmon resonance
SUV	Small unilamellar vesicle
TB	Terrific Broth
TCA	Trichloroacetic acid
TGN	Trans-Golgi network
TIPS	Titerless infected-cells preservation and scale-up
TORC	Target of rapamycin kinase complex
TRAPP	Transport protein particle
VPCS	Vacuole phagophore contact site
VTC	Vacuolar transporter chaperone
WB	Western blot

Summary

Autophagy is a major catabolic pathway, which is conserved in all eukaryotes. It is responsible for the degradation of cytosolic components and organelles by delivering them to the vacuole/lysosome. During the process of macroautophagy, cells form double-membrane vesicles, called autophagosomes. Depending on cargo selection, two different sub-pathways can be distinguished; a specific branch which is e.g. involved in degradation of damaged organelles, and a non-specific branch. The non-specific autophagy pathway degrades bulk cytoplasmic material. Besides its role in energy metabolism, autophagy plays also a role in different diseases as well as in intracellular immune defense and development. The proteins required for autophagy are encoded by 38 autophagy related genes (Atg) in yeast. The Atg1-kinase complex, consisting of the Atg1-kinase and its regulatory subunits Atg13, Atg17, Atg29 and Atg31, is a central regulator of autophagy and is required to recruit vesicles containing the integral membrane protein Atg9 that is essential to initiate the autophagic membrane. However, the molecular mechanism of action of the Atg1-kinase complex has not been understood and recombinantly expressing and purifying the Atg1-kinase complex has remained a major technical challenge. Therefore, all Atg1-kinase complex subunits were recombinantly expressed and analyzed for this study. Assembling the Atg1-kinase complex from its subunits *in vitro* showed that Atg13 bridges the stable trimeric subcomplex formed by Atg17, Atg29, and Atg31 with Atg1-kinase. Furthermore, the phosphorylation dependent disassembly of the Atg1-kinase complex could be recapitulated and it was shown that two stable subcomplexes are formed (Atg17-Atg31-Atg29 and Atg1-Atg13). Analyzing the architecture of the Atg1-kinase complex showed that it forms a dimer of pentamers and that dimerization is mediated by the C-terminal domain of Atg17. Expressing a dimerization deficient mutant of Atg17 in yeast showed a severe effect on dynamics of autophagic membranes. In addition, it was shown that Atg17 directly interacts with Atg9 *in vitro*. Further *in vitro* assays demonstrated that this interaction is regulated by the assembly of the Atg1-kinase complex. The interaction of Atg17 and Atg9 was shown to be required to promote autophagy *in vivo*. These data suggest that the Atg1-kinase complex could function as a membrane tether in autophagy and explain why its assembly is a central regulatory mechanism to promote autophagy.

1. Introduction

1.1. Common principles of vesicular trafficking in eukaryotic cells

Eukaryotic cells contain several membrane enclosed organelles, like the endoplasmic reticulum (ER) or the Golgi complex. Transport of molecules from the cytoplasm to these compartments can be performed by different processes. Proteins can be translocated across membranes by transport proteins e.g. to the ER (Zimmermann et al., 2011) or to mitochondria (Dudek et al., 2013). Gated transport requiring the GTPase Ran is involved in import and export of proteins that are too large for free diffusion through the membrane pores of the nucleus (Aitchison and Rout, 2012). Transport of cargo from one organelle to the other, however, is mediated by shuttling transport vesicles (Bonifacino and Glick, 2004; Palade, 1975). These vesicles can transport material in the biosynthetic secretory pathway to the plasma membrane (PM) and the extracellular space. In the converse endocytic pathway the cell is able to target part of the PM, containing e.g. receptors, for recycling or degradation. Furthermore, through the endocytic pathway nutrients can be

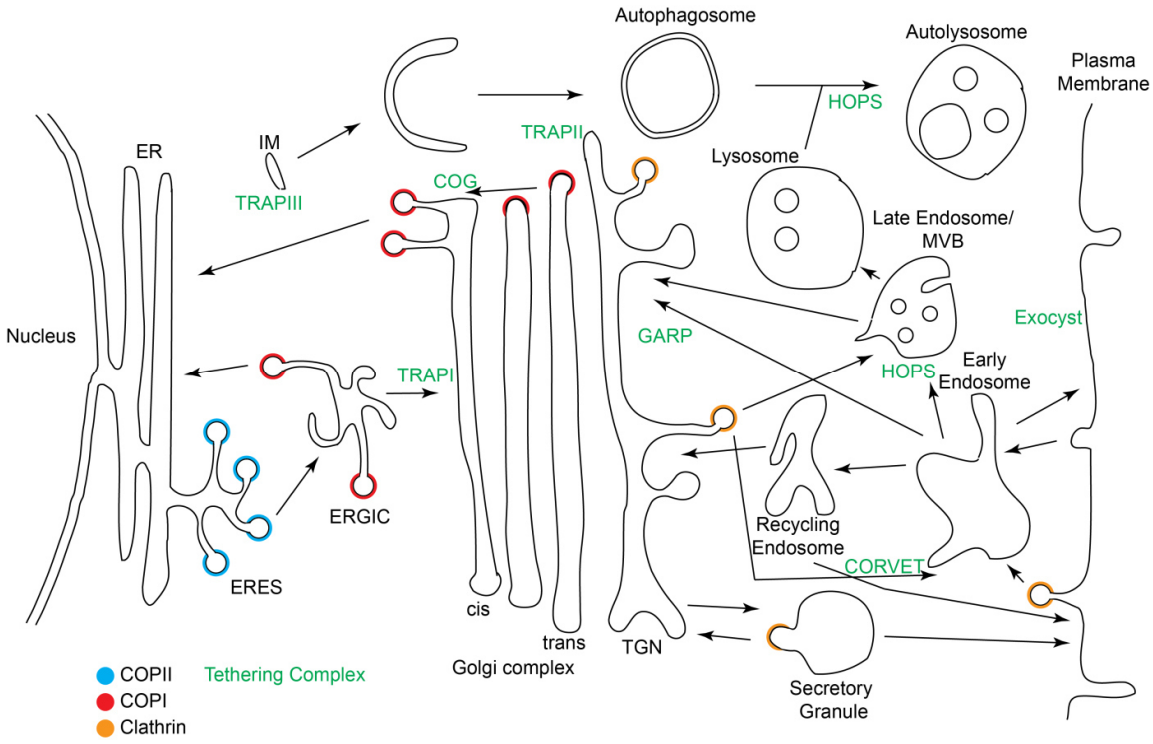

Figure 1: **Vesicular transport in eukaryotic cells.** Material from the ER is transported to the PM through the secretory pathway. The Golgi complex serves as a central sorting platform. Endocytosed material can be sorted for degradation into the lysosome or can be recycled through different routes. The corresponding compartment to the lysosome is the vacuole in yeast cells. Only

selected protein coats and tethering complexes are shown. Adapted and modified from (Scott et al., 2014; Yu and Hughson, 2010).

taken up by the cell. **Figure 1** summarizes vesicular trafficking in eukaryotic cells. Transport vesicles involved in these pathways have to bud off a donor membrane and fuse to a specific acceptor membrane (Bonifacino and Glick, 2004). Several steps are required in budding, transport and fusion of transport vesicles and a diverse set of proteins is involved in these processes.

1.1.1. Transport vesicles require protein coats

Coat proteins are involved in several steps of vesicle formation which are inducing membrane curvature, concentrating cargo, driving vesicle release and membrane scission (D'Arcangelo et al., 2013). The molecular mechanisms underlying these processes are, however, not fully understood (Faini et al., 2013). These processes are mainly regulated by small GTPases of the Ras super-family which are also important to confer specificity to vesicular transport (Mizuno-Yamasaki et al., 2012). Tethering factors recognize the appropriate membrane pairs and bring them into proximity for SNARE (soluble N-ethylmaleimide-sensitive factor attachment protein receptor)-mediated membrane fusion (Jackson et al., 2012). Three different membrane coats are mainly involved in vesicular transport depending on the origin and destination of a vesicle. These membrane coats possess different structural features, but all contain adaptor and cage complexes (Faini et al., 2013).

Vesicles budding off the ER and directed to the ER-Golgi intermediate compartment (ERGIC) are coated by a COPII coat (Barlowe et al., 1994; Szul and Sztul, 2011). These vesicles bud off from defined membrane areas of the ER, called ER exit sites (ERES) (Orci et al., 1991; Stephens, 2003). Five proteins, Sar1, Sec23, Sec24, Sec13 and Sec31, are sufficient to reconstitute vesicle formation *in vitro* (Barlowe et al., 1994; Matsuoka et al., 1998). The adaptor complex comprises the proteins Sec23 and Sec24 and is recruited by the Sar1-GTPase (Miller et al., 2002). The Sec13-Sec31 cage complex forms a protein meshwork. The Sec13-Sec31 cage was suggested to be able to accommodate a membrane vesicle with a diameter of 40 nm and a layer of adaptor complexes (Fath et al., 2007).

Retrograde transport from the ERGIC and the Golgi complex to the ER is mediated by COPI coated vesicles (Bonifacino and Glick, 2004). The adaptor and coat complexes are

part of the coatomer supercomplex that is assembled from seven subunits and is recruited *en bloc* to the membrane (Hara-Kuge et al., 1994). The coatomer is recruited to the membrane by activated Arf1 (Serafini et al., 1991; Yu et al., 2012). It was shown that the coat formed by COPI coatomer is able to adopt different sizes and shapes which is based on conformational flexibility of the coatomer complex (Faini et al., 2012).

Clathrin coated vesicles are involved in vesicular transport from the PM and the endosomal membrane as well as in the trans-Golgi network (TGN). Furthermore, clathrin is involved in numerous specialized pathways like secretory granule formation, antigen presentation, or synaptic vesicle generation (Brodsky, 2012). Different adaptor complexes are involved in these processes. The highly conserved protein AP2 is thought to be recruited by a nucleation module consisting of several proteins to the PM and binds the cytoplasmic tails of PM receptors as well as the PM specific lipid phosphatidylinositol-4,5-bisphosphate ($PI(4,5)P_2$). Furthermore, AP2 interacts with and thereby concentrates cargo (McMahon and Boucrot, 2011). Clathrin plays also a role in intracellular pathways where other adaptor complexes containing AP1, AP3, AP4 and the GGAs (Golgi-localized, γ-ear-containing, ARF-binding proteins) are involved. The respective cargo is recognized by the adaptor complexes through a sorting motif (Robinson, 2004). The recruited cage complex is composed of clathrin light and heavy chains that form triskelia. The legs of the triskelia interact to form the clathrin coat (Fotin et al., 2004).

Assembly and disassembly of the coats described above are only two of many different steps in vesicular trafficking that need to be tightly regulated.

1.1.2. Regulation of vesicular transport by small GTPases

Small GTPases of the Ras super-family are involved in regulating almost every step of vesicular trafficking (Mizuno-Yamasaki et al., 2012). GTPases function as molecular switches that can act on effectors in their active state. They are activated by guanosin nucleotide exchange factors (GEFs) that trigger the release of GDP and binding of GTP. The GTP-bound form is the active state and the inactivation can be triggered by GTPase-activating proteins (GAPs) that enhance the low hydrolytic activity of the GTPase. Inactive small GTPases are dispersed in the cytoplasm and activation recruits them to the

membrane of a specific organelle (Stenmark, 2009). The Arf proteins and the Sar1 protein are so called coat-recruitment GTPases. Active coat recruitment GTPases are targeted to selective membranes by cargo or selective lipids. They insert a hydrophobic helix into the membrane which allows them to recruit downstream factors. Arf proteins are involved in recruiting the COPI and clathrin coat, while the Sar1 protein recruits the COPII coat (Faini et al., 2013). When the coat recruitment GTPases return to their inactive state, they also contribute to release of the vesicle from the membrane of origin (Campelo and Malhotra, 2012) as well as to coat disassembly from the mature vesicle. Rab (Ypt in yeast) GTPases are involved in regulating the subsequent steps which are transport, tethering and fusion of the uncoated vesicles to the respective target membrane by interacting with Rab effector proteins (Stenmark, 2009).

1.1.3. Membrane tethering

Membrane tethering complexes are recruited to specific membranes by small GTPases, coat proteins, lipids, and core components of the fusion machinery. Thereby they establish an initial interaction between these membranes (Jackson et al., 2012). This step was suggested to accelerate the process of bringing two membranes that are supposed to fuse into proximity by applying proteins that span long distances. Tethering factors were separated into two classes. The first class are long coiled-coil homodimer tethering proteins (CCTP) and the second class are multi subunit tethering complexes (MSTC) (Hughson and Reinisch, 2010; Whyte and Munro, 2002). Golgins belong to the CCTP, while the class of MSTC includes the conserved oligomeric Golgi (COG, in yeast Sec34-Sec35 complex) complex, the homotypic fusion and vacuole protein sorting (HOPS) complex and the transport protein particle (TRAPP) complexes (Yu and Hughson, 2010) which are briefly described below.

The CATCHR (complexes associated with tethering containing helical rods) protein family is based on sequence homology of COG complex subunits with other tethering factor subunits (Yu and Hughson, 2010). COG complex is involved in retrograde trafficking at the Golgi complex (Ram et al., 2002). The mammalian COG complex is a heteroctamer (Ungar et al., 2002). Its homologue in yeast is the Sec34-Sec35 complex which also forms a heteroctamer (Suvorova et al., 2002).

Both HOPS and CORVET (class C core vacuole/endosome tethering) complexes are composed of a common core complex that consists of four subunits (Peplowska et al., 2007; Wurmser et al., 2000). The HOPS complex subunits were originally described to be involved in vacuole formation in yeast (Raymond et al., 1992; Wada et al., 1992). For efficient membrane fusion *in vitro*, the HOPS complex required the presence of four vacuolar SNARE proteins, the SNARE disassembly system Sec18-Sec17 (NSF/αSNAP in yeast), the small Rab GTPase Ypt7, and ATP (Stroupe et al., 2009).

Three types of TRAPP complexes have been described which are involved in different pathways. Yeast TRAPPI complex is a heteroheptamer involved in ER to Golgi transport (Sacher et al., 1998). TRAPPII complex includes three additional subunits and is a heterodecamer which acts in intra-Golgi transport (Sacher et al., 2001). Recently, a third complex, TRAPIII was shown to be involved in vesicular transport from early endosomes to the Golgi complex and to be required for autophagy (Lynch-Day et al., 2010; Shirahama-Noda et al., 2013). In contrast to the COG complex which is an effector of the small GTPase Ypt1 (Suvorova et al., 2002), TRAPP complexes were shown to act as Ypt1 GEFs (Lynch-Day et al., 2010; Sacher et al., 2001).

After the tethering event, fusion of membranes needs to occur for delivery of the vesicular content to the organelle of destination. This step is accelerated by SNARE-proteins (Yu and Hughson, 2010).

1.1.4. SNARE-proteins mediated membrane fusion

Specific pairs of SNARE-proteins are located in the vesicles (v-SNARE) and the respective target membrane (t-SNARE) (McNew et al., 2000). SNARE-proteins are largely unstructured, but fold when they interact with their specific partner SNARE (Fasshauer et al., 1997). The interaction between SNARE-proteins is mediated by a SNARE-motif and induces the formation of a 4-helix bundle (Antonin et al., 2002). Membrane fusion is catalyzed by forming this 4-helix bundle in a zipper-like manner from the membrane bound N-termini to the C-termini (Jahn and Scheller, 2006). The folding of SNARE-proteins involves the formation of intermediates in a two-step folding pathway (Li et al., 2014). Molecular dynamics simulations revealed that SNARE-proteins form a stiff platform that brings the vesicle and target membrane into close proximity at the membrane

bound N-termini. Furthermore, the energy that is released during formation of the helix bundle is used for hemifusion (Durrieu et al., 2008; Risselada and Grubmüller, 2012). NSF (N-ethylmaleimide-sensitive factor; Sec18 in yeast), a member of the ATPases Associated with various cellular Activities Plus (AAA^+) family (Hanson and Whiteheart, 2005), is required for disassembly of the 4-helical bundle formed by the SNARE-proteins (Block et al., 1988; Zhao et al., 2012). It requires the peripheral membrane protein soluble NSF Attachment Protein (SNAP; in yeast Sec17) as adaptor. SNAP binds the 4-helical bundle formed by SNARE-proteins after membrane fusion and recruits ATP-bound NSF (Clary et al., 1990; Griff et al., 1992). Hydrolysis of ATP leads to a conformational change of NSF which induces disassembly of the 4-helical bundle (Zhao et al., 2012).

1.2. Recycling and degradation pathways in the cell

Cellular homeostasis requires a tightly tuned balance between anabolic and catabolic processes (Reggiori and Klionsky, 2013). The ubiquitin-proteasome system and the lysosomal/vacuolar system, including endocytosis and autophagy, are the major degradation machineries in the cell.

1.2.1. The ubiquitin-proteasome system

The conjugation of cytosolic proteins to the 8.5 kDa protein ubiquitin, forming poly-ubiquitin chains linked at Lys48, marks them for degradation by the proteasome (Chau et al., 1989; Komander and Rape, 2012). Consuming ATP, ubiquitin is transferred to the target protein by the sequential reaction of an E1, E2, and E3 enzyme which display increasing substrate selectivity (Finley, 2009). In addition to the poly-ubiquitin chain, proteins destined for degradation by the proteasome need to display unfolded regions for initiation of proteasomal degradation (Prakash et al., 2004). The proteasome is formed by a 20 S core particle (CP) and two 19 S regulatory particles (RPs) at the CP caps (Bhattacharyya et al., 2014). The 20 S core particle is formed by 28 subunits. Two heptameric rings composed of the β(1-7)-subunits which confer the proteolytic activity, are sandwiched between two heptameric rings composed of the α(1-7)-subunits which are involved in substrate discrimination (Förster et al., 2013; Groll et al., 1997; Unno et al.,

2002). In mammals, three additional β-subunits (β1i, β2i, β5i) are required to form the immunoproteasome involved in antigen processing upon interferon induction (Unno et al., 2002). The RP contains an AAA-ATPase module and regulates access to the CP by substrate recognition and substrate unfolding (Förster et al., 2013).

1.2.2. Endocytosis in the lysosomal/vacuolar pathway

Lysosomes/vacuoles are specialized organelles that are involved in degrading material from the cytoplasm and the extracellular space. Cargo can be delivered by vesicular transport to the lysosome/vacuole (**Figure 1**). Cargo from the PM and the extracellular space is delivered to the lysosome/vacuole by the process of endocytosis (Bonifacino and Glick, 2004). Receptors that are taken up through endocytosis can be recycled from early endosomes (EE) or degraded by the formation of multivesicular bodies (MVBs) in late endosomes (LE) (Woodman and Futter, 2008). A special degradation pathway is the process of macroautophagy. Thereby a membrane is formed *de novo* to sequester cytoplasmic material and deliver it for degradation to the vacuole/lysosome (Reggiori and Klionsky, 2013). Other forms of autophagy, like microautophagy and chaperone mediated autophagy (CMA) are also involved in transporting cytoplasmic material to the lysosome/vacuole (Kaushik and Cuervo, 2012; Li et al., 2012).

Endosomes are key player in sorting material for recycling or degradation in eukaryotic cells. Vesicles formed from invaginations of the PM take up PM proteins and extracellular material. These vesicles are assumed to fuse to form the EE which takes up and recycles material from the vesicles over a time period of approximately 10 min in mammalian cells (Maxfield and McGraw, 2004). Afterwards EEs undergo a maturation process from EEs to LEs and eventually fuse with and become a lysosome/vacuole (Scott et al., 2014). During this process recycling steps can take place. The EE can directly recycle content to the PM and the TGN or form a recycling endosome that is able to cycle content back to the PM and the TGN. Also LE still possess recycling capacity by routing content to the TGN (Bonifacino and Glick, 2004). The acidification of the LE is required for activation of lysosomal proteins that contribute to the lysosomal degradation machinery (Scott et al., 2014). Receptors from the PM destined for degradation are taken up into the lumen of MVBs formed from EEs that fuse with LEs or lysosomes for degradation (Bissig and

Gruenberg, 2013). More than 30 vesicles with a diameter of about 50 - 100 nm can be internalized per MVB (Huotari and Helenius, 2011).

1.2.3. Autophagy in the lysosomal/vacuolar pathway

Autophagy was defined as a process that delivers cytoplasmic material of a cell to the lysosome/vacuole for degradation more than 50 years ago (de Duve and Wattiaux, 1966; Deter et al., 1967). Autophagy (gr. ‚self-eating') is conserved in all eukaryotes where it is responsible for the degradation of cytosolic components and organelles (Klionsky, 2007). Autophagy fulfills specific housekeeping functions by recycling organelles like mitochondria (mitophagy), peroxisomes (pexophagy), ribosomes (ribophagy) and parts of the ER (reticulophagy) selectively. In yeast, hydrolases are delivered to the vacuole by an additional selective autophagic pathway, the so called cytoplasm to vacuole (cvt) pathway, that has not been identified in mammalian cells (Kraft et al., 2009). A basal level of non-selective autophagy is involved in constant turnover of cytoplasmic material (Mizushima, 2007). However, autophagy is induced under nutrient starvation conditions or in response to stress factors and different physiological signals like hormones (Mizushima, 2007; Noda and Ohsumi, 1998). Special focus has been set on autophagy because it is involved in different diseases, like neurodegenerative diseases or cancer (Choi et al., 2013). Upon starvation induction, so called macroautophagy is strongly induced and cells form double-membranes that engulf cytoplasmic material and eventually fuse to deliver their content to the lysosome/vacuole for degradation. These vesicles originate at the pre-autophagosome structure (PAS) where a precursor membrane, the so called phagophore (isolation membrane (IM) in mammalian cells) is formed.

1.2.3.1. Autophagic pathways

Different types of autophagy that deliver proteins to the lysosome/vacuole have been discovered. **Figure 2** shows an overview over the different autophagic pathways that have been described. In macroautophagy a double membrane is generated *de novo*. This double membrane can engulf cytoplamic material selectively or non-selectively. A special branch of selective autophagy is the cvt pathway that is required for the transport of hydrolases to

the vaculoe. Invaginations in the vacuolar membrane can take up cytoplasmic material selectively or non-selectively. This process is termed microautophagy. Chaperone mediated autophagy (CMA) requires unfolding of the protein that is transported through a channel formed by the protein LAMP-2A.

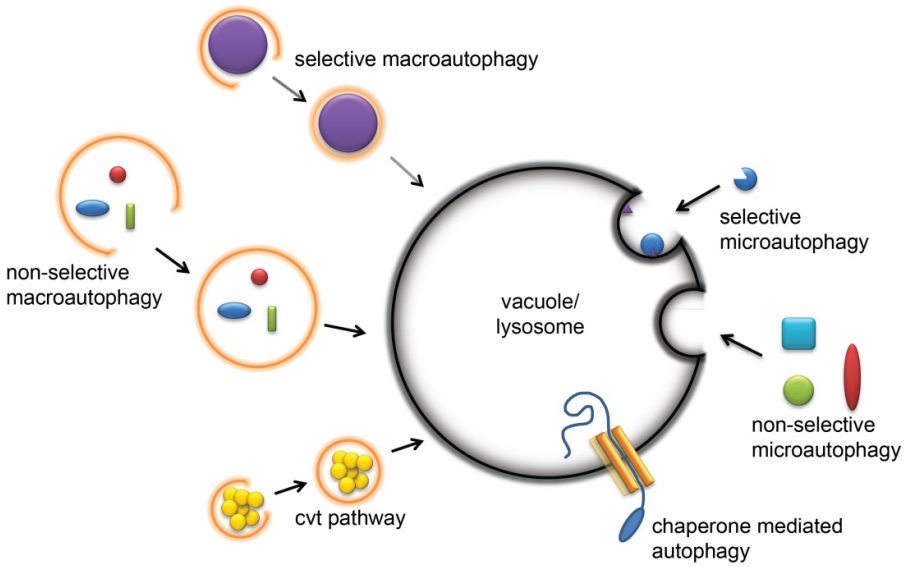

Figure 2: **Different types of autophagy.** Autophagy is defined as the process during which cytoplasmic material is delivered to the vacuole/lysosome for degradation.

a) Selective macroautophagy

Organelles, intracellular pathogens or protein aggregates can be degraded selectively by macroautophagy (Klionsky, 2007; Reggiori and Klionsky, 2013). Selective autophagic degradation of different organelles is termed accordingly, e.g. selective autophagy of mitochondria is termed mitophagy. During selective macroautophagy the cargo is exclusively engulfed and cytoplasm is excluded by the tight contact between cargo and phagophore membrane that is mediated by the respective cargo receptor and the cargo adaptor Atg8 (Kraft et al., 2009). The selective degradation of organelles is required to maintain cellular homeostasis. Failure in removing damaged mitochondria can lead to the accumulation of toxic substances, such as reactive oxygen species (ROS) (Zhang et al., 2007). A special form of selective macroautophagy is the cvt pathway in yeast. At least two hydrolases, α-mannosidase (Ams1) and aminopeptidase I (Ape1) are delivered by the

cvt pathway to the vacuole (Lynch-Day and Klionsky, 2010). The cargo is linked to the autophagic membrane through the action of activated adaptor proteins like Atg19 which bind Atg8, an autophagic protein that is covalently linked to phosphatidylethanolamine (PE) in the phagophore (Sawa-Makarska et al., 2014).

b) Non-selective macroautophagy

Non-selective macroautophagy is mainly induced in response to cellular stress where it functions as a survival mechanism through the degradation of cytoplasmic material (Reggiori and Klionsky, 2013). In contrast to selective macroautophagy, cargo is not recognized by specific interactions with cargo bound adaptors, but engulfed by the growing double membrane (Feng et al., 2014). However, macroautophagy can also modulate biosynthetic pathways by targeting respective enzymes like the fatty acid synthase (FAS) for degradation in the vacuole (Thumm et al., 1994). The cell is able to recycle nutrients that are required for core processes that are required for survival of the cell from the material delivered to the vacuole/lysosome.

In all forms of selective and non-selective macroautophagy the outer membrane of the vesicle subsequently fuses with the vacuole/lysosome to release the inner membrane with its content into the vacuolar/lysosomal lumen for degradation (Nakatogawa et al., 2009).

c) Microautophagy

Other forms of autophagy also lead to transport of cytoplasmic material to the vacuole/lysosome through different mechanisms. Uptake of cytoplasmic material by invaginations in the vacuolar/lysosomal membrane is termed microautophagy (de Duve and Wattiaux, 1966; Li et al., 2012). First, a so called autophagic tube is formed. This membrane structure is a tubular invagination in the vacuolar membrane that is triggered by starvation (Müller et al., 2000; Sattler and Mayer, 2000). At the tip of the tubular invagination a vesicle is formed and expanded. The action of a lateral sorting machinery keeps the vesicular membrane almost free of integral protein and the resulting phase separation facilitates vesicle formation (Müller et al., 2000). Finally, the vacuolar transporter chaperone (VTC) complex is required for scission of the vesicle from the

autophagic tube and the vesicle is released into the vacuolar lumen for degradation (Uttenweiler et al., 2007). Uptake of cytoplasmic material can be selective or non-selective. In addition to its role in cell survival under nitrogen restriction, it is required for maintenance of organellar size and membrane homeostasis (Li et al., 2012; Sahu et al., 2011).

d) Chaperone mediated autophagy

Furthermore, CMA has been described (Chiang et al., 1989). Proteins that are degraded through CMA carry a specific pentapeptide motif (Fred Dice, 1990). The hsc70 (heat shock cognate protein of 70 kDa) chaperone recognizes this pentapeptide and targets the proteins to CMA. The accessibility of this motif is likely to regulate the degradation of the respective proteins. It is assumed that this could serve as a quality control mechanism so that partially unfolded proteins are degraded by CMA (Kaushik and Cuervo, 2012). However, also post-translational modifications can influence the physical properties of the pentapetide motif to alter its affinity for hsc70 (Lv et al., 2011). In CMA, proteins are translocated across the vacuolar/lysosomal membrane by the channel forming protein LAMP-2A (Bandyopadhyay et al., 2008). In order to be translocated by LAMP-2A, proteins need to be unfolded. Chaperone assisted protein unfolding is required for translocation of proteins across the vacuolar/lysosomal membrane during CMA (Agarraberes and Dice, 2001).

1.2.3.2. The autophagic machinery

A combination of genetic screens (Tsukada and Ohsumi, 1993) and biochemical approaches identified 38 Atg proteins in yeast (Lamb et al., 2013b). Out of these 38 Atg proteins, 18 Atg proteins are part of the core autophagic machinery that is required for canonical autophagy (Nakatogawa et al., 2009). They are part of five protein complexes or protein groups including the Atg1-kinase complex (ULK1 complex in mammals), the integral membrane protein Atg9, an autophagy specific phosphatidyinositol-3(PI3)-kinase complex, two interconnected Atg8 conjugation systems, and the Atg18-Atg2 complex.

Furthermore, there are several non-Atg-proteins involved in autophagy. Finally, the outer autophagic membrane fuses with the vacuole/lysosome and the inner membrane with the cytoplasmic material is released for degradation (Mizushima, 2007). **Figure 3** summarizes the role of the Atg-protein subgroups in the formation of the autophagic membrane. Atg1-kinase complex and the integral membrane protein Atg9 are required for phagophore formation (Cheong et al., 2008; Yamamoto et al., 2012). The phagophore is enriched in PI-3-phosphate (PI3P) by an autophagy specific PI3 kinase (Kihara et al., 2001). The PI3P recognizing protein Atg18 is then recruited and involved in organizing the recruitment and disassembly of other Atg-proteins on the phagophore together with Atg2 (Suzuki et al., 2013). Two ubiquitin like conjugation systems transfer Atg8 to PE in the autophagic membrane (Ichimura et al., 2000; Mizushima et al., 1998). On the outer membrane Atg8 forms a membrane scaffold together with other Atg-proteins (Kaufmann et al., 2014). During selective autophagy Atg8 functions also as cargo-adaptor on the concave side of the phagophore (Birgisdottir et al., 2013). A role for the Atg1-kinase complex or some of its subunits in later stages of autophagy and in recycling processes of Atg-proteins from the autophagic membrane has been suggested (Kraft et al., 2012; Reggiori et al., 2004). Finally, the outer autophagic membrane fuses with the vacuole/lysosome and the inner membrane with the cytoplasmic material is released for degradation (Mizushima, 2007).

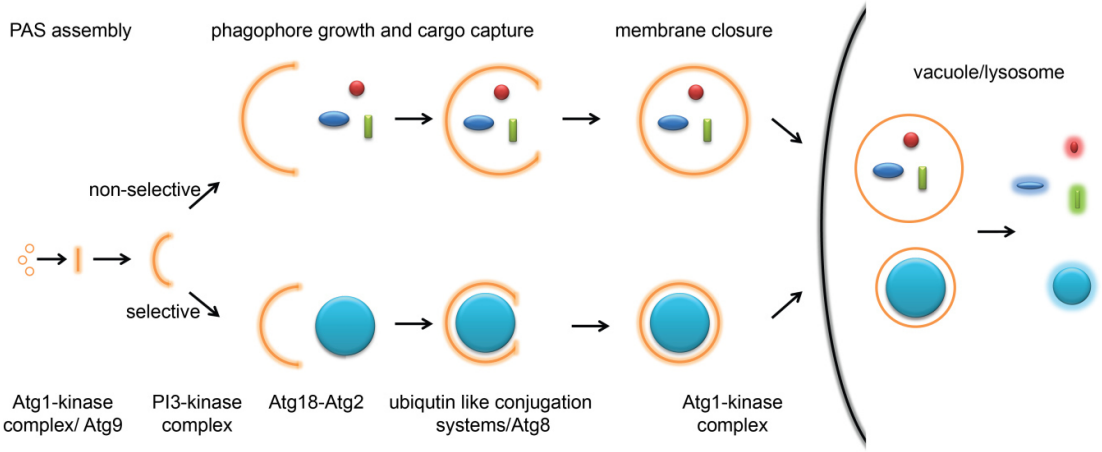

Figure 3: Atg-protein complexes involved in macroautophagy. The sequential action of the indicated protein complexes is required for phagophore nucleation, expansion, closure and fusion with the vacuolar/lysosomal membrane.

a) The Atg1-kinase complex

The first complex to assemble during initiation of autophagosome formation at the PAS is the Atg1-kinase complex which is a heteropentameric complex in yeast, consisting of the Atg1-kinase and its regulatory subunits Atg13, Atg17, Atg29, and Atg31 (Kamada et al., 2000; Kamada et al., 2010). Under starvation conditions, the regulatory subunit Atg13 is dephosphorylated and the Atg1-Atg13 subcomplex associates with a trimeric cytoplasmic complex consisting of Atg17, Atg29 and Atg31. This leads to an increase in the kinase activity of Atg1-kinase (Kamada et al., 2000) and to the recruitment of the Atg1-kinase complex to the PAS (Kabeya et al., 2005). Atg17 is a scaffolding protein that is required for non-selective autophagy (Ragusa et al., 2012) and it was shown that it is required to target Atg9 to the PAS (Sekito et al., 2009). For selective autophagy Atg11 is required and it is speculated that it could be a functional substitute of Atg17 (He et al., 2006). Phosphorylation of Atg29 was shown to be a mechanism that regulates the interaction between Atg29 and Atg11 (Mao et al., 2013). Two human homologues of Atg1-kinase were identified applying si-RNA mediated gene knock down. The Unc51-like kinase-1 (ULK-1) and ULK-2 are required for autophagy in human cells (Chan et al., 2007; Lee and Tournier, 2011). It was shown that the proteins Atg13 and FIP200 are required to form a complex with ULK for signal transduction from TORCI, a major regulator of autophagy. In contrast to the regulation of the Atg1-kinase complex in yeast, in addition to Atg13, ULK is directly phosphorylated by TORCI in human cells which suppresses induction of autophagy (Jung et al., 2009).

b) The integral membrane protein Atg9

Atg9, the only integral membrane protein required for autophagy (Feng et al., 2014; Lang et al., 2000; Noda et al., 2000), interacts with the Atg1-kinase complex to organize the PAS (Sekito et al., 2009) and to deliver lipids for the autophagic membrane (Yamamoto et al., 2012). Active Atg1-kinase complex recruits Atg9 and subsequently other proteins to the PAS which places the Atg1-kinase complex and Atg9 at one of the most upstream positions in the Atg-protein hierarchy (Suzuki et al., 2007). Atg9 was further described to recruit the TRAPPIII complex and the Rab family GTPase Ypt1 to the PAS (Kakuta et al.,

2012). Atg9 contains six trans-membrane helices and the C-terminal and N-terminal part face the cytoplasm (Feng et al., 2014). Atg9 proteins were shown to be organized in a cytoplasmic pool in yeast (Yamamoto et al., 2012). In mammalian cells, Atg9 localizes to the TGN and LE under vegetative conditions (Young et al., 2006). Trafficking of Atg9-vesicles towards the growing autophagic membrane was shown be induced by Atg1-kinase complex dependent phosphorylation of a myosin light chain kinase-like protein that activates the motor protein myosin II in *D. melanogaster* and human cells (Tang et al., 2011). Furthermore, direct phosphorylation of Atg9 by Atg1-kinase was reported to be required to promote autophagy in yeast (Papinski et al., 2014). In addition, transport of Atg9 to the PAS requires Atg23 and Atg27 in yeast (Legakis et al., 2007; Yen et al., 2007). The recruitment of Atg9 to the PAS was further shown to depend on its direct interaction with the N-terminal domain of Atg17 under starvation conditions and with Atg11 under vegetative conditions (He et al., 2006; Sekito et al., 2009).

c) Phosphatidyinositol-3-kinase complex

The PI-3-kinase complex enriches the phagophore with PI3P (Kihara et al., 2001). The complex consists of the PI3-kinase Vps34 and the subunits Vps15, Vps30, Atg14, and Atg38 in yeast. Atg14 is required to constitute an autophagy specific complex (complex I) while the other subunits are also involved in forming a PI3-kinase complex required in the vacuolar protein sorting pathway (complex II) (Araki et al., 2013; Obara et al., 2006). In mammalian cells, three PI3-kinase complexes are involved in autophagy. All contain the PI3-kinase Vps34 and the subunits Belcin1 and p150. Beclin1 can bind several other proteins which was suggested to control the function of the respective PI3-kinase complex in autophagy (Matsunaga et al., 2009; Zhong et al., 2009). The complex containing Atg14L localizes to the IM under starvation conditions and is required to promote autophagy. The mammalian PI3-kinase subunit Beclin1 can exclusively bind Atg14L or the protein UVRAG (Itakura et al., 2008). The composition of the PI3-kinase complex containing UVRAG is more complex, because UVRAG can recruit additional subunits which lead to diverse functions of the fully assembled complex. These functions range from accelerating autophagic flux to membrane deformation and autophagy inhibition which makes the autophagy specific PI3-kinase complex an important regulatory factor (Yang and Klionsky, 2010). In fact, the mammalian PI3-kinase complex was shown to be regulated through phosphorylation of its subunit Beclin1 by the Rho kinase 1 (ROCK1)

and ULK-1 (Gurkar et al., 2013; Russell et al., 2013). However, enrichment of the phagophore with PI3P is required to recruit downstream factors, such as the PI3P binding protein Atg18 (Feng et al., 2014) which interacts with Atg2 (Watanabe et al., 2012). Atg18 is essential for autophagosome formation and temporally regulates recruitment and dissociation of other Atg-proteins to and from the PAS (Suzuki et al., 2013). In Atg18 and Atg1 knockout strains Atg9 accumulates at the PAS indicating that both proteins are required for Atg9 vesicle fusion or Atg9 recycling (Reggiori et al., 2004). In *atg1Δ* cells it was shown that unfused Atg9 vesicles accumulate at the PAS (Mari et al., 2010).

d) Atg8 conjugation machinery

Two interconnected ubiquitin-like conjugation systems are involved in autophagy. Their final aim is to transfer Atg8 to its acceptor lipid PE in the growing autophagic membrane (Mizushima et al., 1998). Before Atg8 is conjugated to the E1-like enzyme Atg7 in an ATP-dependent step, it needs to be activated through proteolytic cleavage by Atg4, which removes a C-terminal Cys to make a Gly residue available (Kirisako et al., 2000). Activated Atg8 is then transferred to the E2-like enzyme Atg3. Atg12 is the E3-like enzyme responsible to transfer Atg8 to PE in the phagophore membrane. Atg12 needs to be activated through sequential reactions with an E1 and E2-like enzyme (Atg7 and Atg10, respectively) itself and is conjugated to Atg5, which further associates with dimeric Atg16 (Mizushima et al., 1998). The Atg12–Atg5-Atg16 complex transfers Atg8 to PE within the phagophore membrane (Ichimura et al., 2000). Atg8 plays a role in autophagic membrane scaffold formation on the outer membrane (Kaufmann et al., 2014) and as cargo adaptor on the inner membrane (Birgisdottir et al., 2013). After the mature autophagosome has been formed, Atg8 is recycled from the cytoplasmic leaflet of the phagophore by Atg4 (Ichimura et al., 2000).

e) Non-Atg proteins involved in autophagy

As described above, small GTPases are involved in regulating almost all steps of vesicular trafficking. The small Rab GTPase Ypt1 was shown to be involved in recruiting Atg1-

kinase to the PAS in yeast (Wang et al., 2013). The activation of Ypt1 requires the TRAPPIII complex which is a GEF of Ypt1 that is specifically recruited to the PAS through its interaction with Atg17 (Lynch-Day et al., 2010; Wang et al., 2013). Moreover, the small GTPase Arf6 was shown to play a role in autophagy in mammalian cells. Arf6 activates its effector PI4P 5-kinase leading to the generation of $PI(4,5)P_2$ at the PM which recruits several effectors to the PM, among them Phospholipase D (PLD) (Moreau et al., 2012). PLD1 is required for the formation of an appropriate number of correctly sized autophagosomes and for starvation response in mice (Dall'Armi et al., 2010), but the direct role of Arf6 in autophagy is unclear (Lamb et al., 2013a). As discussed below, small GTPases regulate autophagy through their effect on TORCI, a central regulator of autophagy (Demetriades et al., 2014). In addition, the small GTPase RalB regulates autophagy through its effector, the Exocyst tethering complex. Under starvation conditions active RalB recruits the autophagy specific subunit Exo84 to the Exocyst complex which leads to release of the negative regulator TORCI and recruitment of Ulk-1 and the autophagy specific PI3-kinase complex (Bodemann et al., 2011). Non-Atg proteins are also involved in membrane tethering and fusion events during autophagy. It was shown that the HOPS complex is required for fusion of the autophagosome with the lysosome in mammalian cells and *D. melanogaster* (Jiang et al., 2014; Takáts et al., 2014). Furthermore, subunits of the COG complex were shown to be required for formation of the phagophore and correct localization of Atg-proteins in yeast (Yen et al., 2010).

After the tethering event, membranes need to fuse. As described previously, SNARE-proteins are required for efficient membrane fusion. SNARE-proteins are involved in different steps of autophagy (Moreau et al., 2013). In mammalian cells, Atg16L1 positive vesicles require VAMP7 together with partner SNARE-proteins (syntaxin-7, syntaxin-8, and VTI1B) for homotypic fusion to contribute to IM formation (Moreau et al., 2011). Other SNARE-proteins were shown to be involved indirectly in autophagosome formation and maturation by playing a role in associated processes. E.g. the movement of Atg9 from peripheral sites to the PAS requires the SNARE-proteins Sso1-Sso2 and Sec9 which are involved in exocytosis in yeast cells (Nair et al., 2011). Furthermore, the SNARE-protein Syntaxin17 (Stx17) which interacts with the HOPS complex, localizes to completed autophagosomes and is required for lysosome/endosome fusion in mammalian cells (Itakura et al., 2012; Jiang et al., 2014). However, the non-Atg proteins described here play important roles in vesicular membrane trafficking which makes it difficult to exclude secondary effects and analyze their detailed role in autophagy.

1.2.3.3. The autophagic membrane

Autophagosomes are unique organelles that are formed from a cup-shaped precursor membrane, the so called phagophore or IM. The origin or donor organelle of the phagophore remains, however, a matter of debate. Vesicular transport of lipids and proteins from different organelles to the phagophore is supposed to be involved in the expansion of the phagophore (Lamb et al., 2013b).

The phagophore is formed at the PAS. In yeast a single PAS is present, while in mammalian cells the PAS is formed at multiple sites upon autophagy induction (Lamb et al., 2013b). The PAS was identified applying fluorescence microscopy of GFP-tagged Atg-proteins (Mizushima et al., 2001; Suzuki et al., 2001; Suzuki et al., 2007). Different models that describe the formation of the PAS exist. It was suggested that extrusions from the ER membrane are formed in specific regions of the ER membrane. These extrusions were called omegasomes and it was hypothesized that omegasomes are precursor structures of autophagosomes (Axe et al., 2008). Further studies observed that autophagosome biogenesis is spatially linked to ERES in yeast and mammalian cells (Graef et al., 2013) as well as to ER-mitochondria contact sites in mammalian cells (Hamasaki et al., 2013). However, in yeast it was also observed that early autophagic proteins assemble at a site close to the vacuole which was suggested to be the PAS (Suzuki et al., 2001) and that the phagophore is also associated with the ER (Suzuki et al., 2013).

Different sources for initial formation as well as for expansion of the phagophore have been described in yeast and in mammalian cells. In the process of omegasome formation in mammalian cells, the IM was suggested to be initially formed by the ER membrane (Simonsen and Stenmark, 2008). The fusion of three Atg9 vesicles was reported to form the phagophore in yeast (Yamamoto et al., 2012). Atg9 is an integral membrane protein in autophagy and resides in a vesicular pool from which single Atg9 vesicles are recruited to the PAS (Mari et al., 2010; Orsi et al., 2012). The ERGIC was described to be essential for early phagophore growth as determined by analyzing the conjugation of the mammalian Atg8 homologue LC3 to the IM in a cell free assay (Ge et al., 2013). Expansion of the phagophore was described to depend on the contribution of different organelles. The Golgi complex was described as a membrane source for growth of the phagophore in yeast (van der Vaart et al., 2010). Also the PM was reported to contribute to growth of the IM,

especially during periods of high autophagy activity in mammalian cells (Ravikumar et al., 2010). Furthermore, Atg9 was described not only to play a role in phagophore initiation, but also in IM expansion in mammalian cells (Orsi et al., 2012). In addition, it was speculated that lipids required for the IM could be synthesized by enzymes that reside in the membranes involved in IM biogenesis (Lamb et al., 2013b). Probably these processes work in concert to generate and expand the phagophore.

1.2.3.4. Regulation of autophagy

Autophagy is regulated mainly by two nutrient factors. Availability of amino acids and sugars (Reggiori and Klionsky, 2013). Different regulatory pathways sense the respective nutrient status and regulate autophagy.

a) Amino acid dependent autophagy regulation

A major regulator of autophagy is the highly conserved target of rapamycin kinase complex I (TORCI) (Cutler et al., 1999; Noda and Ohsumi, 1998) which is regulated by nutrient availability, growth factors and stress (Sengupta et al., 2010). TORCI is composed of the kinase TOR and the subunits Kog1, Tco89, and Lst8 in yeast (RAPTOR, mLST8, PRAS40, and DEPTOR in mammals) which form a dimer with a size of approximately 2 MDa (Loewith and Hall, 2011; Sengupta et al., 2010). Active TORCI acts on downstream effectors like AGC family kinases which leads to cell growth (Loewith and Hall, 2011). In yeast cells, TORCI was shown to localize constitutively to the cytoplasmic face of the vacuolar membrane (Binda et al., 2009) which indicates that localization is not affecting TORCI activity (Loewith and Hall, 2011). In mammalian cells it was demonstrated that activity of TORCI requires localization to the lysosome/LE for activity (Demetriades et al., 2014). One target of TORCI is Atg13, a subunit of the Atg1-kinase complex (Cheong et al., 2008). Under nutrient rich conditions, Atg13 is heavily phosphorylated by TORCI (Kamada et al., 2010), preventing Atg1-kinase complex assembly (Kabeya et al., 2005). In mammalian cells TORCI phosphorylates additionally the Atg1-kinase homologue ULK-1 to inhibit autophagy (Jung et al., 2009). However, if an

non-phosphorylatable mutant of Atg13 is expressed in yeast, autophagy is constantly activated (Kamada, 2010).

b) Glucose dependent autophagy regulation

Different pathways allow yeast to respond to glucose deprivation (Zaman et al., 2008). For regulation of autophagy, protein kinase A (PKA) plays a role (Budovskaya et al., 2004). PKA responds to high levels of AMP in the cell which is a consequence of glucose starvation (Mihaylova and Shaw, 2011). It positively regulates autophagy through direct phosphorylation of Atg1-kinase and Atg13 in yeast (Wang et al., 2001) and in mammalian cells (Kim et al., 2011) under starvation conditions. PKA and TORCI, thus, phosphorylate different sites in Atg13 (Budovskaya et al., 2005). However, also TORCI activity is regulated by glucose availability. In mammalian cells it has been shown that PKA phosphorylates the TSC/TSB complex and the TORCI subunit RAPTOR under starvation conditions which both results in TORCI inhibition (Gwinn et al., 2008). Furthermore, Hexokinase-II which catalyzes the first step of glycolysis, is able to bind and thereby inactivate TORCI under glucose deprivation which induces autophagy (Roberts et al., 2014). Another glucose sensor that negatively regulates autophagy is the protein kinase Sch9. Sch9 inactivation induces autophagy (Stephan et al., 2009; Yorimitsu et al., 2007).

1.2.3.5. Autophagy in disease

Correct function of the autophagic machinery and the factors involved in autophagic membrane biogenesis is crucial for cellular homeostasis. Malfunction of the autophagic system can have serve impact on human health (Choi et al., 2013). Besides the role in catabolic metabolism, autophagy plays also a role in different diseases, including neurodegenerative diseases like Parkinson's, Alzheimer's, and Huntington's disease, as well as cancer (Sarkar et al., 2009) and is involved in intracellular immune defense (Levine et al., 2011).

Reduced autophagic activity leads to an accumulation of toxic protein-aggregates in neurons, which has been shown to contribute to the development of various

neurodegenerative diseases (Wong and Cuervo, 2010). It was shown that autophagy targets aggregate-prone proteins that are linked to neurodegenerative diseases like α-synuclein, synphilin-1, mutant tau or huntingtin which led to the assumption that modulating autophagy could be a therapeutic target (Ravikumar et al., 2002; Wong and Cuervo, 2010). In fact, several FDA approved drugs could be identified as inducers of autophagy and it was shown that they exhibit a protective effect in models of Huntington's disease (Williams et al., 2008). The importance of autophagy in the development of neurodegenerative diseases is further supported by the finding that loss of autophagy leads to neurodegeneration in mice (Komatsu et al., 2006).

The situation is more complex in cancer. Reduced autophagic activity can promote malignant transformation of cells (Brech et al., 2009; Wu et al., 2011). However, once established, higher levels of autophagy protect the tumor from cytochrome c induced, caspase independent apoptosis and metabolic stress (Colell et al., 2007; Guo et al., 2013). Interestingly, mutations in the human autophagy protein BECN1 were found in 40 to 75 % of human breast, ovarian, and prostate tumors (Choi et al., 2013). Therefore, autophagy could represent a target for pharmaceutical intervention. However, whether it is beneficial to induce or inhibit autophagy strongly depends on its role in the respective cancer at a given time.

The selective autophagic pathway that leads to degradation of intracellular pathogens was termed xenophagy (Levine et al., 2011). Intracellular bacteria were shown to be targeted and degraded selectively by autophagy in different cell types (Gutierrez et al., 2004; Nakagawa et al., 2004). The finding that knockout of Atg5 which is essential for autophagy, leads to increased susceptibility for intracellular pathogens in mice further underlines the role of autophagy in degrading intracellular pathogens (Orvedahl et al., 2010; Zhao et al., 2008). However, autophagy was also shown to play a role in immune defense by contributing to MHCII antigen presentation (Lee et al., 2010).

1.2.3.6. Structural and functional insights into the Atg1-kinase complex in yeast

Some insights into the structure of the Atg1-kinase complex are available. Bioinformatic analyses show that the Ser/Thr kinase domain of Atg1-kinase displays high homology to the canonical Ser/Thr kinase fold. *In vitro* as well as X-ray crystallographic analyses of Atg1-kinase complex subunits or subunit domains were performed using the proteins from

the thermophilic yeast strain *L. thermotolerans*. A stable C-terminal domain of Atg1-kinase could be recombinantly expressed which was termed EAT-domain. Atg13 is largely unstructured, but contains a folded HORMA domain which is required for interaction with the autophagy specific PI3-kinase subunit Atg14 (Jao et al., 2013). Recent data show that Atg1-kinase interacts through microtubule interacting and transport (MIT) domains with MIT interacting motifs (MIMs) in Atg13. Two MIT domains, MIT1 and MIT2, constitute the C-terminal EAT-domain of Atg1-kinase and interact with two MIM motifs, MIM(N) and MIM(C), in the intrinsically disordered region of Atg13 (Fujioka et al., 2014). The Atg17-Atg31-Atg29 subcomplex forms an elongated dimer of trimers in solution (Kawamata et al., 2008) and structural analyses showed that it forms an elongated double crescent with Atg31-Atg29 bound to the concave side of the two Atg17 crescents (Chew et al., 2013; Ragusa et al., 2012) (**Figure 4, A**). Dimerization of Atg17 is mediated by its C-terminal tail in a way that the two concave sides of Atg17 face opposite directions. Atg31 directly interacts with Atg17 through its N-terminal helix and bridges it with Atg29 with which the C-terminal part of Atg31 forms a β-sheet sandwich (**Figure 4, B**). However, the overall architecture of the Atg1-kinase complex is still not clear. Insights into the organization of the subunits are only available from pull down assays. It was shown that Atg13 is required for co-immunoprecipitation (IP) of Atg1-kinase with Atg17, while Atg17 is not required for co-IP of Atg1-kinase and Atg13 which led to the hypothesis that Atg13 bridges Atg1-kinase and Atg17 (Kabeya et al., 2005).

To simplify the nomenclature of the Atg1-kinase complex and its subcomplexes, abbreviations shall be used in this work. **Figure 4 C** shows a schematic drawing of the pentameric Atg1-kinase complex and its subcomplexes. The trimeric subcomplex composed of dimeric Atg17, Atg29, and Atg31 will be termed $Atg17^{TC}$. The trimeric subcomplex composed of monomeric $Atg17^{1-320}$ lacking its C-terminal dimerization domain (**Figure 4, A**, highlighted in blue), Atg29, and Atg31 will be termed $Atg17^{monoTC}$. The dimer forming pentameric Atg1-kinase complex will be termed $Atg1^{PC}$. The pentameric Atg1-kinase complex containing monomeric $Atg17^{1-320}$ will be termed $Atg1^{monoPC}$.

Which role exactly the assembly of the Atg1-kinase complex and the Atg1-kinase activity play in autophagy is not fully understood. However, $Atg1^{PC}$ was shown to play a structural role in organizing the PAS and Atg1-kinase activity was shown to be required for recycling of Atg proteins from the PAS (Cheong et al., 2008). Furthermore, some Atg1-

kinase targets have been identified in yeast. Atg1-kinase phosphorylates itself at T226 upon autophagy induction which increases its activity (Kijanska et al., 2010; Yeh et al., 2010). As described above, it was shown that Atg1-kinase directly phosphorylates Atg9 which is required for the recruitment of downstream Atg-proteins (Papinski et al., 2014).

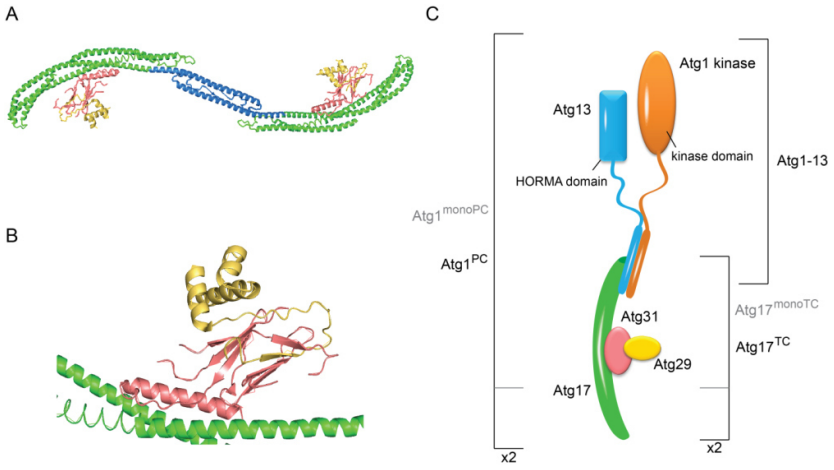

Figure 4: **Structure of the trimeric complex Atg17-Atg31-Atg29 ($Atg17^{TC}$) and subcomplex organization of the Atg1-kinase complex ($Atg1^{PC}$).** (A) Ribbon model of $Atg17^{TC}$ from *L. thermotolerans* was generated using PyMOL (SchrödingerLLC.) from PDB data set 4HPQ (Ragusa et al., 2012). Atg17 is represented in green and its C-terminal dimerization domain is highlighted in blue. Atg31 (salmon) forms an α-helical interaction interface with Atg17 and a β-sheet sandwich with Atg29 (yellow). (B) Zoomed in view of the interaction interfaces of Atg17 and Atg31 as well as of Atg31 and Atg29. (C) Schematic drawing of $Atg1^{PC}$ to introduce abbreviations. Note that Atg17 mediated dimerization is not depicted for simplicity. The dimerization domain highlighted in (A) is lacking in the monomeric $Atg17^{1-320}$-Atg31-Atg29 construct ($Atg17^{monoTC}$).

1.3. Aim of the work

A combinatorial approach using yeast genetics, biochemistry and fluorescence microscopy has identified Atg-proteins and their hierarchy at the PAS (Suzuki et al., 2007; Tsukada and Ohsumi, 1993). However, molecular functions of the Atg-proteins are still unknown. In this study, I explored a novel and highly ambitious approach to investigate the architecture and the molecular mechanism of action of $Atg1^{PC}$. Therefore, full length $Atg1^{PC}$ from yeast *S. cerevisiae* was to be recombinantly expressed and purified. Using the recombinantly expressed proteins, $Atg1^{PC}$ was to be reconstituted. From the reconstitution *in vitro*, details about complex assembly and the physical interaction of the subunits were to be established. Furthermore, applying biophysical methods, the overall architecture of the heteropentameric $Atg1^{PC}$ was to be analyzed.

The structure/function relationship of $Atg1^{PC}$ is poorly understood. Therefore, the function of structural features of $Atg1^{PC}$ identified *in vitro* was to be analyzed *in vivo*.

Furthermore, $Atg1^{PC}$ is recruited to membranes *in vivo*. However, how specificity for autophagic membranes is conveyed has remained unclear. Therefore, the interaction of the recombinantly expressed proteins with membranes and membrane bound Atg-proteins was to be investigated. For this purpose, artificial membranes were to be applied. Moreover, to investigate the specificity of $Atg1^{PC}$ for autophagic membranes, Atg9 containing proteoliposomes (PL) were to be applied for co-floatation assays. The roles of the five different subunits of $Atg1^{PC}$ in the interaction with autophagic membranes were to be investigated.

2. Material and Methods

2.1. Chemicals

If not indicated differently, chemicals were purchased from Carl Roth (Karlsruhe, D), Serva (Heidelberg, D), Sigma-Aldrich (St Louis, Missouri) or AppliChem (Darmstadt, D). All synthetic lipids as well as yeast polar lipid (YPL) extracts were purchased from Avanti Polar Lipids (Alabaster, Alabama).

2.2. Enzymes

If not indicated differently, enzymes were purchased from New England Biolabs (Ipswich, Massachusetts). For polymerase chain reactions (PCRs) *Phusion Polymerase* (New England Biolabs) was used according to the manufacturer's instructions. Proteolytic cleavage of fusion proteins was carried out using PreScission Protease and TEV protease produced by the Core Facility of the Max Planck Institute of Biochemistry (Martinsried, D).

2.3. Media

Ingredients for media were purchased from BD (Franklin Lakes, New Jersey), dissolved in water and autoclaved sterile for 25 min at 121 °C and 1.5 bar. For solid medium 1.5 % (w/v) agar was added.

Table 1: Media for bacteria and yeast used in this study.

Medium	Composition
Luria-Bertani (LB) Medium	5 g/l yeast extract, 10 g/l trypton, 10 g/l NaCl
Terrific Broth (TB) Medium	24 g/l yeast extract, 12 g/l trypton, 5 g/l glycerol, 2.3 g/l KH_2PO_4, 16.4 g/l $K_2HPO_4.3H_20$
Synthetic drop-out medium (for selection using auxotrophy marker)	0.67% yeast nitrogen base, 0.5% ammonium sulphate, 2% glucose, amino acids w/o amino acid used for auxotrophy selection

2.4. Primers

Primers were synthesized by Metabion International AG (Martinsried, D) and delivered in a 100 µM aqueous solution. **Table 2** lists the primers used in this study.

Table 2: Primers used in this study

Number	Sequence (5‘ -> 3‘)	Features
1	*CGCCATTAACCTGATGTTCT*GGGGATGGGAGACATTA AAAATAAAGATCACAC	*Homology sequence*
2	*GTGGTGATGATGATGATGCT*C**GCCCTGAAAATACAG GTTTTC**ATTTTGGTGGTTCATCTTCTGCCTC	*Homology sequence,* **TEV protease cleavage site**
3	*CGCCATTAACCTGATGTTCT*GGGGATGGTTGCCGAAG AGGACATC	*Homology sequence*
4	*GTGGTGATGATGATGATGCT*C**GCCCTGAAAATACAG GTTTTC**ACCTTCTTTAGAAAGGTTCATATCACTCAT G	*Homology sequence,* **TEV protease cleavage site**
5	*GGGCCCCTGGAACAGAACTT*CCAG	*Homology sequence*
6	*CGCCATTAACCTGATGTTCT*GGGG	*Homology sequence*
7	*TCCCGGTCCGAAACCATGAA*ACCCATGAAAATCGAA GAAGG	*Homology sequence*
8	*GCGGCCGCAAGCTTATTAGT*GGTGGTGGTGGTGGTG ATGATGATGATGCTCGC	*Homology sequence*
9	*TAAGCTTGCGGCCGCACTCG*	*Homology sequence*
10	*GGTTTCGGACCGGGATCCGC*	*Homology sequence*
11	*AGATTGCAATTCTGA*AATAATTTTGTTTAACTTTAAG **AAGGAG**ATATACATATGGGCAGCAGC*CATCACCATC ACCATCAC*ATGAATGTTACAGTTACTGTTTATGA	*Homology sequence,* **ribosomal binding site**, *His_6-tag*
12	*CTAAGGATTCTTCAC*GTTGTAA	*Homology sequence*
13	*GTGAAGAATCCTTAG*AATAATTTTGTTTAACTTTAAG **AAGGAG**ATATACATATGATTATGAATAGTACAAAC ACAGTT	*Homology sequence,* **ribosomal binding site**
14	*TCAGAATTGCAATCT*GTCC	*Homology sequence*
15	*TCGAGCTCGATATCG*AATAATTTTGTTTAACTTTAAG	*Homology*

	AAGGAGATATACATATGAACGAAGCAGATGTTAC	*sequence,* **ribosomal binding site**
16	*AATTGTTATCCGCTG*TCATACGGAATTGGAGAGC	*Homology sequence*
17	*ACAACGTGAAGAATCCTTAG*CAGCGGATAACAATTTC ACATCC	*Homology sequence*
18	*CTAAGGATTCTTCACGTTGT*AATTTAAAGTG	*Homology sequence*
19	***CTGTTCCAGGGGCCCATGAA*CGAA**GCAGATGTTAC AAAATTTG	*Homology sequence,* **Prescission protease cleavage site**
20	***GGGCCCCTGGAACAGAACTT*CCAG**ACCCGCGGAGT GATGGTGATGGTGATGGC	*Homology sequence,* **Prescission protease cleavage site**
21	CTTTAAATTACAACGTGAAGAATCCT*GAACAGAAAC TGATTAGCGAAGAAGATCTG*TAGAATAATTTTGTTTA ACTTTAAG	*myc-tag*
22	CTTAAAGTTAAACAAAATTATTCTA*CAGATCTTCTTC GCTAATCAGTTTCTGTTC*AGGATTCTTCACGTTGTAAT TTAAAG	*myc-tag*
23	GATAGCTTCAAAAATTCC*TGA*ACACAAGATATTCAA ACAAC	*Stop codon*, **nucleotide exchanged**
24	GTTGTTTGAATATCTTGTGT***T**CA*GGAATTTTTGAAGC TATC	*Stop codon*, **nucleotide exchanged**
25	*AAGTTCTGTTCCAGGGGCCC*AATACTAATATCGTTAG TATTTTGGAATCTCTG	*Homology sequence*
26	*GAACATCAGGTTAATGGCGT*TTAATTTTGGTGGTTCA TCTTCTG	*Homology sequence*
27	*GATAAATTCGATACTGCGAGGATATTATCAACGTATTTA ACACCT*ATGCGTACGCTGCAGGTCGAC	*Homology sequence*
28	*GATACAATTATTGAATCTTTGTACCGTATCCTTTTTTTCC TTTTTT*CTAATCGATGAATTCGAGCTCG	*Homology sequence*
29	*CTATTAATCTTTAAAGATATTTCCAATCTGATTGATAGCT TCAAAAATTCC*TAACGTACGCTGCAGGTCGAC	*Homology sequence*
30	*CCGGGTTAATTAAGGCGCGCCAGATCTGTTTAGCTTGC CTCGTCC*ATGAACGAAGCAGATGTTACAAAATTTG	*Homology sequence*
31	*GAGATGAGTTTTTGTTCTATGGCTTCATTCAGCTCCGGT TCC*CAACGATCAAGGCGAGTTAC	*Homology sequence*
32	*CTGGGTTTCCATGTC*GCCCGGTACCAGCTTTTG	*Homology sequence*
33	*CGGAATTATTAGGTT*ATGGAGAGAGATGAATACCAG TTACC	*Homology sequence*
34	*GACATGGAAACCCAG*GCTAG	*Homology sequence*

35	*AACCTAATAATTCCG*TGATTTTGATATTTC	*Homology sequence*
36	*CTGGGTTTCCATGTC*GCCCGGTACCAGCTTTTG	*Homology sequence*
37	*CGGAATTATTAGGTT*ATGGAGAGAGATGAATACCAG TTACC	*Homology sequence*

2.5. Vectors

Table 3 lists the vectors used in this study. Vectors were obtained from different sources or generated for this study as indicated.

Table 3: Vectors used in this study.

Name	Origin	Selection marker	Purpose/Description
pCoofy1	Max Planck Institute of Biochemistry, Core Facility	Kanamycin resistance	Vector for expression in *E. coli*, N-terminal His_6-tag with prescission protease cleavage site
pCoofy1-atg1EAT	This study	Kanamycin resistance	Vector for expression of Atg1 kinase EAT domain in *E. coli*, N-terminal His_6-tag with prescission protease cleavage site
pCoofy37	Max Planck Institute of Biochemistry, Core Facility	Kanamycin resistance	Vector for expression in *E. coli*, N-terminal MBP-tag with prescission protease cleavage site, C-terminal His_6-tag
pCoofy37-atg1	This study	Kanamycin resistance	Template for insert amplification for pFastBac-atg1, N-terminal MBP-tag with prescission protease cleavage site, C-terminal His_6-tag with TEV protease cleavage site
pCoofy37-atg13	This study	Kanamycin resistance	Vector for expression of Atg13 in *E. coli*, N-terminal MBP-tag with prescission

			protease cleavage site, C-terminal His_6-tag with TEV protease cleavage site
pFastBac	Invitrogen (Carlsbad, California)	Ampicillin resistance	Vector for expression in insect cells
pFastBac-atg1	This study	Kanamycin resistance	Vector for expression of Atg1 in insect cells, N-terminal MBP-tag with prescission protease cleavage site, C-terminal His_6-tag with TEV protease cleavage site
pST39	(Tan, 2001)	Ampicillin resistance	Vector for polycistronic co-expression in *E. coli*
pST39-his-atg17-atg29-atg31	This study	Ampicillin resistance	Vector for polycistronic co-expression of the trimeric complex Atg17-31-29 in *E. coli*, Atg17 with N-terminal His_6-tag with prescission protease cleavage site
pST39-his-atg17	This study	Ampicillin resistance	Vector for expression of Atg17 in *E. coli*, N-terminal His_6-tag with prescission protease cleavage site
pST39-his-atg17-myc-atg29-atg31	This study	Ampicillin resistance	Vector for polycistronic co-expression of the trimeric complex Atg17-31-29 in *E. coli*, Atg17 with N-terminal His_6-tag with prescission protease cleavage site and C-terminal myc-tag
pST39-his-atg17-myc	This study	Ampicillin resistance	Vector for expression of Atg17 in *E. coli*, N-terminal His_6-tag with prescission protease cleavage site, C-terminal myc tag
pFA6a-hphNT1	Max Planck Institute of Biochemistry, AG Wedlich-Söldner, (Janke et al., 2004)	Hygromycin resistance	Vector for gene deletion in *S. cerevisiae*
pYM21	Max Planck Institute of	Nourseothricin	Vector for

	Biochemistry, AG Wedlich-Söldner, (Janke et al., 2004)	resistance	chromosomal tagging in *S. cerevisiae*
pTL58-atg9	Max Planck Institute of Biochemistry, Dr. Yijian Rao	Ampicillin resistance, LEU2	CEN LEU2 pAbp140 Vector for ectopic expression of Atg9 in *S. cerevisiae*
pTL58-atg9ΔN	Max Planck Institute of Biochemistry, Dr. Yijian Rao	Ampicillin resistance, LEU2	CEN LEU2 pAbp140 Vector for ectopic expression of Atg9ΔN in *S. cerevisiae*
pTL58-atg9ΔcD	Max Planck Institute for Biochemistry, Dr. Yijian Rao	Ampicillin resistance, LEU2	CEN LEU2 pAbp140 Vector for ectopic expression of Atg9ΔcD in *S. cerevisiae*
pTL58-atg9ΔNΔcD	Max Planck Institute of Biochemistry, Dr. Yijian Rao	Ampicillin resistance, LEU2	CEN LEU2 pAbp140 Vector for ectopic expression of Atg9ΔNΔcD in *S. cerevisiae*
pTL58-atg9-promoter-atg9	This study	Ampicillin resistance, LEU2	CEN LEU2 pAbp140 Vector for ectopic expression of Atg9 under the control of its native promoter in *S. cerevisiae*

2.6. Bacterial Strains

Table 4 lists the bacterial strains used in this study. For SLIC (Seamless Ligation Independent Cloning) *E. coli* OmniMax and for all other cloning procedures *E. coli* XL-1 Blue cells were used. *E. coli* Rosetta (DE3) was used as expression strain.

Table 4: Bacterial strains used in this study.

Bacterial strain	Genotype	Origin
E. coli OmniMax	F- [*pro*AB+*lac*Iq *lac*ZΔM15 Tn10(TetR)Δ(*ccd*AB)] *mcr*A Δ(*mrr-hsd*RMS-*mcr*BC) φ80(*lac*Z)ΔM15 Δ(*lac*ZYA-*arg*F) U169 *end*A1 *rec*A1 *sup*E44 *thi*-1 *gyr*A96 *rel*A1 *ton*A *pan*D	Max Planck Institute of Biochemistry, Core Facility
E. coli XL-1 Blue	recA1 endA1 gyrA96 thi-1 hsdR17 supE44 relA1 lac [F′ proAB lacIqZΔM15 Tn10 (Tetr)]	Max Planck Institute of Biochemistry, Core Facility
E. coli	F– ompT hsdSB(rB– mB–) gal dcm	Max Planck Institute of

Rosetta (DE3)	lacY1(DE3) pRARE6 (CmR)	Biochemistry, Core Facility

2.7. Yeast Strains

Table 5 lists the yeast strains used in this study.

Table 5: Yeast strains used in this study.

Yeast strain	Genotype	Origin
S. cerevisiae BY4741	MATa his3Δ leu2Δ met15Δ ura3Δ	Max Planck Institute of Biochemistry, AG Wedlich-Söldner
S. cerevisiae BY4741 *atg9Δ*	MATa his3Δ leu2Δ met15Δ ura3Δ atg9ΔKanR	Max Planck Institute of Biochemistry, AG Wedlich-Söldner
S. cerevisiae BY4741 *gfp-atg8*	MATa his3Δ leu2Δ met15Δ ura3Δ gfp-atg8-natNT2	Max Planck Institute of Biochemistry, Viola Beier
S. cerevisiae BY4741 *atg17Δ*	MATa his3Δ leu2Δ met15Δ ura3Δ atg17Δ::hphNT1	This study
S. cerevisiae BY4741 *atg17*$^{1-320}$	MATa his3Δ leu2Δ met15Δ ura3Δ atg17-Δ963-1251::hphNT1	This study
S. cerevisiae BY4741 *gfp-atg8 atg17Δ*	MATa his3Δ leu2Δ met15Δ ura3Δ gfp-atg8-natNT2 tg17Δ::hphNT1	This study
S. cerevisiae BY4741 *gfp-atg8 atg17*$^{1-320}$	MATa his3Δ leu2Δ met15Δ ura3Δ gfp-atg8-natNT2 atg17-Δ963-1251::hphNT1	This study
S. cerevisiae BY4741 *atg9Δ atg17-3xmyc*	MATa his3Δ leu2Δ met15Δ ura3Δ atg9ΔKanR atg17::atg17-3myc-natNT2	This study
S. cerevisiae BY4741 *atg9Δ pho8Δ60*	MATa his3Δ leu2Δ met15Δ ura3Δ atg9ΔKanR pho8::natNT2-pho8Δ60	This study

2.8. Molecular biological methods

2.8.1. Cloning of the expression vectors using homologous recombination *in vitro*

To avoid incompatibility of restriction enzymes with insertion of DNA fragments at the desired location in the target vector, homologous recombination *in vitro* was applied for cloning. This technique allows cloning into any position of the target vector by linearizing the vector either by PCR or restriction enzyme digestion, and generating an insert with homologous sequences to the linearized vector at the 5' and 3' end of 15 nucleotides

(InFusion HD kit (Clontech, Saint-Germain-en-Laye, F)) or 20 nucleotides (SLIC (Scholz et al., 2013)).

For recombinant expression of Atg1-kinase and Atg13 the genes were amplified from *S. cerevisiae* genomic DNA using primers 1 and 2, and 3 and 4, respectively. They were cloned into linearized pCoofy37 vector (primers 5 and 6) inserting a TEV protease cleavage site in front of the C-terminal His_6-tag applying SLIC. For expression of Atg1-kinase in insect cells, pCoofy37-atg1 was used as a template for insert amplification and the mbp-atg1-his_6 construct was amplified using primers 7 and 8, and cloned into linearized pFastBac vector (primers 9 and 10) applying SLIC.

For co-expression of Atg17, Atg29 and Atg31 the genes were amplified from *S. cerevisiae* genomic DNA using primers 11 (including a His_6-tag sequence) and 12, 13 and 14, and 15 and 16 (all forward primers including a ribosomal binding site (RBS)), respectively. The inserts were cloned in a single step in the above listed order into pST39 vector (linearized by KpnI digest) by homologous recombination *in vitro* using the InFusion HD kit (Clontech) according to the manufacturer's manual.

To express Atg17, pST39-his-atg17-atg29-atg31 vector was linearized using primers 17 and 18. The linearized vector was recirculated applying SLIC.

SLIC was also applied to introduce a Prescission protease cleavage site between the N-terminal His_6-tag and Atg17 with linearization primers 19 and 20.

PCR based mutagenesis using the Quikchange lightning site directed mutagenesis kit from Agilent (Böblingen, D) was applied to insert a C-terminal myc-tag sequence to Atg17 as well as to generate the $Atg17^{1-320}$ and $Atg17^{1-354}$ variants. Mutagenesis primers were primers 21 and 22, and 23 and 24, respectively.

For expression of the EAT domain of *S. cerevisiae* Atg1-kinase, homologous to the EAT-domain of *L. thermotolerans*, the gene region encoding Atg1-kinase residues 589 – 897 was amplified from *S. cerevisiae* genomic DNA using primers 25 and 26, and cloned into linearized pCoofy1 vector (primers 5 and 6).

2.8.2. Chromosomal modification of *S. cerevisiae*

To generate the strains required for the Atg8-PE, GFP-Atg8, Pho8Δ60 and the IP assays, chromosomal modifications had to be introduced.

To modify *S. cerevisiae* chromosomally, a previously described method was applied (Janke et al., 2004). In brief, the respective vector for replacing the chromosomal region with a resistance marker was used as a template for a PCR introducing an approximately 45 bp long homology sequence on the 5' and 3' end of the PCR product. Vectors containing a tag sequence in front of the resistance cassette were used to introduce a tag sequence 3' of the respective ORF.

Table 6 lists the primers and vectors used to generate the PCR products used for chromosomal modification. The PCR products were transformed into competent *S. cerevisiae* BY4741 cells. Yeast cells were made competent by growing a 50 ml culture to OD_{600} of 0.6, harvesting the cells, washing them in 20 ml water and subsequently in 20 ml SORB (10 mM Tris-HCl pH 8.0, 100 mM LiOAC 1 mM EDTA, 1M Sorbitol). Finally, cells were resuspended in 360 µl SORB and frozen in liquid nitrogen. For transformation, 50 µl of competent yeast cells were mixed with 5 µl carrier DNA (Salmon sperm DNA (Invitrogen, Carlsbad, California), incubated for 5 min at 95°C), 12 µl gel extracted PCR product and 300 µl PEG mix (10 mM Tris-HCl pH 8.0, 100 mM LiOAC 1 mM EDTA, 40% PEG 3350). The transformation mix was incubated 1 h at 30 °C. After addition of 35 µl DMSO the cells were heat shocked for 15 min at 42 °C. Finally, cells were spinned down, resuspended in 300 µl YPD medium and incubated over night at 30 °C before they were plated on the respective selection medium.

Table 6: Primers and templates used for chromosomal modification of yeast.

Primers	Template	Strain generated
27 and 28	pFA6a–hphNT1	atg17Δ::hphNT1
29 and 28	pFA6a–hphNT1	atg17-Δ963-1251::hphNT1
27 and 28	pFA6a–hphNT1	gfp-atg8-natNT2 atg17Δ::hphNT1
29 and 28	pFA6a–hphNT1	gfp-atg8-natNT2 atg17-Δ963-1251::hphNT1
30 and 31	pYM21	atg9ΔKanR atg17::atg17-3myc-natNT2
32 and 33	pFA6a-NatNT2-pho8Δ60	atg9ΔKanR pho8::natNT2-pho8Δ60

2.8.3. One-step transformation of plasmids into *S. cerevisiae*

For the Pho8Δ60 assay and the IP assay with Atg9 variants, the plasmids were transformed into the respective *atg9Δ* strains.

Plasmids for ectopic expression of genes were transformed into yeast cells applying a one step protocol. A small amount of cells was picked from a plate and resuspended by vortexing in 95 µl one step buffer (0.24 M LiAc, 47% (v/v) PEG 3550, 0.1 M DTT) with 5 µl carrier DNA (Salmon sperm DNA, incubated 5 min at 95°C) and 3 µl plasmid DNA. The resuspended cells were incubated 30 min at 45 °C and plated on the respective drop-out medium.

2.9. Protein production

2.9.1. Recombinant expression and purification of Atg1-kinase

Atg1-kinase was expressed in insect high five cells (BTI-TN-5B1-4) as an N-terminal MBP fusion protein with a C-terminal His_6-tag applying the titerless infected-cells preservation and scale-up (TIPS) method as described previously (Wasilko et al., 2009) by the Core Facility of the Max Planck Institute of Biochemistry. Insect cells possess a more elaborate protein folding machinery compared to *E. coli* and are able to introduce post-translational modifications (Jarvis, 2009). Therefore, larger or multidomain proteins, that are not properly folded in *E. coli* or require post-translational modifications for folding and/or activity, might be expressed in insect cells.

One g of insect cell pellet was resuspended with 4 ml of lysis buffer (100 mM Tris (pH 7.4), 300 mM NaCl, 5 % (v/v) Glycerol, 20 mM Imidazole, 5 mM β-Mercaptoethanol, 1 % (v/v) Triton-X) supplemented with protease inhibitor cocktail (Sigma-Aldrich) and benzonase. Insect cells were disrupted by high pressure-homogenization. The Atg1-kinase fusion protein was affinity purified using NiNTA His-trap HP columns (GE Healthcare, Uppsala, S) (buffer A: 25 mM Tris (pH 7.4), 300 mM NaCl, 5 % (v/v) Glycerol, 20 mM Imidazole, 5 mM β-Mercaptoethanol, 0.1 % (v/v) Triton-X; buffer B: as buffer A with

500 mM Imidazole), and the MBP and His_6 tags were cleaved by Prescission and TEV protease treatment for 30 min at room temperature before applying the protein to size exclusion chromatography (SEC) (HiLoad Superdex 200 16/600 pg column (GE Healthcare), SEC buffer: as buffer A w/o Triton-X). To remove residual impurities, Atg1-kinase was subjected to re-chromatography. Therefore, the SEC fractions containing Atg1-kinase were applied to a NiNTA His-trap HP column and Atg1-kinase could be collected in the flow through fraction, while impurities were retained on the column.

2.9.2. Recombinant expression and purification of Atg13

Atg13 was expressed as an N-terminal MBP fusion protein with a C-terminal His_6-tag in *E. coli*. Cells were therefore grown in TB medium to an OD_{600} of 0.2 at 37 °C, cooled down to 25 °C and induced at an OD_{600} of 0.5 with 0.3 mM IPTG and expression was performed over 2.5 h at 25 °C.

Cells were resuspended in lysis buffer (100 mM Tris (pH 7.4), 300 mM NaCl, 5 % (v/v) Glycerol, 20 mM Imidazole, 5 mM β-Mercaptoethanol) and lysed by sonication. The Atg13 fusion protein was affinity purified using NiNTA His-trap HP columns (buffer A: 25 mM Tris (pH 7.4), 300 mM NaCl, 5 % (v/v) Glycerol, 20 mM Imidazole, 5 mM β-Mercaptoethanol; buffer B: as buffer A with 500 mM Imidazole), and the MBP- and His_6-tags were cleaved by Prescission and TEV protease treatment for 30 min at room temperature. The protein solution was diluted with dilution buffer (25 mM Tris (pH 7.4), 5 % (v/v) Glycerol) to a NaCl concentration of 125 mM before applying the protein to anion exchange chromatography (AIEX) (MonoQ column (GE Healthcare, Uppsala, S), buffer A: 25 mM Tris (pH 7.4), 125 mM NaCl, 5 % (v/v) Glycerol, 2 mM Dithiothreitol (DTT); buffer B: as buffer A with 1 M NaCl). To separate free Atg13 from the chaperone bound fraction of Atg13, a flat gradient between 0 % and 16 % buffer B was applied over 50 ml.

2.9.3. Recombinant expression and purification of Atg17, Atg17^{TC} and related variants

The respective subunits including Atg17 or Atg17$^{1-320}$ were expressed in *E. coli* with Atg17 carrying a cleavable N-terminal His_6-tag. For the related trimeric complexes Atg17^{TC} and Atg17^{monoTC}, Atg17 or Atg17$^{1-320}$ were co-expressed with Atg29 and Atg31. For expression, cells were grown to an OD_{600} of 0.3 at 37 °C and cooled down to 18 °C. Expression was induced at an OD_{600} of 0.6 with 0.3 mM IPTG and expression was performed over night at 18 °C.

Cells were resuspended in lysis buffer (lysis buffer: 100 mM Tris (pH 7.4), 300 mM NaCl, 20 mM Imidazole), lysed by sonication, and the target protein or complex was (co-)purified by affinity chromatography using a His-trap HP column (buffer A: 25 mM Tris (pH 7.4), 300 mM NaCl, 20 mM Imidazole; buffer B: as buffer A with 500 mM Imidazole). The His_6-tag was cleaved by Prescission protease treatment for 30 min at room temperature before applying the protein or related complexes to SEC on a HiLoad 16/600 Superdex 200 pg column (SEC buffer: 25 mM Tris (pH 7.4), 300 mM NaCl).

2.9.4. Recombinant expression and purification of Atg9

The conserved region of Atg9 from amino acid position 281 to 779 (Atg9^{core}) as well as the truncated constructs of Atg9^{core} (Atg9$^{\Delta N}$ (residues 316-779), Atg9$^{\Delta cD}$ (residues 316-423 and 508-779) were recombinantly expressed in *E. coli* Rosetta and purified by Dr. Yijian Rao. The membrane fraction was resuspended in buffer containing 25 mM Tris (pH 8.0), 150 mM NaCl, and 1% (w/v) LDAO and incubated for 1 h at 4 °C to solubilize the membrane proteins. Solubilized protein was purified by NiNTA-affinity chromatography (buffer A: 25 mM Tris (pH 8.0), 150 mM NaCl, 0.1% (w/v) LDAO, buffer B: as buffer A with 500 mM imidazole). Atg9-containing fractions were pooled, concentrated and subjected to SEC using a Superdex200 10/300GL column (GE Healthcare) for further purification.

2.9.5. Recombinant expression and purification of the EAT-domain of Atg1-kinase

The recombinant expression and purification of the EAT-domain of *L. thermotolerans* Atg1-kinase was described previously (Ragusa et al., 2012). The homologous region of *S. cerevisiae* Atg1-kinase comprising amino acids 589 - 897 was expressed in *E. coli* with a cleavable N-terminal His_6-tag. After cell lysis by sonication, the protein was purified according to the purification protocol for Atg1-kinase described in 2.9.1. (p. 42). Similar buffers were used without Triton-X.

2.10. Mass spectrometry

2.10.1. Electron spray ionization mass spectrometry

To confirm the correct mass of a recombinantly expressed protein or to analyze its posttranslational modifications, protein full masses were analyzed by C4 reversed phase liquid chromatography (LC) coupled electron spray ionization (ESI) mass spectrometry (MS). The analyses were performed at the core facility of the Max Planck Institute of Biochemistry using a MicroTOF ESI-MS (Bruker Daltonics GmbH, Bremen, D). The flow rate was set to 250 µl/min applying a linear gradient over 15 min from 20 % to 80 % solvent B (solvent A: 0.05 % TFA in H_2O, solvent B: 0.05 % TFA in acetonitrile). Protein concentration was adjusted to approximately 0.3 mg/ml.

2.10.2. Tandem mass spectrometry

To analyze the site specific change in post translational modifications, tandem mass spectrometry (MS/MS) was applied. Proteins for MS/MS were used at 1 µM concentrations. Proteolytic digestion was performed over night with LysC under denaturing conditions (8 M Urea) at RT and subsequently with Trypsin for 2 h under native conditions (1:10 dilution in buffer w/o Urea) at 37 °C. For injection to the LTQ Orbitrap (Thermo Fisher, Waltham, Massachusetts) tandem mass spectrometer, the resulting peptides were separated by C18-reversed phase nanoscale liquid chromatography

applying a gradient over 2 h. The analyses were performed in the core facility of the Max Planck Institute of Biochemistry. Data were analyzed using the MaxQuant software package using the label free quantification (LFQ) algorithm (Cox and Mann, 2008).

2.11. Biophysical methods

2.11.1. Surface plasmon resonance

The assembly of the Atg1-kinase complex was monitored by surface plasmon resonance (SPR) measurements using a Biacore^{TM} 2000 (GE Healthcare) instrument. His-tagged Atg17 or his-tagged Atg17^{TC} (1 µM) in buffer containing 25 mM Tris (pH 7.4), 150 mM NaCl and 1 mM DTT was passed at a flow rate of 5 µl/min for a contact time of 600 s over the NiNTA-chip surface for immobilization. Atg13 and Atg1-kinase or buffer and Atg1-kinase (at 1 µM concentrations) were consecutively injected using a flow rate of 10 µl/min for 300 (Atg17) or 600 s (Atg17^{TC}) contact time at indicated time points. Binding of proteins was detected as change in recorded resonance units (RU) and data were evaluated using the BiaEvaluation (Biacore) software. A Ni^{2+}-loaded cell without His-tagged protein was used to correct for background binding. Therefore, the signal from the reference cell was subtracted from the signal from the measuring cell.

2.11.2. Dynamic light scattering

To determine the hydrodynamic radius of a protein or membrane vesicle as well as the polydispersity of the sample, DLS was applied. Prior to DLS measurement, protein solutions were centrifuged 10 min at 17,000 g to remove large particles. Membrane vesicles were extruded through a membrane with the respective pore size. DLS was carried out on a DynaPro Nanostar (Wyatt, Santa Barbara, California) at a wavelength of 658 nm and in a sample volume of 20 – 30 µl. Acquisition time was 5 – 15 s depending on the signal strength and for each sample 15 single measurements were averaged. The DLS data were analyzed using the Dynamics software package (Wyatt).

2.11.3. Multi-angle light scattering

To determine the molar mass of a protein or a protein complex in solution, size exclusion chromatography-multi-angle light scattering (SEC-MALS) was applied. SEC-MALS measurements were performed on a HP1100 HPLC system (Agilent) using a Superdex-200 Increase 10/300GL (GE-Healthcare, Atg1-kinase) or a Superose-6 10/300GL (GE-Healthcare, $Atg1^{PC}$) column. The MALS signal was recorded on-line using a miniDAWN Treos MALS detector (Wyatt) and the corresponding protein concentration was determined with an Optilab t-Rex RI detector (Wyatt). Atg1-kinase was injected at a concentration of 5 mg/ml and $Atg1^{PC}$ at a concentration of 3.4 mg/ml in a volume of 50 µl and 100 µl, respectively. SEC-MALS data were analyzed using the Astra software package (Wyatt) applying the Zimm light scattering model (Zimm, 1948). The molar mass at the concentration peak apex (MW max, refractive index peak apex) and the weight-average molar mass of the respective peak (MW peak, UV peak borders selected manually) were determined.

2.11.4. Analytical ultracentrifugation

To determine the molar mass of a protein in solution, sedimentation velocity experiments were performed on an Optima XL-I analytical ultracentrifuge (Beckman Inc., Palo Alto, CA) using an An 60 Ti rotor and double-sector epon centrepieces (50.000 rpm, 20 °C). Buffer (25 mM Tris (pH 7.4), 300 mM NaCl) density and viscosity was measured using a DMA 5000 densitometer and an AMVn viscosimeter, respectively (both Anton Paar, Graz, A). Protein concentration distribution was monitored at 280 nm. Time-derivative analysis was computed using the SEDFIT software package, version 12.1b (Schuck, 2000), resulting in a c(s) distribution and an estimate for the molecular weight. Experiments and data fitting were performed by Dr. Stephan Uebel.

2.11.5. Generation of large unilamellar vesicles

Large unilamellar vesicles (LUVs) were used for membrane interaction studies in liposome sedimentation assays. To generate the lipid film, the respective synthetic lipids dissolved in chloroform listed in **Table 7** (1 mg total lipid content) were dried using a nitrogen stream in a test tube (8 x 70 mm, Duran, Wertheim, D) and incubated in a vacuum oven with a pressure below 5 mbar at RT over night. The dried lipid film was rehydrated in the respective buffer to a final lipid concentration of 1 mg/ml for 30 min. The suspension was vortexed during the rehydration step five times for 60 s. To generate LUVs of defined sizes, the rehydrated suspension was passed through a filter (Millipore, Billerica, Massachusetts) of corresponding pore size.

2.11.6. Generation of giant unilamellar vesicles

Giant unilamellar vesicles (GUVs) have a size of ~1 – 100 µm in diameter and are therefore suitable for microscopy applications. GUVs were generated by electroformation (Angelova and Dimitrov, 1986). In brief, the lipid mixture listed in **Table 7** (5 µg total lipid) was dried on indium-tin oxide covered glass slides overnight under vacuum. Electroformation was performed in a self-made Teflon chamber filled with 600 mM Sucrose solution by applying an electric AC field (1 V, 10 Hz) for 4 hr at 30°C. GUVs were used immediately after harvesting.

Table 7: Lipid mixes used in this study.

Lipid mix	Composition (%mol)	Application
Yeast polar extract (YPE)	according to manufacturer (Avanti Polar Lipids): 30.7 % PC, 12 % PE, 26.2 % PI, 7.9 % PS, 2 % PA, 0.7 % PG	LUVs, pull downs
Acidic synthetic lipid-mix (ASL)	40 % PC, 30 % PE, 20 % Ch, 10 % PS	LUVs, pull downs
GUV mix	39,9 % PC, 30 % PE, 20 % Ch, 10 % PS, 0.1 % Liss-Rhod-DPPE	GUVs, Fluorescence microscopy

2.11.7. *In vitro* reconstitution of the Atg8 conjugation reaction on GUVs

The Atg8 conjugation reaction was reconstituted as described previously (Kaufmann et al., 2014). In brief, Atg8 (1 µM) was incubated with Atg3 and Atg7 (0.5 µM both) at 30 °C for 30 min in the presence of 0.5 mM ATP-Mg^{2+} and 0.2 mM DTT. Subsequently the reaction was mixed with pre-incubated Atg12–5-16 (0.25 µM) and GUVs. The lipidation reaction was further incubated 30 min at 30 °C and stopped by adding 5 mM DTT.

2.11.8. Reconstitution of Atg9 in proteoliposomes

For floatation assays, $Atg9^{core}$ and its variants were reconstituted in liposomes using the rapid dilution approach by Dr. Yijian Rao. Mulitlamellar vesicles (MLVs) were prepared from mixtures of synthetic lipids containing 20 mol% cholesterol, 10 mol% palmitoyl-oleoyl phosphatidylethanolamine (POPE), 60 mol% palmitoyl-oleoyl phosphatidylcholine (POPC), 10 mol% palmitoyl-oleoyl phosphatidylserine (POPS) or from yeast polar lipid mix (YPL) as described in 2.11.5. Detergent-solubilized $Atg9^{core}$ or its variants were added to the MLV suspension in a protein:lipid ratio of 1:200 and the mixture was 30-fold diluted with hydration buffer (25 mM HEPES (pH 7.0), 100 mM NaCl) and incubated for 30 min at room temperature. Atg9 containing proteoliposomes (Atg9-PL) were harvested by centrifugation (30 min, 650,000 g, 4°C), resuspended in dilution buffer and extruded using a filter with pore size of 200 nm.

2.11.9. Liposome sedimentation and Atg9 floatation assays

To investigate the membrane binding capacity and the interaction of Atg1-kinase complex subunits with Atg9, liposome sedimentation assays and Atg9 floatation assays were performed by Dr. Yijian Rao. YPL was dissolved in chloroform and supplemented with 5 mol% PI(3)P as indicated. MLVs and LUVs were generated as described above (2.11.5). Small unilamellar vesicles (SUVs) were prepared by sonicating the MLV-suspension on ice until the solution became clear and extruded through 30 nm pore-size filters. Liposome sedimentation assays were performed by incubating 100 µl MLVs, LUVs or SUVs with the protein of interest (2 µM final concentration) for 30 min at room temperature. The

liposomes were harvested by centrifugation (30 min, 140,000 g, 4°C) for subsequent analysis using SDS-PAGE.

The interaction of Atg1-kinase complex with liposomes or the interaction of Atg1-kinase complex and its subunits with Atg9-PL was assessed by floatation experiments. Therefore, 250 µl of Atg9-PL were mixed with an equivalent volume of 80% Nycodenz in hydration buffer. A step gradient was generated by overlaying this mixture with 250 µl 30 % Nycodenz and 100 µl hydration buffer. Floating Atg9-PLs accumulated at the Nycodenz-buffer interface and were collected and subsequently analyzed by SDS-PAGE and immunoblotting.

2.12. Fluorescence microscopy

2.12.1. Chemical labeling of proteins with low-molecular fluorescence dyes

To investigate the localization of Atg1-kinase to Atg8 positive membranes *in vitro*, proteins had to be labeled with fluorescent dyes. Proteins were labeled after exchanging the sample buffer of the protein with labeling buffer (25 mM Tris (pH 7.2), 500 mM NaCl) using a desalting column. Equimolar amounts of protein and maleimide dye (Atto-Tec, Siegen, D) were used and the reaction mixtures were incubated for 30 min at RT. Excess dye in the labeling reactions was removed by a desalting step with microscopy buffer (25 mM Tris (pH 7.2), 275 mM NaCl).

2.12.2. Image acquisition in fluorescence microscopy

Fluorescence microscopy was used to investigate Atg1-kinase recruitment to Atg8-positive membranes *in vitro* as well as for visualization and time resolved kinetic analysis of GFP-Atg8 puncta *in vivo*. Images were acquired using a laser scanning microscope LSM 780 (Zeiss, Jena, D). Laser lines as well as excitation and emission filter were selected using the Smart Setup function of the ZEN software (Zeiss, Jena, D) according to the dyes/fluorescent protein used for the respective experiment. Time course experiments with

live yeast cells were performed by acquisition of z-stacks with a 0,6 µm optical slice every 20 s (wt) or every 40 s (Atg17 mutants) over 20 min (wt) or 30 min (Atg17 mutants). Time course analysis was performed with ImageJ (Schneider et al., 2012) by integrating and plotting the GFP-Atg8 puntca intensity in the area of the punctum movement and subtracting the average fluorescence intensity from a control area within the same cell.

2.13. *In vivo* assays in *S. cerevisiae*

2.13.1. Yeast strains and growth conditions

Derivatives of yeast strain *S. cerevisiae* BY4741 (Euroscarf) were used for GFP-Atg8 imaging as well as for GFP-Atg8, Atg8-PE, Pho8Δ60 and IP assays. Strains generated for this study are listed in **Table 6**. Atg9 variants were expressed from pTL58 vectors listed in **Table 3**. For ectopic expression of $Atg9^{WT}$ from the pTL58 vector, the PmaI promoter was exchanged for the endogenous *atg9* promoter to obtain equal expression levels using the InFusion HD kit from Clontech (Saint-Germain-en-Laye, F) with primers 34 and 35 for vector linearization and primers 36 and 37 for insert amplification. The plasmids were transformed into *PHO8Δ60 Δatg9* and *ATG17-myc$_3$ Δatg9* strains.

For all assays, cells were grown in the respective synthetic drop-out media at 30 °C to mid-log phase. For GFP-Atg8 assays and imaging as well as for Atg8-PE assays, autophagy was induced by adding rapamycin to a final concentration of 1 µg/ml. For Pho8Δ60 and IP assays, cells were transferred to synthetic medium without amino acids for starvation for 4 h and 2 h, respectively.

2.13.2. Pho8Δ60 assay

The Pho8Δ60 assay is specific for non-selective autophagy. Mutant alkaline phosphatase (ALP) lacking its targeting sequence is expressed and resides in the cytoplasm under vegetative conditions. ALP is transported to the vacuole upon autophagy induction where it is activated. After cell lysis, active ALP can convert 1-Naphthyl phosphate to 1-Naphtol which can be detected by its specific fluorescence. The amount of 1-correlates with the amount of cytoplasmic ALP that was transported to the vacuole by autophagy.

The pho8Δ60 assay was performed as described previously (Kanki et al., 2009). Briefly, yeast cells corresponding to 4 OD_{600} were harvested by centrifugation (5 min, 500 g) and resuspended in ice cold assay buffer (250 mM Tris (pH 9.0), 10 mM $MgSO_4$, 10 µM $ZnSO_4$). Cells were lysed by vortexing with acid washed glass beads and cleared by centrifugation (20 min, 17,000 g). 5 mM 1-Naphthyl phosphate was added and the enzymatic reaction was stopped after 20 min incubation at 30 °C by adding one volume of stopping buffer (2 M Glycin-NaOH (pH 11.0)). 1-Naphthyl phosphate turnover was determined by measuring the fluorescence using an infinite M1000Pro plate reader (Tecan, Männedorf, CH) with an excitation wavelength of 345 nm and emission wavelength of 472 nm. The fluorescence signal was corrected for the total protein content in the respective sample as determined using the Pierce BCA protein assay kit (Thermo Scientific, Waltham, MA).

2.13.3. Immunoprecipitation assay

To determine whether mutations of Atg9 affected its interaction with Atg17 *in vivo*, co-IP assays were performed. Atg17 was myc-tagged and used for IP while Atg9 was HA-tagged for detection of co-IP by western blotting (WB).

Yeast cells corresponding to 50 OD_{600} were harvested by centrifugation (5 min, 500 g), resuspended in ice-cold lysis buffer (25 mM Tris-HCl pH 7.4, 150 mM NaCl, 200 mM sorbitol, 0.1 % Tween-20 (v/v), supplemented with protease inhibitor cocktail (Sigma-Aldrich) and 1 mM PMSF) and lysed by vortexing with acid washed glass beads for 3 min at 4 °C. Lysates were cleared by centrifugation (20 min, 17,000 g). IP was performed by incubating the cell-lysates with an α-myc antibody (raised in rabbits against a myc-peptide) for 60 min at 4 °C. Magnetic protein A beads (New England Bioloabs) were added and the lysates were incubated for 2 h at 4°C. Beads were washed twice with lysis buffer and resuspended in SDS-sample buffer. Samples were separated on NuPage Bis-Tris gels (Life Technologies) prior to WB.

2.13.4. Trichloroacetic acid precipitation

Trichloroacetic acid (TCA) precipitation from whole cells was performed to analyze the expression levels of tagged proteins by western blotting.

TCA precipitation from yeast cells corresponding to 1 OD_{600} was performed to obtain the samples used to determine expression levels. The cells were harvested (5 min, 2000 g), resuspended in lysis buffer (0.5 M NaOH, 5 % DTT (w/v)) and incubated 15 min on ice. TCA was added to a final concentration of 30 % (w/v) and the sample was incubated for 15 min on ice. Precipitated protein was pelleted (10 min, 17000 g) and resuspended in 1 ml ice cold acetone. After another centrifugation step (10 min, 17000 g), the acetone was removed and the sample was resuspended in SDS-sample buffer. Protein corresponding to 0.25 OD_{600} of cells was loaded onto the SDS-PAGE gel for western blotting.

3. Results

3.1. Purification and characterization of the Atg1^{PC} subunits

Atg1^{PC} is one of the first complexes to assemble at the PAS (Suzuki et al., 2007) where it plays a major role in initiating autophagy (Cheong et al., 2008). Atg1^{PC} is a structural scaffold to recruit other Atg-proteins to the PAS (Sekito et al., 2009). Kinase activity of Atg1-kinase has been shown to be required to recycle other Atg-proteins, including Atg9, from the PAS (Cheong et al., 2008). Atg1^{PC} is a heteropentameric complex consisting of the Atg1-kinase and its regulatory subunits Atg13, Atg17, Atg29, and Atg31 (Kabeya et al., 2005). A main regulator of Atg1^{PC} is the TORCI which constitutively phosphorylates Atg13 under nutrient rich conditions and thereby prevents Atg1^{PC} assembly and activation (Kamada et al., 2010). Other factors like PKA also target Atg1^{PC} (Wang et al., 2001). This makes Atg1^{PC} a central regulator of autophagy. Due to the complexity of autophagy regulation and the highly interconnected protein complexes acting in the autophagic network (Feng et al., 2014) the molecular mechanism of action of Atg1^{PC} remained elusive. *In vitro* reconstitution systems have been applied successfully to address specific molecular questions (Romanov et al., 2012; Wollert and Hurley, 2010). Recombinantly expressed and purified proteins are required for these systems. The recombinant expression and purification of full length Atg1^{PC} has remained, however, a major technical challenge (Ragusa et al., 2012; Stanley et al., 2013).

3.1.1. Purification and characterization of Atg1-kinase

Atg1-kinase was first expressed in *E. coli* as an N-terminal MBP fusion protein with a C-terminal His_6-tag. Soluble Atg1-kinase could be purified from these expressions, but SEC and analytical ultracentrifugation analyses revealed that the protein was aggregated. Atg1-kinase is a multi-domain protein with a molecular mass of 103 kDa. Given the fact that the protein folding machinery of *E. coli* is limited in its ability to fold multidomain proteins, Atg1-kinase was expressed in insect cells to exploit the more elaborate eukaryotic protein folding machinery (Jarvis, 2009). To increase its stability and solubility, Atg1-kinase was

expressed as an N-terminal MBP fusion protein with a C-terminal His_6-tag. After NiNTA-affinity purification (**Figure 5, A**) the tags were removed by proteolytic digestion and Atg1-kinase was further purified by SEC using a Superdex200 column (**Figure 5, B and C**). Atg1-kinase elutes in a peak clearly separated from the void volume, indicating that the protein is properly folded and not aggregated. However, impurities were still present after SEC. To remove these impurities a re-chromatography step was performed (**Figure 5**, **D**).

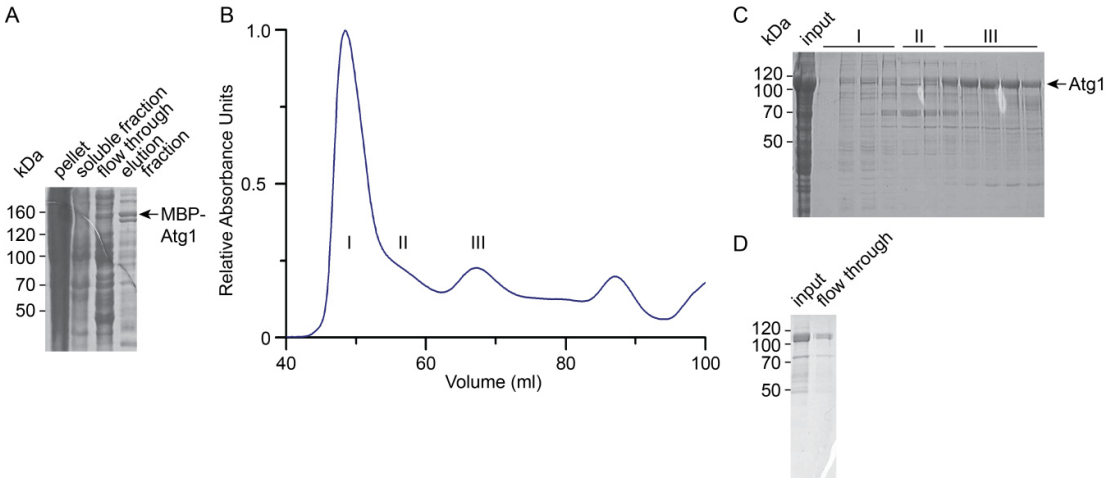

Figure 5: Atg1-kinase purification. (A) SDS-PAGE analysis of NiNTA-affinity purification of Atg1-kinase. Atg1-kinase was expressed as MBP fusion protein. (B and C) SEC profile and corresponding SDS-PAGE analysis of Atg1-kinase purification. I: Aggregated protein, II: impurities, III: Atg1-kinase used for further purification. (D) Pooled fractions from SEC (input) were subjected to NiNTA-affinity re-chromatography. The amount of impurities in the flow through fraction is significantly reduced.

Atg1-kinase displayed two bands on SDS-polyacrylamid gelelectrophoresis (PAGE) gels. Upon phosphatase treatment only the faster migrating band was observed (**Figure 6, A**), suggesting that the second band corresponds to the phosphorylated form of Atg1-kinase. The phosphorylation pattern of Atg1-kinase was further analyzed by MS/MS. **Table 8** lists the phosphorylated sites detected in the slower migrating and faster migrating band of Atg1-kinase. In both cases T226 was found to be phosphorylated. This indicates that Atg1-kinase is active, because T226 autophosphorylation was reported to be required for Atg1-kinase activity (Yeh et al., 2010).

Table 8: Phosphorylation sites detected in recombinantly expressed Atg1-kinase.

Atg1-kinase	Detected phosphorylation sites
Slower migrating (upper) band	48, **226**, 330, 365, 384, 390, 418, 424, 436, 590, 621, 622, 623, 635, 647, 675, 677, 679, 680, 683, 685, 720, 726, 769, 782,783, 865
Faster migrating (lower) band	**226**, 331, 365, 375, 384, 390, 418, 424, 436, 441, 480, 590, 621, 635, 647, 675, 677, 679, 680, 683, 685, 726, 769, 782, 783

Since the isolated EAT-domain of Atg1-kinase from *L. thermotolerans* was reported to form a dimer in solution, the multimerization status of full length Atg1-kinase was investigated. **Figure 6, B** shows the result from a SEC-MALS analysis (2.11.3, p. 47). For full length Atg1-kinase a molar mass of 103 kDa was determined. Comparison with the calculated molar mass (102.7 kDa) indicated Atg1-kinase to be monomeric in solution. This suggests that the isolated EAT-domain of Atg1-kinase might dimerize by exposing hydrophobic protein surfaces that are buried in the full length protein.

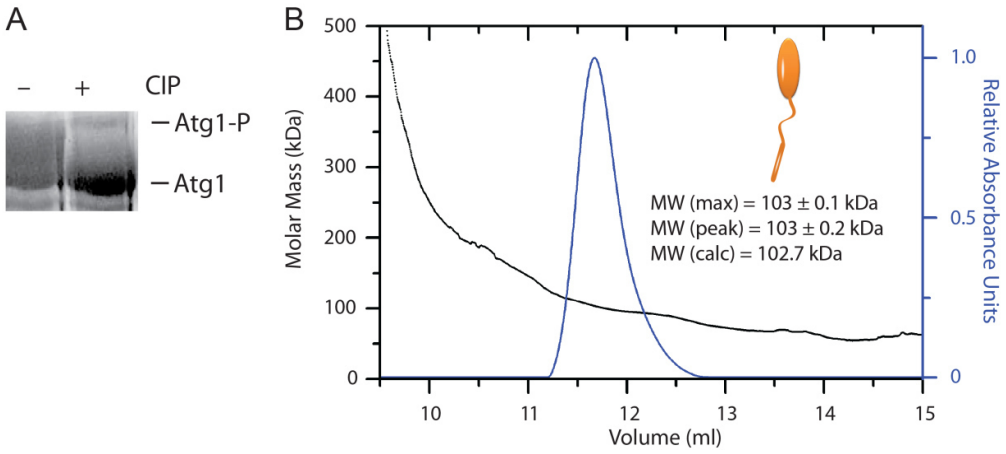

Figure 6: Analysis of Atg1-kinase. (A) Phosphatase treatment of Atg1-kinase. Treatment with calf intenstinal phosphatase (CIP) resulted in increased intensity of the faster migrating band. (B) SEC-MALS analysis of Atg1-kinase shows that full length Atg1-kinase is a monomer in solution. Atg1-kinase elutes as a single peak from the Superdex200 column. MW(max) is the molar mass determined in the peak apex, MW(peak) is the average molar mass determined over the whole peak, MW(calc) is the calculated molar mass of monomeric Atg1-kinase.

3.1.2. Purification and characterization of Atg13

Atg13 was expressed with an N-terminal MBP-tag and a C-terminal His_6-tag and applied to NiNTA-affinity purification (**Figure 7, A**). For further purification, Atg13 was subjected to SEC on a Superdex200 column after proteolytic cleavage of the tags (**Figure 7, B and C**). Two major problems arose when applying Atg13 to SEC. First, the recovery from the column was less than 30 % which indicates strong interaction of Atg13 with the column material. Second, the fraction of Atg13 that was bound by chaperones could not be separated by SEC. To overcome these problems, AIEX was applied instead of SEC. **Figure 7 D and E** show that AIEX separates free Atg13 efficiently from the chaperone bound fraction. Atg13 elutes from the AIEX column between 0 % and 15 % of buffer B

(buffer A: 125 mM NaCl, buffer B: 1 M NaCl) while the chaperone bound fraction elutes at higher salt concentration at around 60 % buffer B.

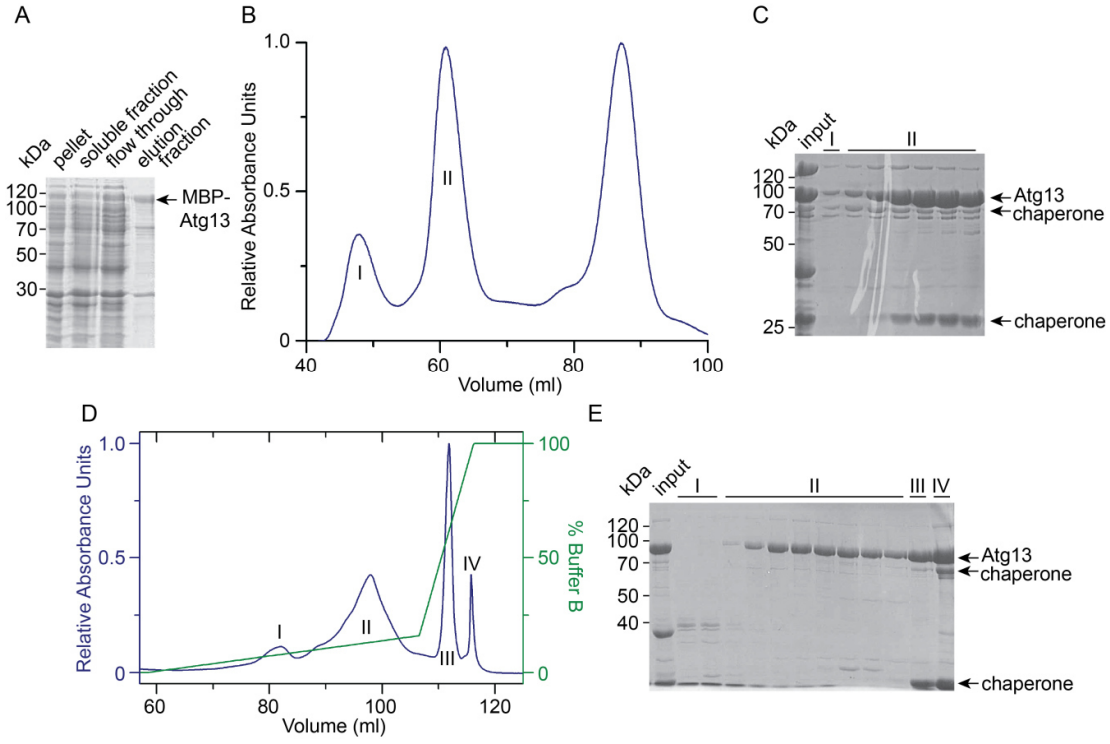

Figure 7: Atg13 purification. (A) SDS-PAGE analysis of NiNTA-affinity purification of Atg13. Atg13 was expressed as MBP fusion protein. (B and C) SEC profile and corresponding SDS-PAGE analysis of Atg13 purification. I: Aggregated protein, II: Atg13 and the chaperone bound fraction of Atg13. (D and E) AIEX profile and corresponding SDS-PAGE analysis of Atg13 purification. I: Impurities, II: Atg13 elutes between 0 % and 15 % of buffer B and was used for further experiments, III and IV: chaperone bound fractions of Atg13.

3.1.3. Purification and characterization of Atg17, Atg17^{TC} and related variants

Atg17 was expressed in *E. coli*. The trimeric subcomplex consisting of Atg17, Atg29, and Atg31 (Atg17^{TC}) was produced by co-expression of the subunits in *E. coli*. Atg17 was fused to an N-terminal His_6-tag for NiNTA-affinity purification. After affinity purification (**Figure 8, A**), Atg17 (**Figure 8, B and C**) and Atg17^{TC} (**Figure 8, D and E**) were subjected to SEC using a Superdex200 column for further purification and to remove aggregated protein. The elution volume of 54 ml for Atg17^{TC} is consistent with the elution volume reported previously for Atg17^{TC} (Kabeya et al., 2009). Atg17^{TC} was further reported to form an elongated dimer of trimers with a hydrodynamic radius (R_H) of 10 nm

(Ragusa et al., 2012). DLS measurement showed that Atg17^{TC} has a R_H of 10 nm consistent with these reports.

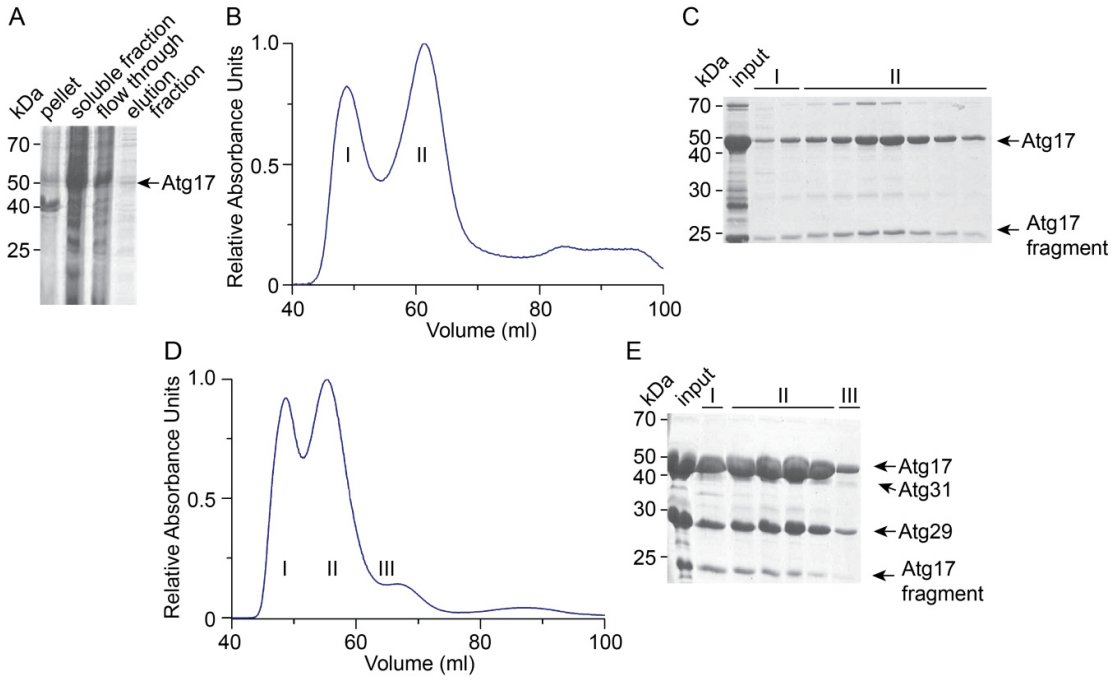

Figure 8: Atg17 and Atg17^{TC} purification. (A) SDS-PAGE analysis of NiNTA-affinity purification of Atg17. Similar purity was observed for Atg17^{TC} and Atg17^{monoTC}. (B and C) SEC profile and corresponding SDS-PAGE analysis of Atg17 purification. I: Aggregated protein, II: Atg17 used for further experiments. (D and E) SEC profile and corresponding SDS-PAGE analysis of Atg17^{TC} purification. I: Aggregated protein, II: the subunits Atg17, Atg29, and Atg31 co-elute from the Superdex200 column in a single peak at 54 ml and are used for further experiments, III: excess of the single subunits Atg17 and Atg29.

In order to analyze the potential function of the Atg17^{TC} dimer, a monomeric variant of this complex was explored which lacked the C-terminal dimerization domain of Atg17 (Atg17$^{1-320}$). **Figure 9** shows that Atg17^{monoTC} eluted at a significantly increased elution volume (Atg17^{TC} 54 ml, Atg17^{monoTC} 66 ml) from the Superdex200 column indicating Atg17^{monoTC} to be monomeric.

To confirm that Atg17^{monoTC} is a monomer, the sample was subjected to analytical ultracentrifugation analysis (**Figure 10**), which was performed by Dr. Stephan Uebel as described (2.11.4, p. 47). To exclude that dimerization occurs at higher protein concentrations, the experiment was performed with different protein concentrations. At the tested concentrations no protein species with higher molar masses was detected. The fitted molar masses correspond to the calculated molar mass for the monomeric Atg17^{monoTC} (71 kDa). Furthermore, a R_H of 4.3 nm was determined by analytical ultracentrifugation

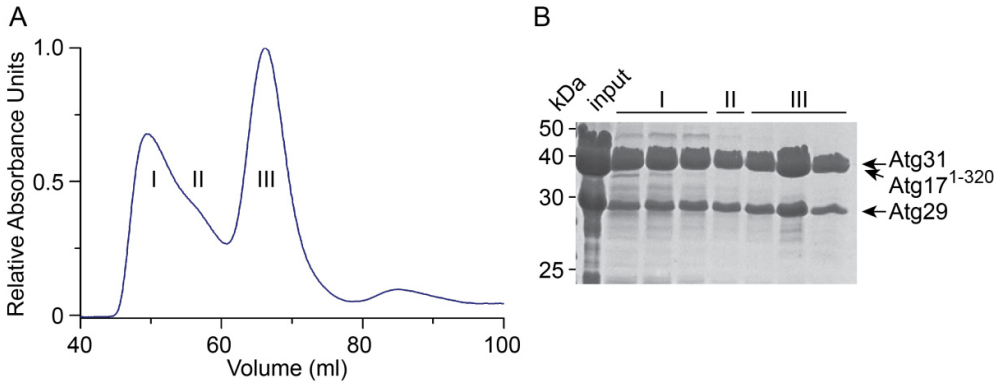

Figure 9: Atg17^{monoTC} purification. (A and B) SEC profile and corresponding SDS-PAGE analysis of Atg17^{monoTC} purification. I and II: Aggregated protein and impurities, III: The subunits Atg17$^{1-320}$, Atg29, and Atg31 co-elute from the Superdex200 column in a single peak and are used for further experiments. The elution volume is significantly shifted compared to Atg17^{TC} from 54 ml to 66 ml.

for Atg17^{monoTC}, which is significantly reduced compared to the R_H of Atg17^{TC} (10 nm). Taken together, all Atg1^{PC} subunits could be expressed and purified and were available for further analysis of Atg1^{PC} assembly and architecture.

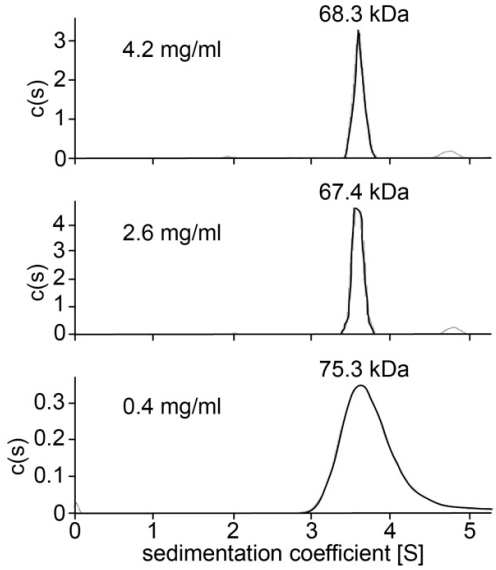

Figure 10: Analysis of Atg17^{monoTC} by analytical ultracentrifugation. Sedimentation velocity runs were performed with different protein concentrations as indicated. Independent of the protein concentration the molar mass corresponding to the monomeric Atg17^{monoTC} (calculated molar mass: 71 kDa) was detected. Experiment was performed and analyzed by Dr. Stephan Uebel.

3.2. Atg1^{PC} assembly and characterization

Analyzing the assembly and architecture of Atg1^{PC} remained a challenging task *in vivo* as well as *in vitro*. Furthermore, conflicting data exist, describing that Atg1^{PC} assembles from Atg17^{TC} and the single Atg1-kinase and Atg13 proteins (Kabeya et al., 2005) or from Atg17^{TC} and a constitutive complex formed by Atg1-kinase and Atg13 (Alemu et al., 2012). Active Atg1^{PC} was suggested to be dimeric, but the mechanism of dimerization remained unclear. It was suggested that besides dimeric Atg17 (Chew et al., 2013; Ragusa et al., 2012), the EAT-domain of Atg1-kinase could mediate dimerization (Ragusa et al., 2012) or that dimerization is mediated by Atg13 driven Atg1-kinase self-association (Yeh et al., 2011). To distinguish between previously published dimerization mechanisms, Atg1^{PC} was assembled *in vitro*.

Atg17^{TC} was co-expressed and formed an elongated dimer. The Atg1-Atg13 subcomplex, however, had to be reconstituted from its purified subunits. **Figure 11 A and C** shows that Atg1-kinase and Atg13 elute in a single peak from a Superdex200 column, indicating that they form a stable complex. To reconstitute Atg1^{PC}, all subunits were mixed in a stoichiometric molar ratio of Atg1-kinase:Atg13:Atg17^{TC} = 1:1:1 and analyzed on a Superose6 column (**Figure 11**, **B and C**). All subunits were found to elute in a single peak from a Superose6 column suggesting that they are part of the same complex. To investigate whether Atg17 is the only protein conferring dimerization of Atg1^{PC}, a pentameric complex containing dimerization deficient Atg17$^{1-320}$ (Atg1^{monoPC}) was reconstituted *in vitro* from purified Atg1-kinase, Atg13 and Atg17^{monoTC} and subjected to SEC. Atg17^{monoTC} was forming a stable complex with Atg1-kinase and Atg13. The elution volume of Atg1^{monoPC} containing the monomeric Atg17^{monoTC} was significantly increased compared to the elution volume of Atg1^{PC} (**Figure 11**, **B and C**), suggesting that dimerization of Atg1^{PC} is mediated by the C-terminal domain of Atg17. To confirm that Atg1^{PC} is a dimer of pentamers, the mass of Atg1^{PC} in solution was determined by SEC-MALS (2.11.3, p. 47). The determined mass of 684 ± 35 kDa (**Figure 11, D**) corresponds to the mass of a dimer of pentamers with a calculated mass of 568 kDa. The higher apparent molar mass in SEC-MALS is likely caused by aggregates that interact with the column material and elute together with Atg1^{PC}. Interestingly, DLS data showed that Atg1^{PC} has a R_H of 13 nm which is only slightly larger than the R_H of Atg17^{TC} (10 nm).

This indicates that Atg1-kinase and Atg13 are accommodated within the crescent of the Atg17 scaffold.

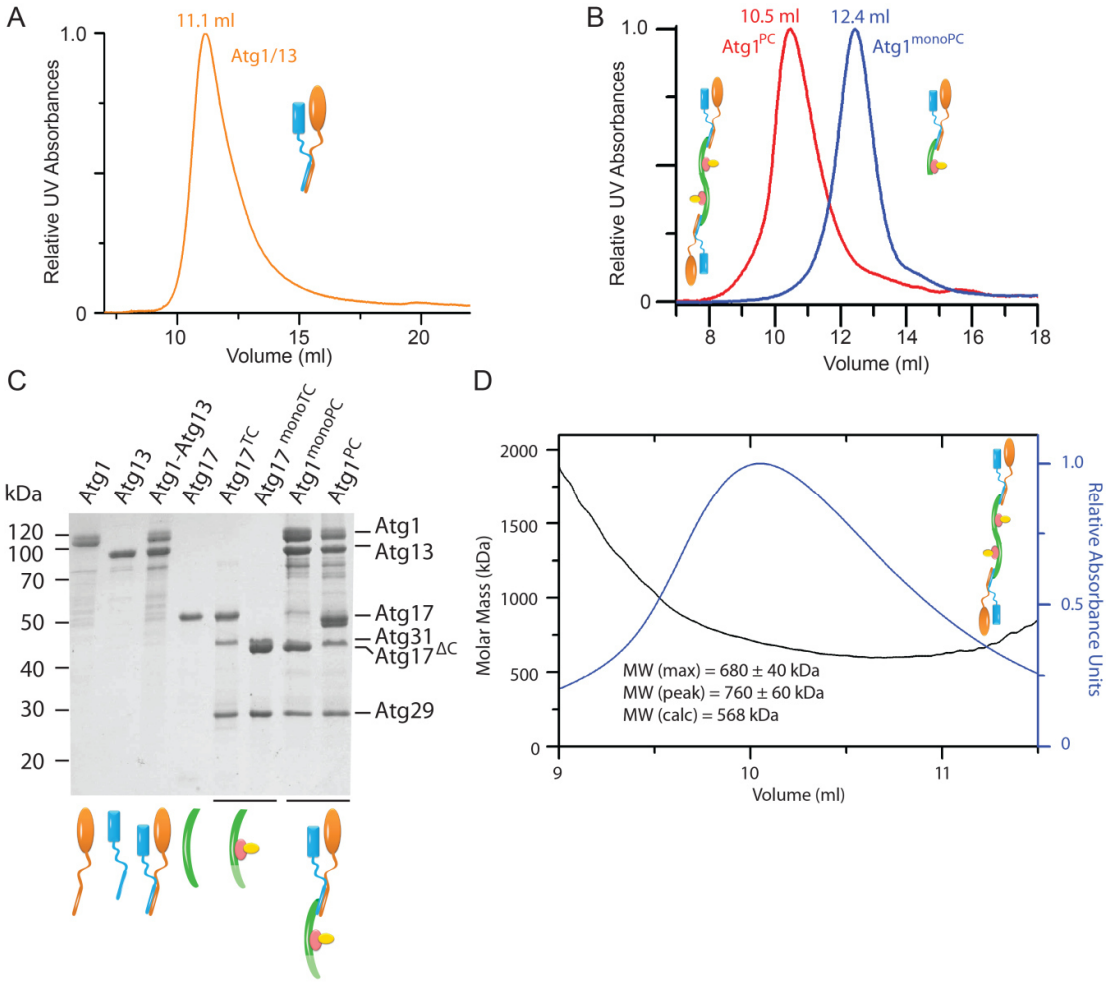

Figure 11: Assembly and characterization of Atg1^{PC} (A) SEC profile of Atg1-Atg13 on a Superdex200 column. Both subunits elute in a single peak. (B) SEC profiles of Atg1^{PC} (red line) and Atg1^{monoPC} (blue line) on a Superose6 column. The elution volume is significantly shifted to higher volumes for Atg1^{monoPC}. (C) SDS-PAGE analysis of purified Atg1^{PC} subunits. Atg17^{TC} and Atg17^{monoTC} were co-expressed and co-purified, respecitvely. Atg1-Atg13, Atg1^{monoPC} and Atg1^{PC} were reconstituted from the purified components and subjected to SEC. Samples of the pooled peak fractions from (A) and (B) were applied to SDS-PAGE. (D) SEC-MALS analysis of Atg1^{PC} shows that it is a dimer of pentamers in solution. Atg1^{PC} elutes from the Superose6 column as a single peak and the molar mass determined on-line by MALS corresponds to the calculated molar mass of an Atg1^{PC} dimer. MW(max) is the molar mass determined in the peak apex, MW(peak) is the average molar mass determined over the whole peak, MW(calc) is the calculated molar mass of dimeric Atg1^{PC}.

Previous studies showed that for co-IP of Atg17 and Atg1-kinase, Atg13 is required and that the N-terminal region of Atg17 is required for the interaction of Atg17 with Atg13 (Kabeya et al., 2005). SEC analyses in this study show that Atg1^{PC} assembles from its subunits *in vitro*. However, which subunits interact directly to assemble Atg1^{PC} still needed to be investigated. In order to recapitulate the ordered assembly of Atg1^{PC} from its subunits

Atg1-kinase, Atg13 and Atg17^{TC}, SPR experiments (2.11.1, p. 46) were performed. To investigate the interactions involved in Atg1^{PC} assembly, a NTA chip was coated with His-tagged Atg17. Atg13 and Atg1-kinase were injected subsequently to the coated chip (**Figure 12, A**, red line). Clear responses upon Atg13 and Atg1-kinase injection show the direct interaction of these subunits. However, if buffer is injected instead of Atg13 (**Figure 12, A**, grey line), the interaction of Atg1-kinase with Atg17 is abolished, showing that Atg13 directly interacts with Atg17 and bridges Atg17 and Atg1-kinase. To test whether Atg29 and Atg31 are involved in the interaction, Atg13 was injected to a NTA chip coated with Atg17^{TC} (**Figure 12, B**). In the presence of Atg29 and Atg31 the interaction between Atg17 and Atg13 was still observed, indicating that they do not interfere with the interaction (**Figure 12**, **B**). The binding kinetics of Atg1-kinase to Atg13, however, are altered. In the presence of Atg29 and Atg31, both binding and dissociation kinetics of Atg1-kinase are significantly reduced. This indicates that these subunits influence Atg1-kinase binding directly through interaction with Atg1-kinase or indirectly by sterically interfering with Atg1 kinase binding. The fact that binding sites for Atg31 and Atg13 on Atg17 as well as for Atg17 and Atg1-kinase on Atg13 are in close proximity (Fujioka et al., 2014), supports the latter hypothesis. Taken together, these results show how Atg1^{PC} can be assembled from its subunits and that Atg13 plays a central role in bridging Atg17^{TC} and Atg13.

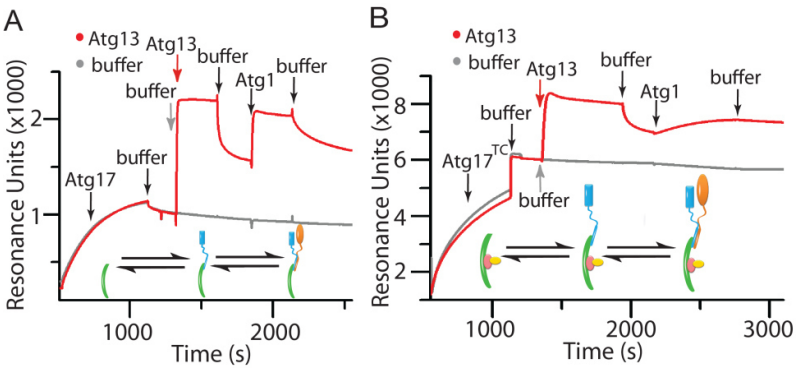

Figure 12: SPR allows real time observation of Atg1^{PC} assembly. (A and B) The NTA chip is first coated with His-tagged Atg17 (A) or Atg17^{TC} (B). Sequentially Atg13 (red line) or buffer (grey line) and Atg1-kinase are injected. A clear response can be observed after injection of both proteins. If buffer is injected instead of Atg13, Atg1-kinase does no longer interact with Atg17 or Atg17^{TC}. (B) Atg13 binding kinetics are not altered compared to (A). Atg1-kinase binding and dissociation kinetics are reduced in the presence of Atg29 and Atg31.

3.3. Atg1-kinase phosphorylates Atg1^{PC} subunits *in vitro*

Previous studies reported that Atg1^{PC} assembly was mainly dependent on the phosphorylation status of Atg13. Under nutrient rich conditions, Atg13 is constantly phosphorylated by TORCI at several sites (Kamada, 2010) and phosphorylation of Atg13 prevents Atg1^{PC} formation and induction of autophagy under vegetative growth conditions (Kawamata et al., 2008). Atg1^{PC} could be assembled from its subunits in this study, suggesting that Atg13 was not phosphorylated. Electron spray ionization (ESI)-mass spectrometry (MS) was applied to investigate the phosphorylation status of the recombinantly expressed Atg1^{PC} subunits. As expected, the proteins expressed in *E. coli* were not phosphorylated. Atg1-kinase expressed in insect cells showed several mass peaks corresponding to phosphorylated Atg1-kinase species. To test Atg1-kinase activity and the effect on complex assembly of Atg1^{PC}, ATP was added to Atg1^{PC}. As indicated by their electrophoretic mobility shift, Atg1-kinase phosphorylates itself, Atg13 and Atg29 *in vitro* (**Figure 13, A**). To test whether phosphorylation induces disassembly of Atg1^{PC}, unphosphorylated and phosphorylated Atg1^{PC} were subjected to SEC. Unphosphorylated

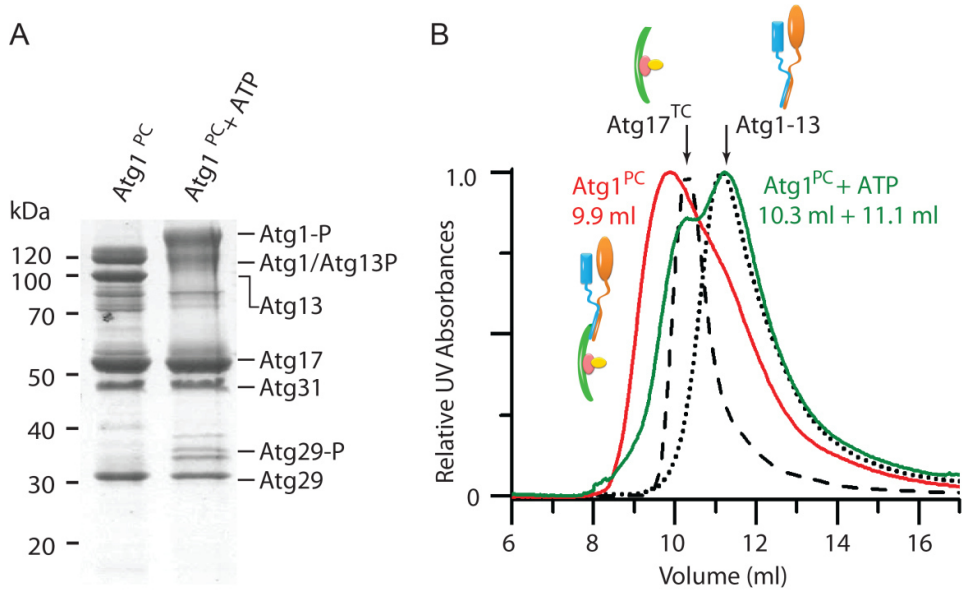

Figure 13: Atg1^{PC} phosphorylation leads to complex disassembly. (A) SDS-PAGE analysis of unphosphorylated and phosphorylated Atg1^{PC}. Phosphorylation of Atg1-kinase, Atg13 and Atg29 is indicated by their electrophoretic mobility shift upon ATP addition. (B) SEC profiles of unphosphorylated Atg1^{PC} (red line) and phosphorylated Atg1^{PC} (green line). Unphosphorylated Atg1^{PC} elutes in the void volume of the Superdex200 column. After phosphorylation Atg1^{PC} elutes in two peaks, corresponding to Atg17^{TC} (dashed line) and the Atg1-Atg13 complex (dotted line).

Atg1^{PC} elutes from a Superdex200 column in the void volume. After addition of 1 mM ATP it elutes in a double peak corresponding to the elution volume of Atg17^{TC} and the Atg1-Atg13 subcomplex (**Figure 13, B**). This shift indicates that upon phosphorylation Atg1^{PC} is disassembled into the stable subcomplexes Atg17^{TC} and Atg1-Atg13. This finding supports the idea that Atg1-Atg13 is a stable subcomplex that does not dissociate upon Atg13 phosphorylation. However, Atg1-kinase presumably phosphorylates Atg1^{PC} subunits in an unregulated manner *in vitro*. To test whether the previously described regulatory phosphorylation sites on Atg1-kinase (Kijanska et al., 2010), Atg13 (Kamada et al., 2010) and Atg29 (Mao et al., 2013) are phosphorylated in this *in vitro* assay, a MS/MS based analysis of unphosphorylated and phosphorylated Atg1^{PC} was performed (2.10.2, p. 45). **Table 9** lists the previously reported regulatory sites on Atg1^{PC} subunits that were found to be phosphorylated by Atg1-kinase *in vitro*. Importantly, phosphorylation of Atg1-kinase at T226 was detected already in the sample without ATP. Atg1-kinase autophosphorylation at T226 was reported to be required for the activity of Atg1-kinase which is required for inducing autophagy (Yeh et al., 2010). For all other Atg1^{PC} subunits no phosphorylated peptides were detected. The only exception is the peptide containing S5 and T8 of Atg29 which was also detected carrying a phosphorylation in the sample without ATP. The phosphorylated fraction of Atg29, however, is very small since it could not be detected by ESI-MS. After addition of ATP, Atg1-kinase phosphorylates itself at its autophosphorylation site T226 which is important for its activity (Yeh et al., 2010). In addition, three other regulatory sites in Atg1-kinase are phosphorylated. S351, S356 and S533 were described to be phosphorylated upon autophagy induction (Kijanska et al., 2010), but whether Atg1-kinase is responsible for these phosphorylations *in vivo* is unclear. Atg13 phosphorylation by TORCI is a main regulatory process during autophagy inhibition and Atg1^{PC} disassembly (Kabeya et al., 2005; Noda and Ohsumi, 1998). Atg13 was found to be phosphorylated on four out of eight characterized TORCI dependent regulatory sites. The phosphorylation sites S437, S438, S646 and S649 were found applying MS/MS (Kamada et al., 2010). Out of these Atg13 residues only S649 could be detected to be phosphorylated by Atg1-kinase *in vitro*. Other regulatory TORCI dependent phosphorylation sites within Atg13 were found by homology search. These sites are S348, S496, S541 and S535 (Kamada et al., 2010). Out of these sites three could be detected to be phosphorylated in the *in vitro* assay (S496, S535 and S541). In addition, instead of being phosphorylated at S348, Atg13 was found to be phosphorylated on the same peptide at S346. However, the phosphorylation on these sites was sufficient to induce the

disassembly of Atg1^{PC}. Atg29 was reported to contain mainly three regulatory phosphorylation sites in its C-terminal region at positions S197, S199 and S201 (Mao et al., 2013). Out of these three phosphorylation sites only one could be detected at S201. Other detected phosphorylation sites in Atg29 are all located in the unstructured C-terminal part of the protein, except for S5 and T8. Taken together, these data show that Atg1-kinase is able to phosphorylate Atg13 at the regulatory sites required for Atg1^{PC} disassembly *in vitro*. Furthermore, other sites in Atg1-kinase, Atg13 and Atg29 are phosphorylated which might play a role in Atg1^{PC} disassembly or in other processes. Therewith assembly and disassembly of Atg1^{PC} could be recapitulated *in vitro* and Atg1^{PC} architecture could be analyzed. Why Atg1^{PC} is an elongated dimer of pentamers, however, remained a matter of debate.

Table 9: Atg1-kinase phosphorylates Atg1^{PC} subunits at regulatory sites *in vitro*.

Protein	Positions of phosphorylations	Peptide sequence	w/o ATP (log(intensity))	+ 1 mM ATP (log(intensity))
Atg1	T226	FLPNTSLAE**T**LC GSPLYMAPEILN YQK	7.8	8.3
	S351 or S356	GIVE**S**NMFV**S**EY LSK	-	7.9
	S351 and S356	GIVE**S**NMFV**S**EY LSK	-	8.3
	S533	ALGIA**S**TR	-	7.7
Atg13	S346	SL**S**LSPCTR	-	8.7
	S496	KTSGNNPPNINIS D**S**LIR	-	7.6
	(S535 and S543) or (S533 and S543) or (S533 and S541)	GRSD**S**H**S**PLPSI**S** P**S**MHYGSLNSR	-	8.5
	S643 or S644	FK**SS**ISPR	-	8.5
	(S649 and S654) or (S649 and S656) or (S652 and S656) or (S655 and S656)	**S**IDSI**SSS**FIK	-	8.7
Atg29	S5 or T8	MIMN**S**TN**T**VVYI K	5.6	6.6
	S106	YSNDQVNEGM**S** DLIHK	-	8.8
	S125	YTPTLQNDNLLN V**S**ASPLTTER	-	8.6
	S136 or T144 or S154	QD**S**EEVETEV**T**N EALQHLQT**S**K	-	8.7
	S201	**S**ALEEALMDR	-	7.6

SEC purified Atg1^{PC} was incubated with or without 1 mM ATP. Some peptides were found to be phosphorylated at different and/or multiple positions as indicated. The table lists the previously identified regulatory sites in Atg1-kinase and Atg13 that were also found to be phosphorylated in

this analysis (except for Atg13, S346 instead of S348 was detected to be phosphorylated). All phosphorylation sites detected in Atg29 are listed. Atg29, phosphorylated at S5 or T8 in the absence of ATP, represents a minor fraction of the preparation, because no mass corresponding to phosphorylated Atg29 was detected by ESI-MS. Phosphorylation sites detected in Atg17 and Atg31 are not listed since no electrophoretic mobility shift was detected for these proteins in SDS-PAGE (see Figure 13) and only the masses corresponding to unphosphorylated proteins could be detected by ESI-MS. The listed intensities are average values from four independent experiments.

3.4. Role of the Atg17 dimerization domain *in vivo*

3.4.1. Dimerization of Atg17 is required for autophagy

Dimerization of $Atg1^{PC}$ is mediated by the C-terminal domain of Atg17. To investigate the role of $Atg1^{PC}$ dimerization *in vivo*, yeast *S. cerevisiae* strains $ATG17^{1\text{-}320}$ and *atg17Δ* were generated. To follow autophagic flux, the GFP-Atg8 assay was used. GFP-Atg8 is recruited to the autophagic membrane where it is conjugated to PE by the Atg8 conjugation machinery (Hanada et al., 2007; Ichimura et al., 2000). A certain amount of GFP-Atg8 which is conjugated to the inner autophagic membrane or unselectively taken up from the cytoplasm is transported to the vacuole upon autophagy induction. In the vacuole the Atg8 moiety is rapidly degraded while GFP is more stable preventing it from rapid proteolytic digestion. The GFP-moiety can therefore be detected by WB. By comparing band intensities of GFP-Atg8 and GFP in WB, the overall autophagic flux can be monitored. **Figure 14 A** shows GFP-Atg8 turn over in $ATG17^{WT}$, $ATG17^{1\text{-}320}$ and *atg17Δ* cells. Autophagic turnover is significantly impaired in cells expressing the monomeric $Atg17^{1\text{-}320}$ mutant and in the *atg17Δ* cells indicating that the dimerization domain of Atg17 is practically important. Semi-quantitative analysis of the band intensities shows that in $ATG17^{1\text{-}320}$ cells autophagic flux is reduced compared to *atg17Δ* cells (**Figure 14**, **B**), suggesting that monomeric $Atg17^{1\text{-}320}$ exerts a dominant negative effect. Atg11 is a scaffold protein that is required for selective autophagy and was suggested to be a functional homologue of Atg17 for PAS formation during vegetative growth (Cheong et al., 2008). In the absence of Atg11 the expression of a monomeric Atg17 mutant results in complete inhibition of autophagy (Ragusa et al., 2012) supporting the findings in this study. However, non-selective autophagy specific Pho8Δ60 assay showed that unselective autophagy turnover is almost completely blocked in *atg17Δ* cells (Cheong et al., 2005), indicating that the residual GFP-Atg8 turnover is mediated by Atg11 dependent selective

autophagy. Non-functional Atg17$^{1-320}$ could therefore compete with Atg11 during autophagy.

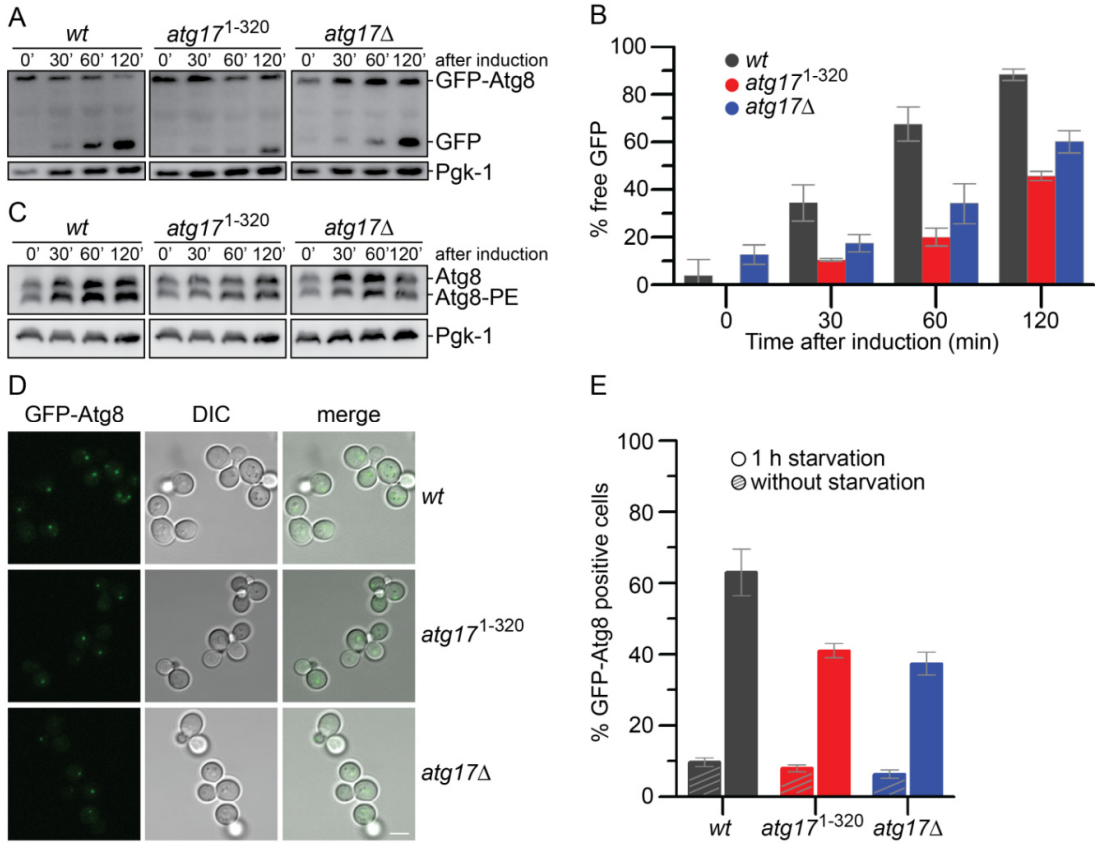

Figure 14: The Atg17 dimerization domain plays an important role in autophagy. (A) WB of the GFP-Atg8 assay to monitor autophagic flux in *ATG17*^{WT}, *ATG17*$^{1-320}$ and *atg17Δ* cells. The intensity of the band corresponding to free GFP is significantly decreased in *atg17*$^{1-320}$ and *atg17Δ* cells compared to *ATG17*^{WT} cells. (B) Semi-quantitative analysis of data shown in (A). Bars represent integrated band intensities as average of three independent experiments and error bars represent the standard deviation. (C) WB of the Atg8-PE assay to monitor induction of autophagy and early steps leading to conjugation of Atg8 to PE. Atg8 is conjugated to PE efficiently in all strains. (D) Fluorescence microscopy analysis of GFP-Atg8 distribution 1 h after induction of autophagy by rapamycin. In all strains GFP-Atg8 puncta were observed. (E) Quantification of data shown in (D). The bars represent the average of three independent analyses of 100 cells, respectively. Error bars indicate standard deviation.

Since the GFP-Atg8 assay monitors the overall autophagic flux, it is impossible to identify the step in the autophagic process that is affected. Therefore, the Atg8-PE assay was used to monitor steps that lead to the conjugation of Atg8 to the autophagic membrane. **Figure 14 C** shows that the conjugation of Atg8 is not influenced in *ATG17*$^{1-320}$ and *atg17Δ* cells, because none of the tested mutations affected the formation of Atg8-PE. This suggests that Atg17 is not required for induction of Atg8 conjugation, but needed in another step of the autophagic process. Furthermore, these findings suggest that dimeric Atg1^{PC} is also required for later stages of autophagy. Since Atg8 conjugation remains unaffected in

ATG17$^{1-320}$ cells, it is likely that cargo delivery is slowed down or that delivery of GFP-Atg8 to the vacuole is only mediated by specific autophagy in the respective mutant strains. To further investigate whether defective initiation of autophagy is the only reason for inhibition of the autophagic flux, the amount of cells positive for GFP-Atg8 puncta was determined (**Figure 14**, **C and D**). The number of GFP-Atg8 positive cells is reduced in *ATG17*$^{1-320}$ and in *atg17Δ* cells. The reduction in number is, however, not as significant as the reduction in autophagic flux as determined by the GFP-Atg8 assay. Taken together, these results show that Atg17 dimerization is required for autophagy and that early steps in autophagy are not exclusively affected by the dimerization defect. To investigate the role of Atg17 and Atg1^{PC} in membrane dynamics closer, single GFP-Atg8 puncta were observed and their kinetics recorded.

3.4.2. Single PAS-analysis reveals altered autophagic membrane dynamics in the Atg17 dimerization mutant

In this study it was shown that autophagic flux was significantly decreased in *ATG17*$^{1-320}$ and *atg17Δ* cells. The fluorescence intensity of GFP-Atg8 puncta was therefore monitored over time to resolve autophagic membrane dynamics (2.12.2, p. 50). **Figure 15 A** shows the intensity curves for the GFP-Atg8 signal on the autophagic membrane in cells expressing different Atg17 constructs. The maximum average fluorescence intensity observed in *ATG17*^{WT} cells was set to 1 and used for normalization. A striking effect for autophagic membrane kinetics can be observed in *ATG17*$^{1-320}$ and *atg17Δ* cells. Both, the elongation and the recycling phase are extended. Moreover, a significant increase in GFP-Atg8 fluorescence intensity at the PAS was observed in *ATG17*$^{1-320}$ and *atg17Δ* cells. The increase in autophagic membrane life time and the increase in GFP-Atg8 fluorescence intensity (**Figure 15**, **B**) indicate a role for Atg17 dimerization in regulating phagophore expansion. In contrast to Cvt vesicles with a size of ~150 nm in diameter (Molecular and Cellular EndocrinologyBaba et al., 1997), autophagosomes are significantly larger and can be observed by fluorescence microscopy. As mentioned before, the GFP-Atg8 turn over in *ATG17*$^{1-320}$ and in *atg17Δ* cells is likely mediated by selective autophagy. Nevertheless, membrane structures with higher GFP-Atg8 density compared to that in *ATG17*^{WT} cells are observed in mutant background. Since cargo delivery to the vacuole in *atg17Δ* cells is

likely to be mediated by selective autophagy (Cheong et al., 2005) the observed large membrane structures are not forming productive autophagosomes. This further suggests that Atg1^{PC} plays a role in coordinating phagophore expansion and that dimerization of Atg1^{PC} is required for this function. A detailed picture of the interaction of Atg1^{PC} with autophagic membranes is, however, still missing.

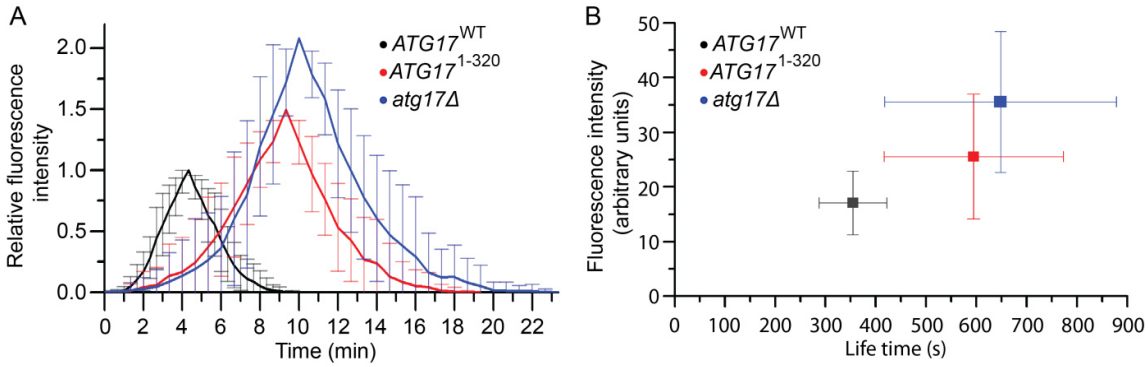

Figure 15: Membrane dynamics analyzed by fluorescence microscopy. (A) The curves represent the average fluorescence intensity at a given time point after appearance of the GFP-Atg8 punctum in *ATG17^{WT}* (black line), *ATG17$^{1-320}$* (red line) and *atg17Δ* (blue line) cells. All phases of GFP-Atg8 conjugation and deconjugation are increased in the mutant *ATG17$^{1-320}$* and *atg17Δ* strains. Fluorescence profiles represent the average of more than 30 single puncta. (B) Data from (A) analyzed for life time and fluorescence intensity. Both, life time and fluorescence intensity of GFP-Atg8 puncta are increased in the mutant *ATG17$^{1-320}$* (red square) and *atg17Δ* (blue square) strains. The strongest effect is observed in *atg17Δ* cells. (A and B) Error bars represent the standard deviation.

3.5. Recruitment of Atg1^{PC} to the autophagic membrane

3.5.1. Atg1-kinase binds Atg8-positive membranes

Assembly and disassembly of Atg1^{PC} is regulated by phosphorylation of the subunits. In their phosphorylated form the subunits of Atg1^{PC} form the Atg17^{TC} and the Atg1-Atg13 subcomplexes. However, Atg1^{PC} subunits show different distribution patterns along the autophagic membrane. Atg1-kinase was found to be distributed all over the autophagic membrane while Atg13 and Atg17 localize to the vacuole-phagophore contact site (VPCS) (Suzuki et al., 2013). This suggests that Atg1-kinase and Atg1^{PC} might exert different functions. It was shown that Atg8 binds Atg1-kinase by recognizing an Atg8 interaction motif (AIM) which led to the assumption that Atg1-kinase plays a role in later steps in autophagy (Alemu et al., 2012; Kijanska and Peter, 2013; Kraft et al., 2012). The Atg8 lipidation reaction was reconstituted *in vitro* (Romanov et al., 2012) and a Atg8 dependent

autophagic membrane scaffold was dicrovered (Kaufmann et al., 2014). It was shown that Atg8 forms a membrane scaffold together with Atg12–Atg5 and Atg16 which has a meshwork like architecture (Kaufmann et al., 2014). To overcome the limitation in analyzing protein-protein and protein-membrane interactions *in vivo*, the GUV based Atg8-lipidation system was applied to analyze Atg1-kinase recruitment to Atg8-positive membranes and its effect on the formation of autophagic membrane scaffolds. Therefore, fluorescently labeled Atg8 was conjugated to PE in GUVs *in vitro* (2.11.7, p. 49) and fluorescently labeled Atg1-kinase was added. **Figure 16 A** shows that Atg1-kinase is recruited to Atg8 positive GUVs, but not to GUVs without Atg8. Fluorescence recovery after photobleaching (FRAP) is a method to investigate the diffusion of molecules in or attached to a membrane. Therefore, a certain area of the membrane is photobleached. The recovery rate of the fluorescence in the bleached area depends on the mobility and the diffusion coefficient of the analyzed molecule. FRAP experiments showed Atg8 to be immobilized on membranes by the Atg12–Atg5/Atg16 complex. The interaction of Atg8 and Atg12 was shown to be mediated by an AIM in Atg12 (Kaufmann et al., 2014). Therefore it was tested whether Atg1-kinase can compete with Atg12 for Atg8 binding through its AIM. When Atg1-kinase is added to the membrane scaffold, Atg8 remains immobile on the membrane (**Figure 16, B**), indicating that the interaction between Atg8 and Atg12 is not affected by Atg1-kinase. Atg1-kinase bound to the autophagic membrane scaffold is also immobile which further indicates that the exchange kinetics of Atg1-kinase are slow once it is bound to Atg8. This *in vitro* experiment supports the idea that Atg1-kinase plays different roles in autophagy when it is part of $Atg1^{PC}$, forming a complex with Atg13 or acting as uncomplexed Atg1-kinase. Atg1-kinase is distributed along the whole autophagic membrane (Suzuki et al., 2013). The FRAP data indicate that Atg1-kinase plays a regulatory role on the autophagic membrane that is not directly involved in autophagic membrane scaffold disassembly by competing with Atg12 for AIM dependent Atg8 binding.

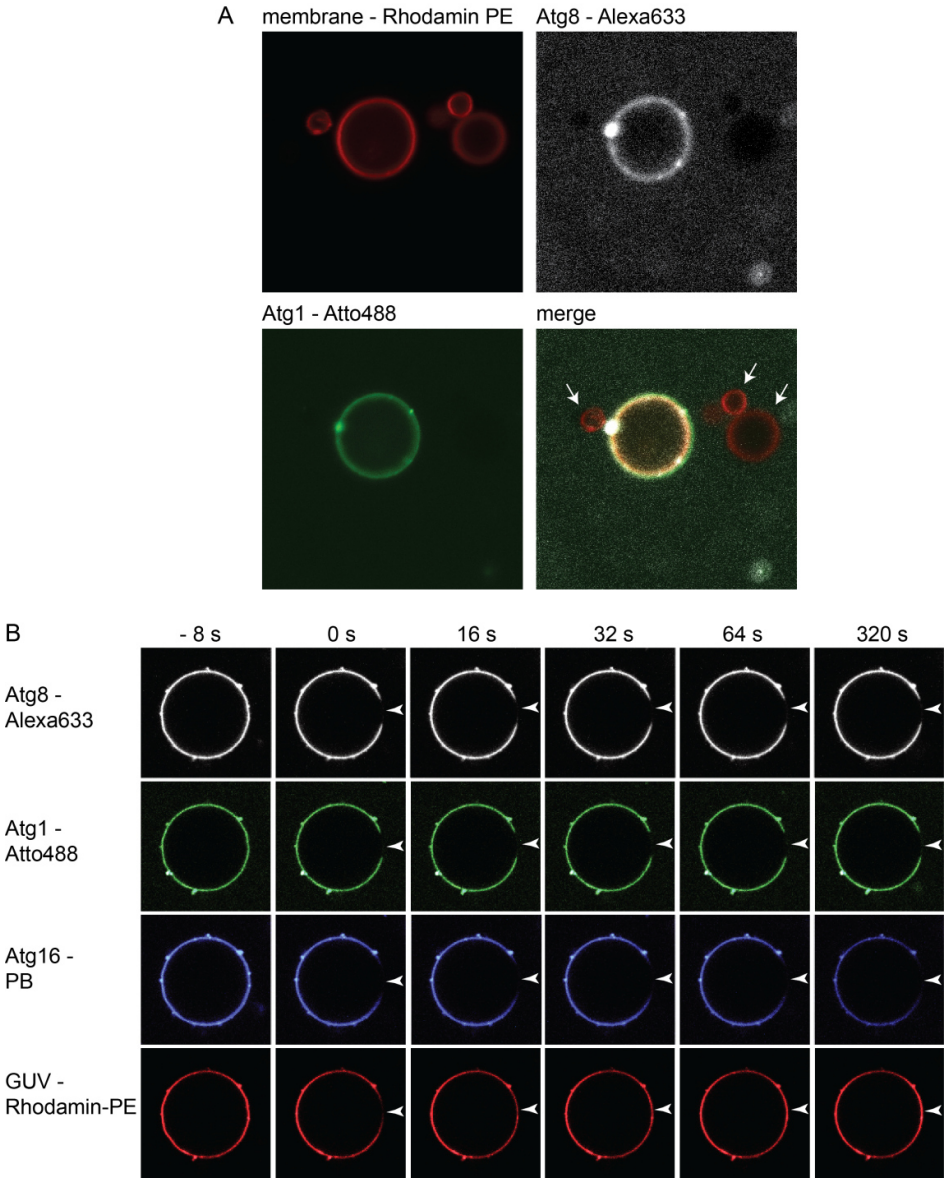

Figure 16: Atg1-kinase is recruited to Atg8-positive membranes *in vitro*. (A) Atg1-kinase is recruited to Atg8-positive GUVs, but not to GUVs without Atg8 (white arrows). (B) FRAP experiment to test the integrity of the autophagic membrane scaffold and Atg1-kinase mobility. Images were acquired at indicated time points before and after photobleaching. Bleached areas are marked (white arrowheads). The fluorescence of the labeled lipid in the GUV recovers rapidly. Atg1-kinase behaves like the scaffold forming Atg8 and Atg16 and is not recovering in the bleached area within the observed time span.

3.5.2. Atg1-kinase and Atg13 specifically bind PI-containing membranes

The EAT-domain of Atg1-kinase was found to interact with membranes directly without requiring any adaptor proteins (Ragusa et al., 2012). Furthermore, the human homolog of Atg1 kinase (Ulk-1) and Atg13 were found to be membrane associated and membrane

localization of Ulk-1 was mediated by its C-terminal domain which corresponds to the EAT-domain of Atg1-kinase in yeast (Chan et al., 2009). However, whether the full length proteins display direct membrane binding capacity has not been analyzed. To investigate the membrane binding capacity of $Atg1^{PC}$ subunits, liposome sedimentation assays were performed by Dr. Yijian Rao (2.11.9, p. 49). First, the proteins were incubated with liposomes prepared from yeast polar lipid extracts (YPL) of different diameter. A clear preference for small YPL-LUVs with high membrane curvature was observed for Atg1-kinase and Atg13 (**Figure 17**, **A**). $Atg17^{TC}$ and Atg17 did not interact with YPL-LUVs of any size (**Figure 17**, **A**). Protein-membrane interactions are often mediated by charge dependent interactions of basic amino acid residues with charged lipids, such as phosphatidylserine (PS) (Cho and Stahelin, 2005). Therefore, binding to highly charged membranes containing 20 mol% PS (acidic synthetic lipid-mix, ASL) was compared to that to YPL membranes. Interestingly, Atg1-kinase and Atg13 were only recruited efficiently to YPL-LUVs and not to ASL-LUVs (**Figure 17**, **B**). This suggests that the interaction of Atg1-kinase and Atg13 with YPL-LUVs is not charge dependent, but mediated by a specific lipid in the YPL-LUVs. The autophagic membrane is enriched in PI3P which is produced by an autophagy specific PI3-kinase complex containing the Vps34 PI3-kinase (Kihara et al., 2001; Obara et al., 2008). However, $Atg1^{PC}$ acts upstream of the PI3-kinase complex (Suzuki et al., 2007) and human Atg1-kinase (Ulk-1) was shown to be a regulator of the PI3-kinase complex (Russell et al., 2013). To test whether Atg1-kinase requires PI for interaction with membranes, $Atg1^{PC}$ subunit binding was tested to LUVs containing PI. LUVs containing PI and PI3P, were applied to mimic the autophagic membrane at different maturation stages. Both, Atg1-kinase and Atg13 bound efficiently to PI containing membranes (**Figure 17**, **B**). Addition of PI3P did not further increase membrane binding (**Figure 17**, **B**), which is also consistent with the recruitment of $Atg1^{PC}$ as one of the first complexes to the early phagophore membrane (Suzuki et al., 2007). To confirm that the increased interaction of Atg1-kinase and Atg13 with YPL liposomes was not due to the effect of another lipid than PI present in the complex YPL mixture, synthetic lipid mixes were used for liposome sedimentation assays. Atg1-kinase and Atg13 interacted only with acidic synthetic lipid (ASL) liposomes containing PI (**Figure 17**, **C**), confirming that both proteins specifically recognize PI.

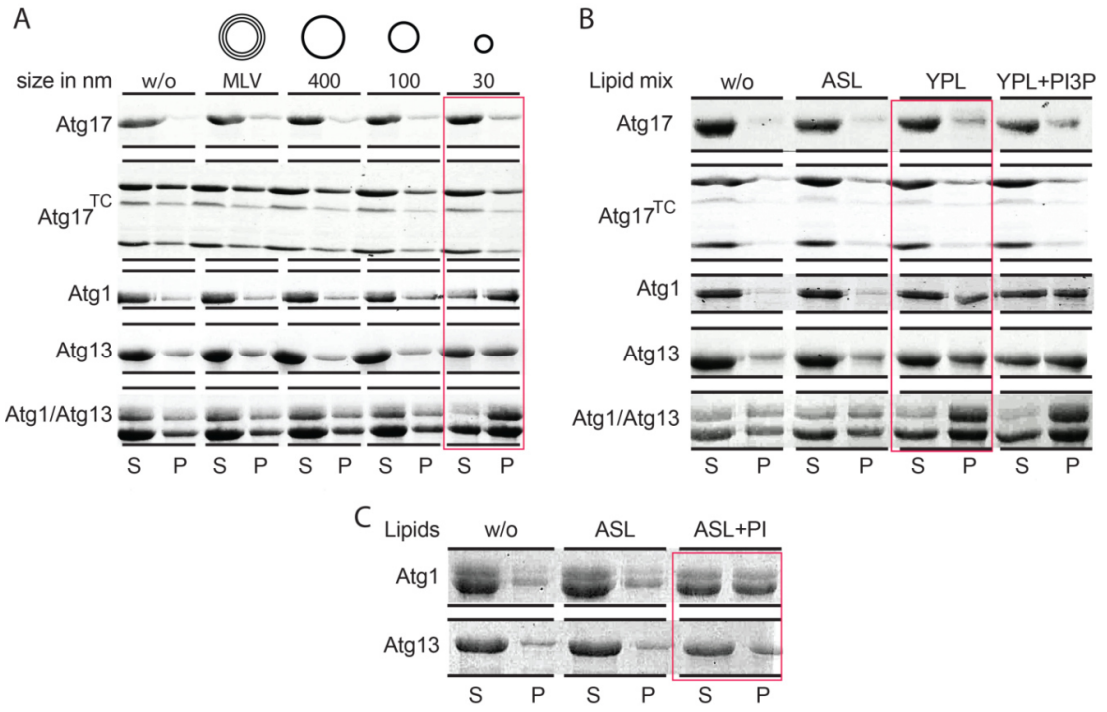

Figure 17: Analysis of the liposome sedimentation assays with Atg1^{PC} subunits. (A) Liposome sedimentation assays with YPL-MLVs or YPL-LUVs of defined sizes. Atg17 and Atg17^{TC} do not interact with liposomes of any size. Atg1-kinase and Atg13 show a strong preference for highly curved liposomes. (B) Liposome sedimentation assays with 30 nm vesicles with different lipid compositions (ASL, YPL and YPL supplemented with 5 mol% PI3P). Atg17 and Atg17^{TC} do not interact with liposomes of any lipid composition. Atg1-kinase and Atg13 show a strong preference for liposomes containing PI (YPL). Addition of PI3P does not further increase binding of Atg1-kinase or Atg13. (C) Liposome sedimentation assay with 30 nm ASL liposomes without and with 10 mol% PI as indicated. Atg1-kinase and Atg13 bind to PI supplemented vesicles. Assays were performed by Dr. Yijian Rao. (A, B, and C) Red boxes indicate best binding conditions. S = supernatant, P = pellet.

The Atg1-Atg13 subcomplex assembles at the PAS with Atg17^{TC} to form Atg1^{PC} (Kabeya et al., 2005). To test whether PAS recruitment of Atg1^{PC} is mediated by direct interactions of Atg1-kinase and Atg13 with PI, Atg1^{PC} membrane binding was analyzed by a floatation assay with YPL-LUVs of different sizes performed by Dr. Yijian Rao (2.11.9, p. 49). **Figure 18** shows that Atg1^{PC} retains the same preference for highly curved PI-containing membranes as observed for Atg1-kinase and Atg13. This indicates that the fully assembled Atg1^{PC} is targeted to highly curved, PI-containing membranes. Membrane binding and the dimeric architecture of Atg1^{PC} suggest that it functions as a membrane tether.

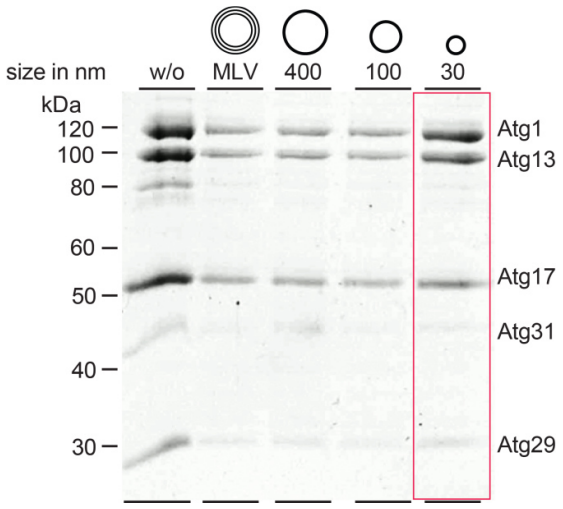

Figure 18: Analysis of the liposome floatation assay with Atg1^{PC}. Atg1^{PC} was incubated with yeast polar lipid extract YPL-MLVs or YPL-LUVs of defined sizes as indicated. Bound protein co-floated with liposomes and the floating (top) fraction was analyzed by SDS-PAGE. Atg1^{PC} shows a strong preference for highly curved PI-containing membranes. Assay was performed by Dr. Yijian Rao.

3.5.3. Membrane tethering *in vitro*

The structure of Atg17^{TC} revealed an elongated shape with two distant membrane binding regions (Ragusa et al., 2012) resembling the architecture of canonical membrane tethering factors (Yu and Hughson, 2010). Furthermore, the EAT-domain of Atg1-kinase from *L. thermotolerans* tethers LUVs *in vitro*. Atg1^{PC} assembly and disassembly could be recapitulated in this study. Furthermore, Atg1^{PC} dimerization was analyzed and it was shown that the dimerization of Atg1^{PC} is mediated by the Atg17 dimerization domain. To test the tethering capacity of Atg1^{PC} and its subunits DLS experiments with YPL-LUVs extruded trough a 30 nm pore filter were performed (2.11.2, p. 46). As shown in **Figure 17**, Atg1-kinase and Atg13 are binding 30 nm YPL-LUVs efficiently. **Figure 19** shows the measured diameter of the LUVs in absence and presence of the different Atg1^{PC} subunits. The EAT-domain of Atg1-kinase from *S. cerevisiae* shows membrane tethering activity. However, all other subunits as well as the Atg1-Atg13 subcomplex and Atg1^{PC} do not show any tethering of LUVs. Interestingly, also full length Atg1-kinase does not display any tethering function. This is not surprising since Atg1-kinase is, in contrast to the isolated EAT-domain of Atg1-kinase, monomeric (**Figure 6**) and not dimeric (Ragusa et al., 2012). Thus, the EAT-domain might specifically interact with membranes. However,

its tethering activity is likely to be mediated by artificial dimerization. Taken together, these data show that under *in vitro* conditions, Atg1^{PC} does not tether membranes. However, Atg9 vesicles were shown to be 30 - 60 nm in diameter *in vivo* (Yamamoto et al., 2012). It is likely that tethering is impaired due to the size difference of the vesicles *in vivo* and the LUVs applied in the *in vitro* tethering assay. The LUVs extruded through 30 nm pores display a diameter of ~80 nm. Thus, Atg1^{PC} could probably only accommodate two vesicles of the appropriate size without steric hindrance.

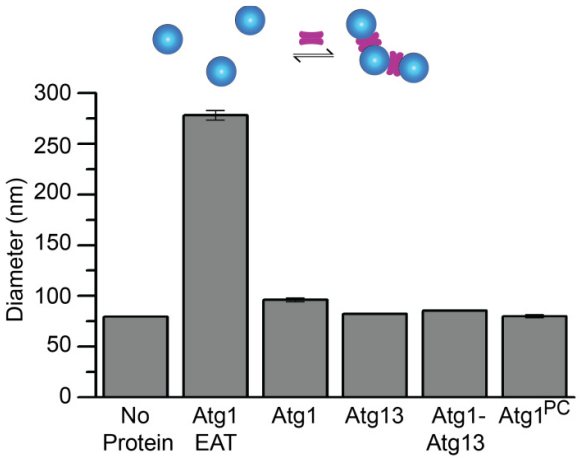

Figure 19: DLS analysis of YPL-LUVs in absence and presence of Atg1^{PC} subunits. LUVs were incubated with or without protein as indicated, and the diameter was determined by DLS. Bars represent the average of three independent experiments and error bars represent the standard deviation.

3.5.4. Atg17 senses Atg9 positive membranes

PI is found in membranes of all cellular organelles (Zinser et al., 1991). In addition, almost all of these organelles possess membranes with high curvature. Atg1^{PC} therefore needs to be directed to autophagic membranes by a different marker. Atg9 is a six-helix transmembrane protein involved in autophagy and is recruited to the PAS by Atg17 (Sekito et al., 2009). However, direct interaction between these two proteins has not been proven. To analyze whether the interaction of Atg17 with Atg9 directs Atg1^{PC} to the PAS, co-floatation assays with Atg17 and Atg9- PL, containing the conserved core region of Atg9 (Atg9^{core}) were performed. Atg9^{core} comprises amino acids from position 281 to 779 without the unstructured cytoplasmic N- and C-termini. Atg9^{core} was recombinantly expressed in *E. coli* by Dr. Yijian Rao and purified by solubilizing the membrane protein in buffer containing 1 % (w/v) LDAO. Atg9^{core} was reconstituted in liposomes to generate

Atg9-PL (2.11.9, p. 49). A floatation assay was applied to investigate the interaction of Atg17 with Atg9-PL (**Figure 20, A**). To perform semi-quantitative analyses, Atg17 was expressed with a C-terminal myc-tag for WB. As shown in **Figure 20 B**, Atg17 directly interacts with Atg9-PL, but not with liposomes without $Atg9^{core}$. However, the binding region for Atg17 in Atg9 remained to be analyzed.

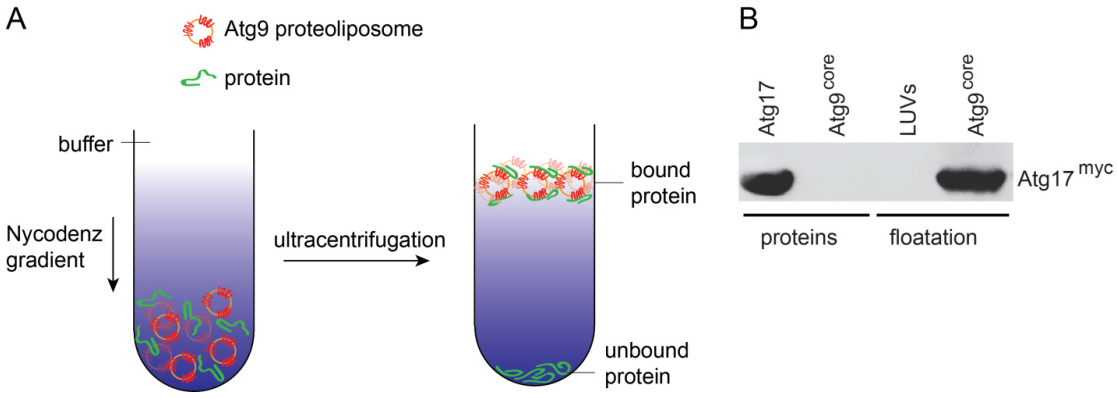

Figure 20: Co-floatation assay with Atg9-PL. (A) Schematic representation of the experimental setup. Protein and Atg9-PL are incubated and subjected to ultracentrifugation in a Nycodenz gradient. Atg9-PL and bound protein accumulate at the interface between the Nycodenz gradient and buffer. (B) WB analysis of a co-floatation experiment as described in (A). LUVs or Atg9-PL were incubated with Atg17-myc. Bound protein co-floated and the floating (top) fraction was analyzed by SDS-PAGE and WB. Atg17-myc interacts with Atg9-PL, but not with LUVs lacking Atg9. Assay was performed by Dr. Yijian Rao.

3.5.5. Deletion of Atg9 N-terminal and central regions interferes with Atg17 binding

In vivo studies showed that the interaction between Atg17 and Atg9 occurs in the N-terminal region of Atg9 (Sekito et al., 2009). However, this region was deleted in the $Atg9^{core}$ construct used for the floatation experiments. To test which part of $Atg9^{core}$ directly recognizes Atg17, co-floatation assays were performed with $Atg9^{core}$ variants lacking the cytosolic N-terminal part present in $Atg9^{core}$ ($Atg9^{\Delta N}$), the cytoplasmic middle domain ($Atg9^{\Delta cD}$) or both domains ($Atg9^{\Delta N \Delta cD}$). Interestingly, the removal of either one of the two domains reduces the affinity of Atg17 for the respective Atg9 construct significantly (**Figure 21**). This indicates that Atg9 N-terminal and cytoplasmic domain are forming an extended interaction interface with Atg17.

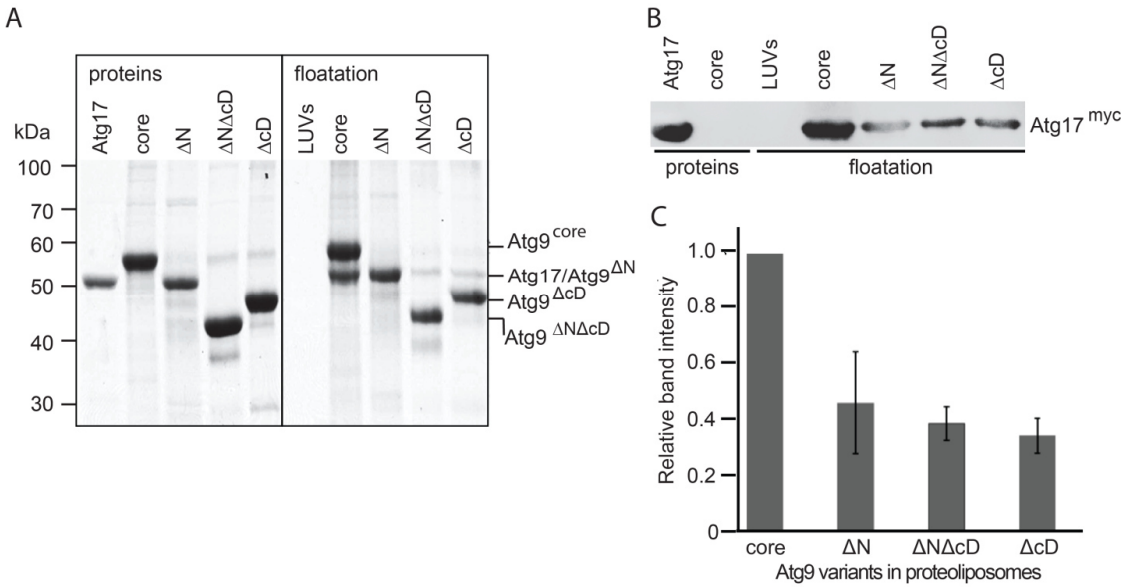

Figure 21: Atg17 interaction with Atg9 is impaired in Atg9 mutants. (A) SDS-PAGE gel showing the protein samples used for floatation (protein) and the floating fraction from the floatation assay (floatation). Atg17 and Atg9$^{\Delta N}$ are running at the same size and cannot be separated. (B) WB of samples shown in (A) to detect Atg17-myc in all samples. (C) Semi-quantitative analysis of WB shown in (B). Bars represent integrated band intensities as average of three independent experiments and error bars represent the standard deviation. A significant decrease in interaction of Atg17-myc with all mutants is detected. Intensity of Atg17-myc in the co-floatation sample with Atg9^{core} was set to 1 and used for normalization. Assay was performed by Dr. Yijian Rao.

3.5.6. Analysis of Atg9 variants *in vivo*

To confirm that the interaction between Atg17 and Atg9 is dependent on the N-terminal and cytoplasmic domains of Atg9 identified in the floatation assays, and that this interaction is required to promote autophagy, *in vivo* assays were performed. For floatation assays the truncated Atg9^{core} construct was applied. However, the cytoplasmic N- and C-terminal domains are involved in interaction with other binding partners (Webber and Tooze, 2010). To interfere specifically with the interaction between Atg17 and Atg9, only the domains from Atg9^{core} identified in the floatation assays to be involved in the interaction between Atg17 and Atg9 were removed from full length Atg9 (**Figure 22, A**). Similar expression levels of these Atg9 constructs were required to perform the *in vivo* assays. **Figure 22 B** shows the expression levels of the Atg9 constructs ectopically expressed in *ATG17-myc$_3$ atg9Δ* cells under the control of a PmaI promoter. In addition, Atg9^{WT} was ectopically expressed under the control of its endogenous promoter. The levels of all Atg9 constructs decrease upon starvation induction. However, Atg9^{WT} under

the control of the PmaI promoter is greatly overexpressed. In contrast, comparable expression levels of $Atg9^{WT}$ under the control of its endogenous promoter and Atg9-variants under the control of the PmaI promoter have been observed. Therefore, $Atg9^{WT}$ was expressed under the control of its endogenous promoter for the co-IP assays (2.13.3, p. 52). Atg17-myc_3 was immunoprecipitated (IPed) and IP was assessed by a α-myc WB. The amount of co-IPed Atg9 was determined by an α-HA WB (**Figure 22, C**). Interestingly, the amount of co-IPed Atg9 is similar for all tested Atg9 variants under non starvation conditions. Furthermore, the interaction of Atg17 and $Atg9^{WT}$ or its variants was apparently unaffected under vegetative growth conditions suggesting that under these conditions a different mode or indirect interaction between Atg17 and Atg9 takes place. However, upon starvation, Atg9 expression levels decrease (**Figure 22, B**), but interaction between Atg17 and Atg9 is dramatically upregulated while the interaction between Atg17 and the Atg9-varaints is greatly reduced (**Figure 22, C**). This shows that the mutations in Atg9 affect the interaction between Atg17 and Atg9 *in vivo*. The effect of the respective Atg9-truncations on Atg17 interaction *in vivo* is even larger than the effect *in vitro*.

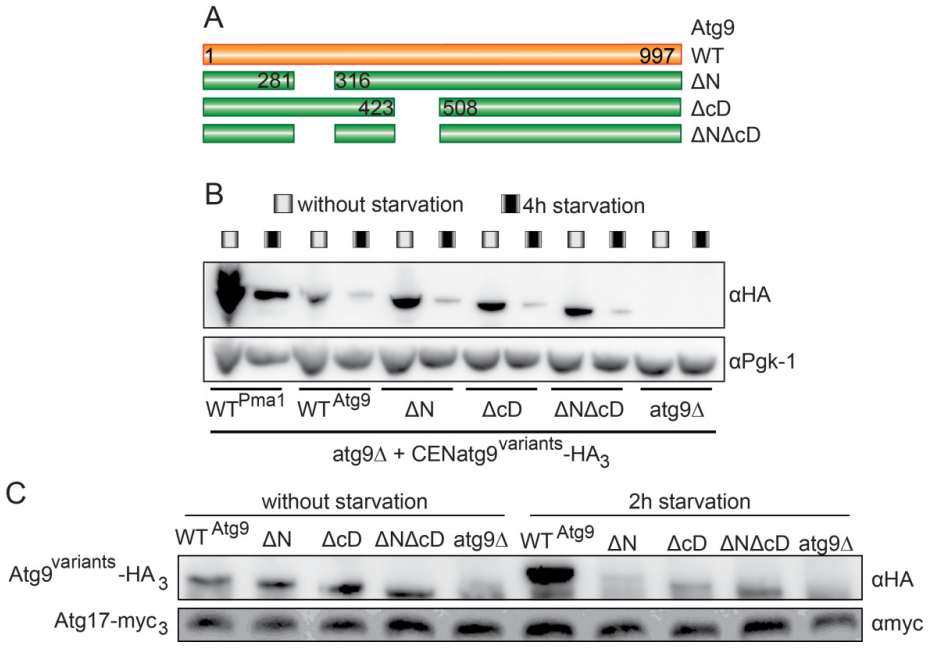

Figure 22: Atg9 interacts with Atg17 *in vivo*. (A) Schematic representation illustrates Atg9-variants generated for *in vivo* experiments. (B) Expression levels of Atg9-variants under non-starvation and starvation conditions as indicated. (C) IP of Atg17-myc_3 from $ATG9^{WT}$, $ATG9^{\Delta N}$, $ATG9^{\Delta cD}$ or $ATG9^{\Delta N\Delta cD}$ and *atg9*Δ cell-lysates without and after 2 h starvation. Atg9 co-IP was assessed by a α-HA WB. Under non-starvation conditions interaction of Atg9-varaints with Atg17 is comparable to $Atg9^{WT}$ while interaction between Atg17 and the Atg9-variants is impaired upon autophagy induction.

3.5.7. Atg17 interaction with Atg9 is required to promote autophagy

To investigate the role of the interaction between Atg17 and Atg9 for autophagy *in vivo*, the Pho8Δ60 assay was applied. ALP transport to and its activation in the vacuole can be monitored using this assay which is a measure for non-selective autophagy flux (2.13.2, p. 51). For this assay the Atg9 variants described under 3.5.6 (**Figure 22, A**) were used. HA-tagged Atg9-variants were ectopically expressed from a plasmid in *PHO8Δ60 atg9Δ* cells. In accordance with the data obtained in the co-floatation and co-IP experiments, autophagic flux is significantly decreased in cells expressing one of the Atg9-variants (**Figure 23**). This shows that the interaction between Atg17 and Atg9 is required to promote autophagy *in vivo*. Interestingly, the difference between Pho8Δ60 activity in cells expressing Atg9 under the control of the PmaI or its endogenous promoter is only about 20 %. The change in expression level between Atg9 expressed under the control of these two promoters is significantly larger (**Figure 22, B**). This indicates that Atg9 expression levels do not influence its activity dramatically. It was reported that during autophagy initiation three Atg9-vesicles (each Atg9 vesicle containing ~27 Atg9-molecules) assemble at the PAS (Yamamoto et al., 2012). Probably only a certain amount of Atg9-molecules is required to provide enough lipids from Atg9-vesicles to initiate the nucleation of the phagophore. Taken together, the Pho8Δ60 assay and the co-IP assay show that the interaction interface between Atg17 and Atg9 is important to promote autophagy and that there might be different modes of interaction between Atg17 and Atg9 dependent on nutrient status.

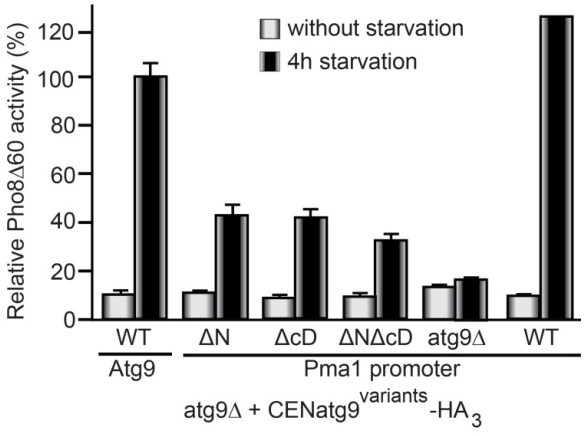

Figure 23: Cytoplasmic domains of Atg9 are required to promote autophagy. Pho8Δ60 assay of non-starved (white bars) and starved (black bars) $ATG9^{WT}$, $ATG9^{\Delta N}$, $ATG9^{\Delta cD}$ or $ATG9^{\Delta N\Delta cD}$ and *atg9*Δ cells (under the control of Atg9- or Pma1-promoter as indicated). The Pho8Δ60 activity of starved $ATG9^{WT}$ cells (Atg9-promoter) was set to 100 % and used for normalization. Bars represent the average of three independent experiments and error bars represent the standard deviation.

3.5.8. Atg1-kinase and Atg13 activate Atg17^{TC} for Atg9 binding

As observed in the IP assay, the interaction between Atg17 and Atg9 is greatly enhanced upon autophagy induction (**Figure 22**). However, how this increase is regulated remained unknown. Upon induction of starvation Atg13 is dephosphorylated and Atg1^{PC} assembles (Kamada, 2010) which indicates that Atg1^{PC} assembly could play a role in regulating the interaction of Atg17 with Atg9. Furthermore, Atg31 and Atg29 were proposed to exhibit an inhibitory effect on Atg17^{TC} binding to Atg9 (Chew et al., 2013; Ragusa et al., 2012; Stanley et al., 2013). The *in vitro* assay developed in this study allowed the regulation of Atg1^{PC} to be directly addressed. To test these hypotheses, floatation assays were performed with Atg9-PLs and different combinations of Atg1^{PC} subunits by Dr. Yijian Rao (**Figure 24**, **A and B**). Atg17^{TC} showed significantly reduced interaction with Atg9 indicating that Atg29 and Atg31 indeed interfere with binding by blocking the concave side of Atg17. Atg1-kinase does not release this inhibition. However, Atg13 directly interacts with Atg17^{TC} and bridges this subcomplex and Atg1-kinase (**Figure 12**). Accordingly, Atg13 is able to release the inhibition by Atg29 and Atg31 which is shown by the increased binding capacity of Atg17^{TC} to Atg9. Atg17^{TC} interaction with Atg9 is fully restored to Atg17 level in the presence of the Atg1-Atg13 subcomplex. This shows that the interaction between Atg17 and Atg9 depends on Atg1^{PC} assembly.

The observation that Atg1-kinase phosphorylates Atg1PC subunits in vitro and thereby disassembles Atg1PC into its subcomplexes (**Figure 13**) led to the question whether Atg1^{PC} induced phosphorylation impacts on the interaction of Atg17 with Atg9. Atg1^{PC} was therefore incubated with 1 mM ATP in the presence of Atg9-PL. Atg1-kinase, Atg13 and Atg29 were phosphorylated as indicated by their electrophoretic mobility shift (**Figure 24**, **C**). No band shift was observed for the interaction partners Atg17 and Atg9^{core} as well as for Atg31 which indicates that these proteins are not phosphorylated. Upon phosphorylation, interaction of Atg17 and Atg9-PL is almost completely abolished (**Figure 24**, **A and B**). Considering that phosphorylation leads to disassembly of the complex into Atg17^{TC} and the Atg1-Atg13 subcomplexes, the interaction strength of Atg17^{TC} with Atg9-PL in the presence of ATP was expected to be similar to the level observed for Atg17^{TC} in the absence of ATP. Because Atg17 and Atg9^{core} are not phosphorylated, the strong decrease in interaction between Atg17^{TC} and Atg9-PL needs to be caused by one of the other phosphorylated subunits. The only phosphorylated subunit in Atg17^{TC} is Atg29, and

it is therefore likely that this subunit is involved in regulating the interaction between Atg17^{TC} and Atg9-PL. The phosphorylation sites detected in Atg29 are located in its C-terminal domain (**Table 9**) and are not involved in interaction with Atg31 (Ragusa et al., 2012). Furthermore, Atg29 phosphorylation in its C-terminal domain was described to be important for activating Atg29 and to promote autophagy (Mao et al., 2013).

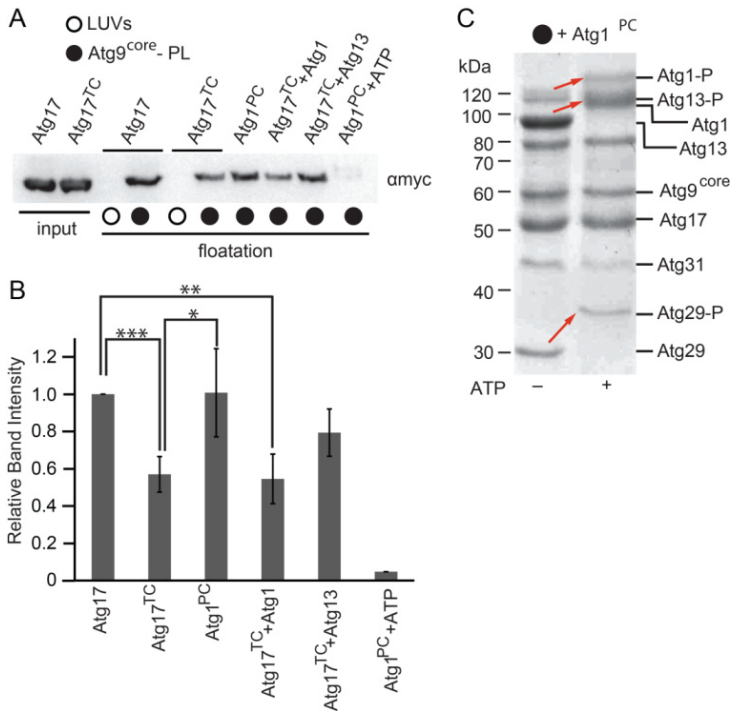

Figure 24: Atg1^{PC} assembly and phosphorylation regulates interaction of Atg17 with Atg9-PL. (A) Different combinations of Atg1^{PC} subunits were tested for their effect on the interaction of Atg17 with Atg9-PL as indicated. The floating fraction was applied to SDS-PAGE and analyzed by WB for Atg17-myc. (B) Semi-quantitative analysis of (A). Bars represent integrated band intensities as average of three independent experiments and error bars represent the standard deviation. The average intensity of Atg17-myc from floatation experiments with Atg9-PLs was set to 1 and used for normalization. P values were calculated using two-tailed Student's T-test (*, $p<0.05$; **, $p<0.01$; ***, $p<0.001$). (C) Atg1-kinase phosphorylates itself, Atg13 and Atg29 in the presence of Atg9-PL. Shifted bands are indicated (red arrows). (A, B and C) Assays were performed by Dr. Yijian Rao.

3.5.9. Atg17 possesses two Atg9 binding sites

Atg17^{TC} is a dimer of trimers (Kabeya et al., 2009) suggesting that it functions as a scaffold for a tethering complex with two binding sites for Atg9 vesicles (Ragusa et al., 2012; Stanley et al., 2013). To test whether dimerization is required for binding of Atg17^{TC} to Atg9-PL, Atg17^{monoTC} was co-floated with Atg9-PL. Atg17^{monoTC} still interacts with Atg9-PL (**Figure 25, A**), indicating that dimerization is not required for the interaction of Atg17 with Atg9. This also shows that Atg17-dimerization provides two independent binding sites for Atg9-PL. Atg17$^{1-320}$ could only be expressed in complex with Atg29 and Atg31, because the isolated protein was prone to aggregation. To analyze the effect of Atg17-dimerization on Atg9 binding, functional Atg17 was required as reference. To generate a stable monomeric Atg17 in the absence of Atg29 and Atg31, only the dimerization domain needed to be removed without affecting the overall structure of the helical bundle in the core region of Atg17. The structure of Atg17 from *S. cerevisae* was calculated as a homology model based on the *L. thermotolerans* template (Ragusa et al., 2012) using the SWISS-MODEL program (Arnold et al., 2006) (**Figure 25, B**). The resulting Atg17 construct comprising amino acids 1-354 (Atg17$^{1-354}$) could be expressed as soluble protein as well as part of the trimeric Atg17$^{1-354}$-Atg31-Atg29 complex (Atg17$^{(1-354)TC}$). Atg17$^{1-354}$ co-floated with Atg9-PL (**Figure 25, C**), confirming that the dimerization domain is not required for Atg17 interaction with Atg9. To analyze the regulation of Atg17$^{(1-354)TC}$ binding to Atg9-PL, Atg1-kinase and Atg13 were combined with Atg17$^{(1-354)TC}$ to form the truncated Atg1$^{(1-354)PC}$ complex. In contrast to the situation with Atg17^{TC}, Atg13 and Atg1-kinase were not able to release Atg17$^{(1-354)TC}$ inhibition. This suggests that the C-terminal part of Atg17 plays a central role in regulating the interaction of Atg1^{PC} with Atg9. Taken together, these results show that Atg17^{TC} is activated for Atg9 binding by assembly of Atg1^{PC} with Atg13 and Atg1-kinase. The C-terminal part of Atg17 thereby plays an important role in regulating Atg1^{PC} interaction with Atg9. Atg1^{PC} architecture suggests that two Atg9 vesicles of the appropriate size can be brought into close proximity by Atg1^{PC}. This suggests a model in which Atg1^{PC} binds highly curved PI containing vesicles through the membrane interacting components Atg1-kinase and Atg13. Specificity for autophagic membranes is conveyed by Atg17 which directly interacts with Atg9.

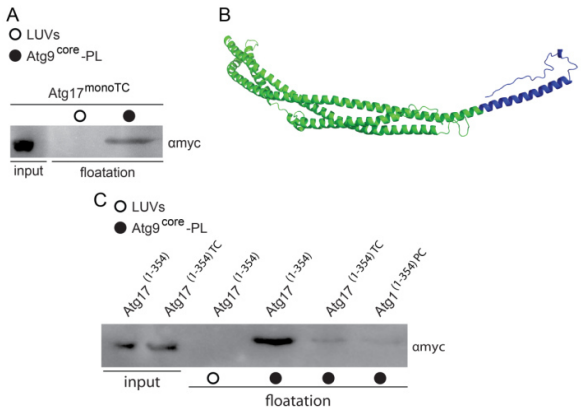

Figure 25: Atg17 dimerization domain is not required for interaction with Atg9-PL, but for regulation of Atg17^{TC} binding. (A) Atg17^{monoTC} is able to interact specifically with Atg9-PL. (B) Ribbon model of Atg17^{TC} from *S. cerevisiae* based on the Atg17^{TC} structure from *L. thermotolerans.* The model was calculated using PDB data set 4HPQ (Ragusa et al., 2012) and the program SWISS-MODEL (Arnold et al., 2006). The ribbon model was generated using PyMOL (SchrödingerLLC.). The part of the dimerization domain of Atg17 which is not involved in forming the triple helix bundle (amino acids 354 - 417) is highlighted in blue. (C) Atg17$^{1-354}$ is able to interact specifically with Atg9-PL. The presence of Atg13 and Atg1-kinase does not influence Atg17$^{(1-354)TC}$ binding capacity to Atg9. (A and C) The floating fraction was applied to SDS-PAGE and analyzed by WB for Atg17$^{1-320}$-myc (A) or Atg17$^{1-354}$-myc (C).

4. Discussion

4.1. Atg1^{PC} assembly, disassembly and architecture

Atg1-kinase is one of the most important regulators of autophagy and plays an indispensable role in organizing the PAS (Cheong et al., 2008; Kawamata et al., 2008). It integrates signaling pathways from upstream nutrient-sensing kinases such as TORCI (Noda and Ohsumi, 1998) and PKA (Wang et al., 2001) and serves as a scaffolding complex while its kinase activity is required to regulate the recruitment and recycling of Atg proteins, such as Atg9 (Cheong et al., 2008). However, how Atg1^{PC} is assembled and which subcomplexes constitute Atg1^{PC} remained under debate. It was shown that in *atg17Δ* cells the interaction between Atg1-kinase and Atg13 was not affected. In contrast, in *atg13Δ* cells the interaction between Atg1-kinase and Atg17 was impaired (Kabeya et al., 2005). The SPR experiments in this study (**Figure 12**) show that Atg13 directly interacts with Atg17 and thereby bridges Atg17 and Atg1-kinase which is in line with the previous results. Recombinantly expressed Atg13 is lacking any phosphorylation as confirmed by MS/MS analysis (**Table 9**) which is the phosphorylation state of Atg13 suggested to be required for assembly of Atg1^{PC} (Kamada et al., 2010). Atg17 forms a complex with Atg29 and Atg31 so that these proteins could play a role in the interaction of Atg13 with Atg17. The SPR experiments with Atg17 and Atg17^{TC} (**Figure 12**) allow addressing this question easily. The results show that Atg17 can interact with Atg13 independently of the presence of Atg29 and Atg31. However, since binding kinetics of Atg1-kinase to Atg13 differ in the presence of Atg29 and Atg31, a role for the Atg29-Atg31 subcomplex in Atg1^{PC} assembly is likely. The presence of Atg29-Atg31 leads to slower binding and dissociation kinetics which could indicate that these subunits influence Atg1^{PC} assembly by sterically hindering Atg1-kinase binding or by inducing conformational changes in the Atg17^{TC}-Atg13 subcomplex. Recent data show that the binding sites of Atg31 and Atg13 are located close to each other on Atg17. Furthermore, it was shown that the Atg17 binding site and the Atg1-kinase binding site on Atg13 are also located in close proximity (Fujioka et al., 2014). Sterical hindrance and the need for conformational rearrangement of the proteins could therefore influence Atg1^{PC} complex assembly in the presence of the Atg31-Atg29 subcomplex. In addition, Atg29 is an intrinsically disordered protein (IDP) (Mao et al., 2013) which remains unstructured in its C-terminal part even upon Atg17^{TC} formation

(Ragusa et al., 2012). It is therefore tempting to speculate that the unstructured C-terminal part of Atg29 is involved in altering Atg1-kinase binding kinetics. The exact role of the C-terminal part of Atg29 is poorly understood, although a role in switching between selective and non-selective autophagy has been proposed (Mao et al., 2013). Interaction of Atg29 with other binding partners dependent on its phosphorylation status could lead to structuring its C-terminal part and therewith be an additional mechanism for autophagy regulation.

The assembly and disassembly of $Atg1^{PC}$ is regulated through the phosphorylation status of Atg13 (Kamada et al., 2010), rendering the latter to be a central regulator for complex formation. In this study, the disassembly of $Atg1^{PC}$ could be recapitulated *in vitro* (**Figure 13**). Atg1-kinase mediated phosphorylation *in vitro* led to disassembly of $Atg1^{PC}$ into the $Atg17^{TC}$ and Atg1-Atg13 subcomplexes. Some of the previously found regulatory phosphorylation sites in Atg13 (Kamada et al., 2010) were found to be phosphorylated in this assay (**Table 9**). *In vivo* the regulatory sites in Atg13 were shown to be phosphorylated by other kinases than Atg1-kinase such as TORCI or PKA (Budovskaya et al., 2004; Cutler et al., 1999). However, to recapitulate disassembly the unregulated phosphorylation of $Atg1^{PC}$ by Atg1-kinase was sufficient. Whether phosphorylation of $Atg1^{PC}$ by Atg1-kinase plays a role *in vivo* is unclear. The capability of Atg1-kinase to phosphorylate $Atg1^{PC}$ subunits *in vitro*, indicates that Atg1-kinase could exert self-limiting functions leading to disassembly and deactivation of $Atg1^{PC}$. Another possibility is that the free subcomplexes are required for later steps in autophagy. Atg1-kinase phosphorylated a wide range of sites without a clear consensus pattern which indicates that the incubation time was long enough that most of the accessible phosphorylatable residues present in $Atg1^{PC}$ were targeted by Atg1-kinase in this assay. Even under these highly phosphorylated conditions, however, the subcomplexes remained stable. This supports the idea that Atg1-Atg13 forms a stable subcomplex that is constitutively formed under vegetative and starvation conditions, independent of its phosphorylation state. This is further supported by the finding that the only conserved regulatory residues in Atg13 are S494 and S496 which are in contact with the MIM2 domain of Atg1-kinase (Fujioka et al., 2014). Especially S469 which is located in the MIM(C)-motif of Atg13 is in close contact with the MIT1-domain of Atg1-kinase (**Figure 26**). This residue was found to be phosphorylated in the *in vitro* assay in this study (**Table 9**) which did not influence the formation of the Atg1-Atg13 subcomplex. However, as discussed below, other factors could lead to disassembly of this subcomplex.

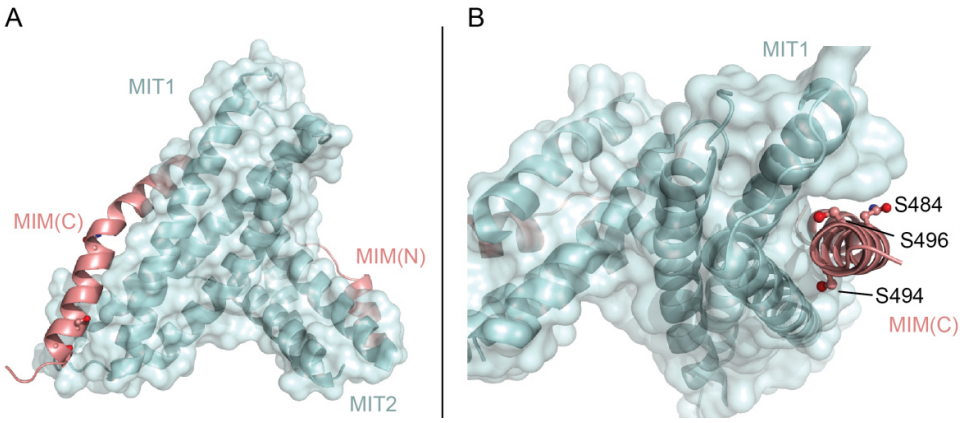

Figure 26: Crystal structure of the Atg1-kinase MIT-domains in complex with the Atg13 MIM-motif containing peptides. (A) Overview of the Atg1-kinase MIT-domains in complex with the MIM-motif containing peptides of Atg13. (B) View of the binding region of the Atg1-kinase MIT1-domain and the MIM(C)-motif of Atg13. The conserved residues S484, S494, and S496 are shown. S496 is in close contact with the MIT1-domain. (A and B) The ribbon and protein surface model was generated using PyMOL (SchrödingerLLC.) from PDB file 4P1N (Fujioka et al., 2014) by Dr. Thomas Wollert.

Previous studies suggested different models for $Atg1^{PC}$ architecture. Dimerization of $Atg1^{PC}$ was suggested to be conferred by an Atg13-induced dimerization of Atg1-kinase (Yeh et al., 2011). More recent data showed that Atg17 forms an elongated double crescent and that Atg17 possesses a C-terminal dimerization domain, arguing that Atg17 leads to dimerization of $Atg1^{PC}$ (Chew et al., 2013; Ragusa et al., 2012). Furthermore, Atg1-kinase has been suggested to be dimeric through dimerization of its EAT-domain (Ragusa et al., 2012). Analysis of full length Atg1-kinase in this study showed that Atg1-kinase is monomeric excluding the possibility that Atg1-kinase mediates dimerization. Moreover, the Atg1-Atg13 subcomplex runs at an elution volume in SEC that corresponds to a sterical heterodimer, arguing that Atg13 does not mediate or induce dimerization of Atg1-kinase. Data from this study showed that $Atg1^{PC}$ is a dimer of pentamers and that removal of the dimerization domain of Atg17 leads to a dimerization defect in $Atg1^{PC}$ (**Figure 11**). **Figure 27** shows a model for $Atg1^{PC}$ organization. Atg13 thereby bridges Atg17 and Atg1-kinase. R_H of $Atg1^{PC}$ measured by DLS is only increased by 3 nm compared to $Atg17^{TC}$ which indicates that Atg13 and Atg1-kinase could be flexibly attached or align along the axis of Atg17.

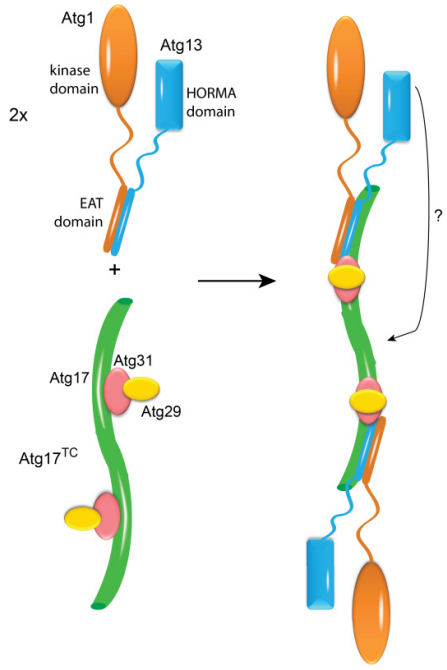

Figure 27: Atg1^{PC} architecture based on structural data and the results from this study. Atg17^{TC} forms an elongated dimer with a C-terminal dimerization domain. Atg13 bridges Atg1-kinase and Atg17 by binding both of them. Atg1^{PC} assembly leads to structural reorganization within Atg17^{TC}. The Atg31-Atg29 subcomplex is moved in a way that the proposed Atg9 binding site on Atg17 becomes available.

4.2. Regulation of Atg9 binding to Atg17^{TC}

After initiating the assembly of Atg1^{PC} at the PAS, Atg9-positive vesicles are recruited in an Atg17 dependent manner (Sekito et al., 2009). The interaction of Atg17 and Atg9 was found to be induced upon starvation (**Figure 22**) suggesting that Atg1^{PC} assembly is involved in regulating this activity. How the interaction of Atg17 with Atg9 is regulated remained obscure. The *in vitro* data from this study show that Atg1^{PC} assembly is a main regulator of the interaction between Atg17 and Atg9. The structure of Atg17^{TC} revealed that the Atg31-Atg29 subcomplex blocks the concave side of Atg17 (Chew et al., 2013; Ragusa et al., 2012) and it was suggested that the Atg31-Atg29 subcomplex has to be shifted in order to allow Atg9 to bind to Atg17 (Stanley et al., 2013). However, experimental evidence for a role of the Atg31-Atg29 subcomplex in regulating Atg17 interaction with Atg9 has been missing. Furthermore, according to the model derived from the structure of Atg17^{TC}, Atg9 is sufficient to induce a conformational change in Atg17^{TC} that allows Atg9 to bind Atg17 (Ragusa et al., 2012; Stanley et al., 2013). This model does not include a regulatory mechanism for the induction of the interaction between Atg17 and

Atg9. Co-IP assays in this study, however, clearly show that the interaction between Atg17 and Atg9 is induced upon starvation mediated induction of autophagy (**Figure 22**). This means that the interaction between Atg17 and Atg9 is inhibited under vegetative conditions. This is in line with the finding that $Atg17^{TC}$ shows reduced affinity to Atg9-PL when compared to Atg17 *in vitro* (**Figure 24**). The reduced affinity further supports the idea that the Atg31-Atg29 subcomplex inhibits Atg9 binding by blocking the concave face of Atg17. Only fully assembled $Atg1^{PC}$ restores the interaction of Atg17 with Atg9-PL to the level observed when only Atg17 is co-floated with Atg9-PL (**Figure 24**). Furthermore, the floatation data show that the underlying regulatory mechanism involves the dimerization domain of Atg17. If the dimerization domain is missing, $Atg17^{1-354}$ still binds Atg9-PL efficiently. However, a regulatory effect of Atg1-kinase and Atg13 on binding of $Atg17^{(1-354)TC}$ to Atg9-PL is not observed suggesting that the C-terminal dimerization domain of Atg17 is required for regulation (**Figure 25**). C-terminal of its dimerization domain, Atg17 contains a region with a short α-helix and a short β-strand (**Figure 4**). Since this region of Atg17 is not directly involved in dimerization (Ragusa et al., 2012), it could play a role in regulation. As discussed before, R_H of $Atg1^{PC}$ is only slightly increased compared to R_H of $Atg17^{TC}$ suggesting that Atg13 and Atg1-kinase are folded along the axis of Atg17. The putative regulatory peptide at the C-terminus of Atg17 could provide an interaction interface with Atg13 and/or Atg1-kinase to align these proteins along the Atg17 crescent. As observed during $Atg1^{PC}$ assembly, the binding kinetics of Atg1-kinase to the $Atg17^{TC}$-Atg13 complex are reduced in the presence of the Atg29-Atg31 subcomplex (**Figure 12**). This could be an effect of the close proximity of binding sites for Atg13 and Atg31 on Atg17 and for Atg1-kinase and Atg17 on Atg13 leading to steric hindrance. However, this could also indicate that Atg1-kinase is sterically hindered in aligning along the Atg17 axis by the Atg29-Atg31 subcomplex. The conformational reorganization of the Atg31-Atg29 subcomplex, that is required for the interaction of $Atg17^{TC}$ with Atg9, could be mediated by orienting Atg13 and Atg1-kinase through an interaction with the C-terminal peptide of Atg17. This reorganization could take place as a consequence of different effects. By positioning Atg13 and Atg1-kinase along the axis of Atg17, the Atg31-Atg29 subcomplex could be moved passively. Another possibility is that the regulatory peptide on the C-terminus of Atg17 could interact with the largely unstructured C-terminal domain of Atg29. Once Atg13 and Atg1-kinase bind, they could compete with Atg29 for interaction with the regulatory peptide. Once Atg29 does no longer interact with the C-terminal part of Atg17, the whole Atg31-Atg29 subcomplex would become more

flexible which would facilitate Atg9 binding to Atg17. This would also mean that binding sites for Atg9 and Atg31 are not fully overlapping on Atg17 which is supported by the finding that these subunits are not replaced by Atg9 in floatation assays. The Atg31-Atg29 subcomplex would rather be moved apart. This would allow $Atg17^{TC}$ to return quickly to its inactive state once $Atg1^{PC}$ has been disassembled.

4.3. $Atg1^{PC}$ membrane interaction and role as a tethering factor

In this study it was shown that $Atg1^{PC}$ contains two binding sites for autophagic membranes. These sites are located on opposite sides of the double crescent formed by Atg17 and a role of $Atg1^{PC}$ as a tethering complex in autophagy has been suggested based on the structure of $Atg17^{TC}$ and on the membrane tethering capacity of the EAT-domain of Atg1-kinase (Ragusa et al., 2012; Stanley et al., 2013). Tethering of membranes precedes fusion. Tethering factors thereby capture the membranes that are subsequently fused by SNARE-proteins which accelerate rate limiting steps in membrane fusion and directly provide energy by forming a 4-helix bundle (Yu and Hughson, 2010). However, in contrast to the isolated EAT-domain of Atg1-kinase, full length Atg1-kinase was shown to be monomeric in solution (**Figure 6**) and did not possess membrane tethering capacity (**Figure 19**). In liposome sedimentation assays, Atg1-kinase showed a strong preference to bind PI-containing membranes, indicating that it is not able to tether membranes itself. It can, however, confer tight binding of $Atg1^{PC}$ to membranes (**Figure 17**). Conformational rearrangement within $Atg1^{PC}$ mediates the specific interaction with autophagic membranes by recognizing the specific marker Atg9 and by providing close contact through Atg1-Atg13 membrane binding. In *atg1Δ* and *atg13Δ* cells Atg9-vesicles accumulate at the PAS, which indicates that these subunits are required for nucleation of the phagophore (Mari et al., 2010). In agreement with the *in vivo* observations, the ability of Atg17 to bind to Atg9-PL further supports the idea that $Atg1^{PC}$ could be an autophagy specific tethering factor. Especially the fact that $Atg17^{TC}$ dimerization is not required for Atg9-PL binding (**Figure 25**) demonstrates the presence of two independent Atg9-PL binding sites in full length $Atg17^{TC}$. Another tethering factor that was reported to be involved in autophagy is the TRAPPIII complex (Lynch-Day et al., 2010). Its effector Ypt1, was shown to be recruited to the PAS by Atg9 to mediate homotypic fusion of Atg9-vesicles (Kakuta et al., 2012). In addition, the TRAPPIII complex was shown to play mainly a role in Atg9 trafficking and

to be especially important in the cvt pathway (Shirahama-Noda et al., 2013). However, this does not exclude the presence of another tethering complex that is specific for autophagy. The different tethering complexes could act at different steps in phagophore biogenesis or take over different roles. Tethering factors span long distances to tether two membranes (Yu and Hughson, 2010) which is only partly done by $Atg1^{PC}$ since the dimerization domain of Atg17 is the only part that separates the two membrane binding sites. Architecture of $Atg1^{PC}$ therewith does not allow spanning long distances. This suggests that $Atg1^{PC}$ and membrane contact might trigger SNARE-mediated fusion by accelerating SNARE-priming. A sequential mechanism in which Atg9 vesicles are first tethered by other autophagy specific tethering complexes and subsequently transferred to $Atg1^{PC}$ that is involved in regulating phagophore formation and growth could explain both, the architecture of $Atg1^{PC}$ and the requirement for other tethering factors. In other words, first capturing of Atg9 vesicles is performed by long ranging tethering factors and then phagophore formation and expansion is regulated by the short ranging docking factor $Atg1^{PC}$.

To be able to act as a tethering factor, dimerization of $Atg1^{PC}$ is required. However, *in vivo* analyses of autophagy in this study show that early steps in autophagy are only partially affected if $Atg1^{PC}$ dimerization is inhibited. Atg8 conjugation to PE still takes place in *atg17Δ* and $ATG17^{1\text{-}320}$ cells while the number of Atg8 puncta is reduced (**Figure 14**). The conjugation of Atg8 to PE is still promoted indicating on one hand that the regulatory function of $Atg1^{PC}$ in autophagy induction is largely unaffected. On the other hand, the generation of GFP-Atg8 puncta is impaired which indicates that initiation of the phagophore is affected. Analysis of membrane dynamics further revealed altered kinetics of autophagic membranes in *atg17Δ* and $ATG17^{1\text{-}320}$ cells (**Figure 15**) indicating that not only the initiation of the phagophore, but also its expansion is affected. Atg9 localizes to the edges of the growing autophagic membrane. Atg17 and Atg13 are localized to the vacuole-phagophore contact site (VPCS) while Atg1-kinase is distributed all over the autophagic membrane (Suzuki et al., 2013). Therefore, on one edge Atg9 co-localizes with Atg1-kinase, Atg13 and Atg17. The curvature sensing activity of Atg1-Atg13 could be responsible for restricting their interaction partners, including Atg17 and its interaction partner Atg9, to the VPCS. This indicates that these proteins work in concert at the VPCS and that $Atg1^{PC}$ could have a function as a membrane tether required for expansion of autophagic membranes. This is supported by the finding that expansion kinetics of

autophagic membranes are affected in *atg17Δ* and *ATG17*$^{1-320}$ cells. Taken together, the role of Atg1^{PC} dimerization seems to be complex. Whereas the kinase activity of Atg1-kinase was described to be essential for Atg protein dynamics at the PAS (Cheong et al., 2008), the importance of Atg1-kinase dimerization was poorly analyzed due to the lack of detailed knowledge about Atg1^{PC} dimerization. However, in line with the findings in this study, increase in Atg1-kinase dimerization has been shown to increase autophagic flux (Yeh et al., 2011).

4.4. Roles of Atg1^{PC} in the context of its assembly state

Three Atg9 vesicles were shown to be involved in initiating the autophagic membrane (Yamamoto et al., 2012). Atg9 was further shown to be a target of Atg1-kinase and that Atg1-kinase mediated phosphorylation of Atg9 is required for autophagy (Papinski et al., 2014). Atg9 phosphorylation mainly affected the recruitment of Atg18. This emphasizes the dual role of Atg1^{PC}, as a structural factor in PAS organization and as a kinase in autophagosome maturation. Whether phosphorylation of Atg9 by Atg1-kinase influences its binding properties to Atg17 could not be analyzed. The phosphorylation sites in Atg9 targeted by Atg1-kinase are mainly located in the unconserved C-terminal region of Atg9. This region is not present in the Atg9^{core} construct used in this study. Therefore, it cannot be excluded that phosphorylation of Atg9 also affects its binding properties to Atg17. However, Atg9 has to be released from Atg1^{PC} in a regulated manner. Data from this study suggest that Atg1-kinase mediated phosphorylation can induce release of Atg9. The disassembly of Atg1^{PC} into its subunits should already be sufficient to reduce affinity of Atg17^{TC} to Atg9 by the influence of the Atg29-Atg31 subcomplex. The disassembly of Atg1^{PC} would furthermore make Atg1-kinase and Atg13 available for functions that require them not to be part of Atg1^{PC} as suggested by their different localizations on the autophagic membrane (Suzuki et al., 2013). In addition, Atg1^{PC} might need to be released from the site of tethering before SNAREs could facilitate membrane fusion after SNARE-priming.

Atg1^{PC} assembles from its subcomplexes upon autophagy induction. Once Atg1^{PC} assembles *in vitro*, it can be disassembled in a phosphorylation dependent manner. MS/MS analyses showed that in this case some of the regulatory phosphorylation sites of Atg13 are phosphorylated (**Table 9**) including the conserved residue S496 (**Figure 26**). Nevertheless,

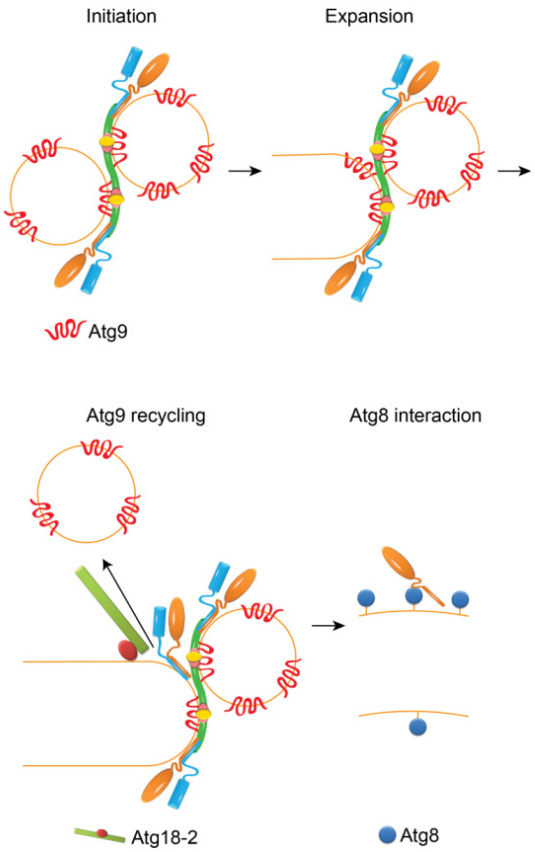

Figure 28: Atg1-kinase could play different roles in autophagy. Localization analysis and data from this study support the idea that Atg1-kinase plays different roles in autophagy depending on its interaction with other Atg1^{PC} subunits.

Atg1-kinase and Atg13 still form a complex whereas they dissociate from Atg17^{TC} which also forms a stable complex upon phosphorylation. This supports the finding that Atg1-kinase and Atg13 form a constitutive complex. However, upon autophagy induction Atg1-kinase and Atg13 were found to display distinct distributions along the autophagic membrane in a fine mapping analysis (Suzuki et al., 2013). Atg1-kinase is found on the whole autophagic membrane, while Atg13 only localizes to the VPCS. This could be due to disassembly of the Atg1-Atg13 complex by additional phosphorylations introduced by other regulatory kinases or by replacement of Atg13 by other binding partners.

Figure 28 summarizes possible roles for Atg1-kinase in different Atg1^{PC} assembly states. Due to its architecture as well as its Atg9 and membrane binding capacity, Atg1^{PC} possesses the structural features to act as a tethering factor (**Figure 27**). Since defects in Atg17 dimerization do not only affect the initiation step of autophagy (**Figure 14** and **Figure 15**), a role as a tethering factor in membrane expansion is also likely. The Atg1-Atg13 subcomplex was shown to be involved in Atg9 recycling from the autophagic

membrane (Reggiori et al., 2004). Furthermore, Atg8 was reported to be a scaffold for Atg1-kinase recruitment to the autophagic membrane (Alemu et al., 2012), which could be confirmed *in vitro* in this study (**Figure 16**). This indicates that Atg1-kinase could play a role in autophagic membrane scaffold dynamics. Taken together, these data suggest a mechanism where different $Atg1^{PC}$ assembly states are required for different tasks during autophagy. Fully assembled $Atg1^{PC}$ is required for early stages of autophagy (Cheong et al., 2008). However, $Atg1^{PC}$ as well as the free subcomplexes and subunits are likely to play also a role in later stages.

4.5. Atg17 and Atg11 in phagophore expansion

Atg1-kinase functions not only under starvation conditions, but also during vegetative conditions by mediating specific autophagy (Kraft et al., 2009). In *atg17Δ* cells, GFP-Atg8 turnover is not fully inhibited (**Figure 14**). However, Pho8Δ60 assays showed that non-selective autophagy is almost completely blocked (Cheong et al., 2005). At the same time larger, but less abundant GFP-Atg8 positive membrane structures are observed in *atg17Δ* cells (**Figure 14** and **Figure 15**). Thus, an autophagic membrane is being formed and expands, suggesting that nucleation and expansion do either not entirely depend on Atg17 or that redundant mechanisms could take over. Atg11 was suggested to be a scaffold protein in the selective cvt pathway (Shintani and Klionsky, 2004). Furthermore, it was shown that Atg9 recruitment to the PAS is impaired in *atg11Δ atg17Δ* cells (Suzuki et al., 2007) and that Atg11 interacts with Atg1-kinase and Atg13 in the cvt pathway (Kamada et al., 2000). Moreover, Atg11 is interacting with Atg9 under vegetative and under starvation conditions as shown by co-IP assays (Sekito et al., 2009). Taken together, these data suggest that Atg11 could be a functional homologue of Atg17 in selective autophagy. The mechanism by which the shape of the phagophore membrane is determined in the non-selective autophagy pathway is not clear. However, in selective autophagy Atg11 recognizes cargo through binding sites and assists in forming the autophagic membrane in close contact around the cargo (Yorimitsu and Klionsky, 2005). If Atg11 replaces Atg17 in starvation-induced autophagy, this could result in a combination of effects. Due to a defect in regulating expansion of the phagophore, larger autophagosomes are produced. These autophagosomes are likely to be in contact with cargo due to the cargo binding property of

Atg11. The large structures are not delivering cytoplasmic cargo to the vacuole (Cheong et al., 2005) and therefore need to be disassembled and recycled in the cytoplasm.

4.6. Switching between selective and non-selective autophagy

How the switch between the selective and the non-selective pathway of autophagy is mediated is poorly understood. Recently it was suggested that the phosphorylation of Atg29 in its C-terminal regulatory peptide could be involved in regulating the interaction of Atg29 with Atg11 (Mao et al., 2013). Three phosphorylation sites in the C-terminal part of Atg29 were identified to be required for interaction of Atg29 with Atg11. In this study it was shown that phosphorylated $Atg17^{TC}$ does no longer interact with Atg9 (**Figure 24**). The only subunit that was found to be phosphorylated was Atg29 (**Table 9**). Atg17 interaction with Atg9 is much weaker under vegetative conditions than under starvation conditions *in vivo* (**Figure 22**). The *in vitro* floatation experiments with Atg9-PL and $Atg17^{TC}$ or $Atg1^{PC}$ which are mimicking the vegetative and starvation conditions, respectively, show a significantly smaller difference in interaction strength between Atg17 and Atg9 compared to the *in vivo* data (**Figure 24**). This already indicates that the interaction of Atg17 with Atg9 is regulated by additional mechanisms other than $Atg1^{PC}$ complex assembly. In contrast to Atg17 which strongly interacts with Atg9 under starvation conditions, Atg11 was found to interact with Atg9 under both, vegetative and starvation conditions similarly (Sekito et al., 2009). This indicates that affinity of Atg17 for Atg9 could be an important regulatory factor for induction of non-selective autophagy. However, a second role of phosphorylation of Atg29 in autophagy is reasonable. It is important to note that Atg29 is phosphorylated under starvation conditions (Mao et al., 2013) when Atg17 and Atg9 interaction is increased. In the *in vitro* assays in this study phosphorylation was introduced by Atg1-kinase in an unregulated manner. Whether these phosphorylations introduced by Atg1-kinase are also present *in vivo* remains unclear. Nevertheless, the possibility exists that these phosphorylations are introduced by Atg1-kinase or another regulatory kinase *in vivo* to release Atg9 from $Atg1^{PC}$. In concert with phosphorylating Atg13 which leads to complex disassembly, this could be a regulatory mechanism to allow sequential binding of several Atg9-vesicles to the growing

phagophore. The release of Atg9 would have to be tightly regulated and synchronized with later membrane fusion steps.

5. Outlook

Assembly and disassembly of Atg1^{PC} could be reconstituted *in vitro* and a role for dimeric Atg1^{PC} subunits at different steps of autophagic membrane formation was suggested in this study. A role for Atg1-kinase in later stages has been proposed previously on the basis of its interaction with Atg8 (Kijanska and Peter, 2013). However, how assembly and disassembly of Atg1^{PC} are regulated in a spatio-temporal manner in the cell still needs to be investigated in detail. The model proposed for the different roles of Atg1-kinase in autophagy while being part of different Atg1^{PC} subcomplexes, requires tight regulation of Atg1^{PC} assembly and disassembly. Kinases and interaction partners regulating the assembly status of Atg1^{PC} can only be identified *in vivo*. A screen to analyze the effect of deletion of regulatory kinases would be required to address this question.

The findings of this study strongly suggest that Atg1^{PC} functions as a membrane tether. Tethering factors act upstream and downstream of small GTPases for regulation of vesicular trafficking and promote SNARE-mediated fusion (Yu and Hughson, 2010). Therefore, the respective SNARE-proteins could be reconstituted in Atg9-PL containing fluorescent dyes for fluorescence resonance energy transfer (FRET) based fusion assays. Different technical solutions for this assay have been developed, down to single fusion event analysis (Diao et al., 2012). This *in vitro*-system would also allow investigating the regulatory role of different small GTPases.

This study demonstrates that Atg1^{PC} assembly regulates binding of Atg17 to Atg9. It is likely that binding of Atg13 and Atg1-kinase induce a conformational change in Atg17^{TC} that allows binding of Atg17 to Atg9. The regulation of the interaction between Atg17 and Atg9 could be further analyzed in detail. The role of the C-terminal putative regulatory peptide in Atg17 could be addressed in *in vitro* assays employing the respective Atg17-variants. The influence of the regulatory peptide on the interaction of Atg proteins and the autophagic flux could be addressed using standard co-IP and autophagy assays *in vivo*.

The kinase activity of Atg1-kinase has been shown to be dispensable for recruiting downstream Atg-proteins (Sekito et al., 2009), but to be required for recycling Atg9 together with Atg18 and Atg2 (Reggiori et al., 2004). The factors required for the Atg9 recycling process, like the membrane budding and scission machinery, have not been determined. Despite the fact that Atg9 was found to be recycled (Reggiori et al., 2004), this

study shows that a large portion of Atg9 is degraded upon induction of autophagy. This suggests that Atg9 is in the autophagic membrane when fusion with the vacuole takes place indicating that Atg9 from the outer autophagic membrane could be transferred to the vacuolar membrane. However, Atg9 has not been found to reside on the vacuolar membrane suggesting that it could be recycled from the vacuole. Reconstituting this process is not possible yet, but *in vivo* analysis could clarify the mechanisms by tracking Atg9, Atg1-kinase, Atg18 and Atg2 during autophagosome biogenesis.

In *atg17Δ* cells, non-selective autophagy is blocked (Kabeya et al., 2005) while a GFP-Atg8 positive membrane is formed as shown in this study. Given the fact that Atg17 is the central unit of $Atg1^{PC}$ conferring its Atg9 vesicle tethering capacity, this role needs to be taken over by another protein so that autophagic membrane growth is still taking place in the absence of Atg17. As discussed above, Atg11 is a scaffold protein that is required for selective autophagy and that is able to interact with Atg9 (He et al., 2006). It is likely that it plays a similar role like Atg17, but in selective autophagy. The interaction of Atg11 with $Atg1^{PC}$ subunits has to be analyzed in the first place to determine the complex composition under vegetative conditions. The phosphorylation status of the proteins involved will be an important question to be investigated in order to understand how the switch between selective and non-selective autophagy is regulated. To investigate the morphology of the GFP-Atg8 positive membrane that is formed in *atg17Δ* cells and to get insight into the step that is impaired in the absence of Atg17, e.g. membrane closure or membrane fusion with the vacuole, electron microscopy is a powerful tool. Furthermore, *in vitro* reconstitution analyses in combination with *in vivo* autophagy assays addressing specifically the selective and non-selective autophagic pathways can help to elucidate the detailed role of Atg11.

Only by combining the advantages of *in vitro* and *in vivo* assays the regulation and the molecular mechanisms underlying the autophagic pathway will be fully uncovered. A detailed understanding of this process will be essential to modify autophagy efficiently for therapeutic purposes.

6. Literature

Agarraberes, F.A., and Dice, J.F. (2001). A molecular chaperone complex at the lysosomal membrane is required for protein translocation. J Cell Sci *114*, 2491-2499.

Aitchison, J.D., and Rout, M.P. (2012). The yeast nuclear pore complex and transport through it. Genetics *190*, 855-883.

Alemu, E.A., Lamark, T., Torgersen, K.M., Birgisdottir, A.B., Larsen, K.B., Jain, A., Olsvik, H., Øvervatn, A., Kirkin, V., and Johansen, T. (2012). Atg8 family proteins act as scaffolds for assembly of the ULK complex: sequence requirements for LC3-interacting region (LIR) motifs. J Biol Chem *287*, 39275-39290.

Angelova, M.I., and Dimitrov, D.S. (1986). Liposome electroformation. Faraday Discuss Chem Soc *81*, 303-311.

Antonin, W., Fasshauer, D., Becker, S., Jahn, R., and Schneider, T.R. (2002). Crystal structure of the endosomal SNARE complex reveals common structural principles of all SNAREs. Nat Struct Mol Biol *9*, 107-111.

Araki, Y., Ku, W.-C., Akioka, M., May, A.I., Hayashi, Y., Arisaka, F., Ishihama, Y., and Ohsumi, Y. (2013). Atg38 is required for autophagy-specific phosphatidylinositol 3-kinase complex integrity. J Cell Biol *203*, 299-313.

Arnold, K., Bordoli, L., Kopp, J., and Schwede, T. (2006). The SWISS-MODEL workspace: a web-based environment for protein structure homology modelling. Bioinformatics *22*, 195-201.

Axe, E.L., Walker, S.A., Manifava, M., Chandra, P., Roderick, H.L., Habermann, A., Griffiths, G., and Ktistakis, N.T. (2008). Autophagosome formation from membrane compartments enriched in phosphatidylinositol 3-phosphate and dynamically connected to the endoplasmic reticulum. J Cell Biol *182*, 685-701.

Baba, M., Osumi, M., Scott, S.V., Klionsky, D.J., and Ohsumi, Y. (1997). Two distinct pathways for targeting proteins from the cytoplasm to the vacuole/lysosome. J Cell Biol *139*, 1687-1695.

Bandyopadhyay, U., Kaushik, S., Varticovski, L., and Cuervo, A.M. (2008). The chaperone-mediated autophagy receptor organizes in dynamic protein complexes at the lysosomal membrane. Mol Cell Biol *28*, 5747-5763.

Barlowe, C., Orci, L., Yeung, T., Hosobuchi, M., Hamamoto, S., Salama, N., Rexach, M.F., Ravazzola, M., Amherdt, M., and Schekman, R. (1994). COPII: A membrane coat formed by Sec proteins that drive vesicle budding from the endoplasmic reticulum. Cell *77*, 895-907.

Bhattacharyya, S., Yu, H., Mim, C., and Matouschek, A. (2014). Regulated protein turnover: snapshots of the proteasome in action. Nat Rev Mol Cell Biol *15*, 122-133.

Binda, M., Péli-Gulli, M.-P., Bonfils, G., Panchaud, N., Urban, J., Sturgill, T.W., Loewith, R., and De Virgilio, C. (2009). The Vam6 GEF controls TORC1 by activating the EGO complex. Mol Cell *35*, 563-573.

Birgisdottir, Å.B., Lamark, T., and Johansen, T. (2013). The LIR motif – crucial for selective autophagy. J Cell Sci *126*, 3237-3247.

Bissig, C., and Gruenberg, J. (2013). Lipid sorting and multivesicular endosome biogenesis. Cold Spring Harbor Perspectives in Biology *5*.

Block, M.R., Glick, B.S., Wilcox, C.A., Wieland, F.T., and Rothman, J.E. (1988). Purification of an N-ethylmaleimide-sensitive protein catalyzing vesicular transport. PNAS *85*, 7852-7856.

Bodemann, B.O., Orvedahl, A., Cheng, T.L., Ram, R.R., Ou, Y.H., Formstecher, E., Maiti, M., Hazelett, C.C., Wauson, E.M., Balakireva, M., *et al.* (2011). RalB and the Exocyst mediate the cellular starvation response by direct activation of autophagosome assembly. Cell *144*, 253-267.

Bonifacino, J.S., and Glick, B.S. (2004). The mechanisms of vesicle budding and fusion. Cell *116*, 153-166.

Brech, A., Ahlquist, T., Lothe, R.A., and Stenmark, H. (2009). Autophagy in tumour suppression and promotion. Mol Oncol *3*, 366-375.

Brodsky, F.M. (2012). Diversity of clathrin function: new tricks for an old protein. Annu Rev Cell Dev Biol *28*, 309-336.

Budovskaya, Y.V., Stephan, J.S., Deminoff, S.J., and Herman, P.K. (2005). An evolutionary proteomics approach identifies substrates of the cAMP-dependent protein kinase. PNAS *102*, 13933-13938.

Budovskaya, Y.V., Stephan, J.S., Reggiori, F., Klionsky, D.J., and Herman, P.K. (2004). The Ras/cAMP-dependent protein kinase signaling pathway regulates an early step of the autophagy process in *Saccharomyces cerevisiae*. J Biol Chem *279*, 20663-20671.

Campelo, F., and Malhotra, V. (2012). Membrane fission: the biogenesis of transport carriers. Annu Rev Biochem *81*, 407-427.

Chan, E.Y.W., Kir, S., and Tooze, S.A. (2007). siRNA screening of the kinome identifies ULK1 as a multidomain modulator of autophagy. J Biol Chem *282*, 25464-25474.

Chan, E.Y.W., Longatti, A., McKnight, N.C., and Tooze, S.A. (2009). Kinase-inactivated ULK proteins inhibit autophagy via their conserved C-terminal domains using an Atg13-independent mechanism. Mol Cell Biol *29*, 157-171.

Chau, V., Tobias, J., Bachmair, A., Marriott, D., Ecker, D., Gonda, D., and Varshavsky, A. (1989). A multiubiquitin chain is confined to specific lysine in a targeted short-lived protein. Science *243*, 1576-1583.

Cheong, H., Nair, U., Geng, J.F., and Klionsky, D.J. (2008). The Atg1 kinase complex is involved in the regulation of protein recruitment to initiate sequestering vesicle formation for nonspecific autophagy in *Saccharomyces cerevisiae*. Mol Biol Cell *19*, 668-681.

Cheong, H., Yorimitsu, T., Reggiori, F., Legakis, J.E., Wang, C.W., and Klionsky, D.J. (2005). Atg17 regulates the magnitude of the autophagic response. Mol Biol Cell *16*, 3438-3453.

Chew, L.H., Setiaputra, D., Klionsky, D.J., and Yip, C.K. (2013). Structural characterization of the *Saccharomyces cerevisiae* autophagy regulatory complex Atg17-Atg31-Atg29. Autophagy *9*, 1467 - 1474.

Chiang, H., Terlecky, Plant, C., and Dice, J. (1989). A role for a 70-kilodalton heat shock protein in lysosomal degradation of intracellular proteins. Science *246*, 382-385.

Cho, W., and Stahelin, R.V. (2005). Membrane-protein interactions in cell signaling and membrane trafficking. Annu Rev Biophys Biomol Struct *34*, 119-151.

Choi, A.M.K., Ryter, S.W., and Levine, B. (2013). Autophagy in human health and disease. N Engl J Med *368*, 651-662.

Clary, D.O., Griff, I.C., and Rothman, J.E. (1990). SNAPs, a family of NSF attachment proteins involved in intracellular membrane fusion in animals and yeast. Cell *61*, 709-721.

Colell, A., Ricci, J.E., Tait, S., Milasta, S., Maurer, U., Bouchier-Hayes, L., Fitzgerald, P., Guio-Carrion, A., Waterhouse, N.J., Li, C.W., *et al.* (2007). GAPDH and autophagy preserve survival after apoptotic cytochrome c release in the absence of caspase activation. Cell *129*, 983-997.

Cox, J., and Mann, M. (2008). MaxQuant enables high peptide identification rates, individualized p.p.b.-range mass accuracies and proteome-wide protein quantification. Nat Biotech *26*, 1367-1372.

Cutler, N.S., Heitman, J., and Cardenas, M.E. (1999). TOR kinase homologs function in a signal transduction pathway that is conserved from yeast to mammals. Mol Cell Endocrinol *155*, 135-142.

D'Arcangelo, J.G., Stahmer, K.R., and Miller, E.A. (2013). Vesicle-mediated export from the ER: COPII coat function and regulation. Mol Cell Res *1833*, 2464-2472.

Dall'Armi, C., Hurtado-Lorenzo, A., Tian, H., Morel, E., Nezu, A., Chan, R.B., Yu, W.H., Robinson, K.S., Yeku, O., Small, S.A., *et al.* (2010). The phospholipase D1 pathway modulates macroautophagy. Nat Commun *1*, 142.

de Duve, C., and Wattiaux, R. (1966). Functions of lysosomes. Annu Rev Physiol *28*, 435-492.

Demetriades, C., Doumpas, N., and Teleman, Aurelio A. (2014). Regulation of TORC1 in response to amino acid starvation via lysosomal recruitment of TSC2. Cell *156*, 786-799.

Deter, R.L., Baudhuin, P., and Deduve, C. (1967). Participation of lysosomes in cellular autophagy induced in rat liver by glucagon. J Cell Biol *35*, C11-C16.

Diao, J., Ishitsuka, Y., Lee, H., Joo, C., Su, Z., Syed, S., Shin, Y.-K., Yoon, T.-Y., and Ha, T. (2012). A single vesicle-vesicle fusion assay for in vitro studies of SNAREs and accessory proteins. Nat Protocols *7*, 921-934.

Dudek, J., Rehling, P., and van der Laan, M. (2013). Mitochondrial protein import: Common principles and physiological networks. Mol Cell Res *1833*, 274-285.

Durrieu, M.-P., Lavery, R., and Baaden, M. (2008). Interactions between neuronal fusion proteins explored by molecular dynamics. Biophys J *94*, 3436-3446.

Faini, M., Beck, R., Wieland, F.T., and Briggs, J.A.G. (2013). Vesicle coats: structure, function, and general principles of assembly. Trends Cell Biol *23*, 279-288.

Faini, M., Prinz, S., Beck, R., Schorb, M., Riches, J.D., Bacia, K., Brügger, B., Wieland, F.T., and Briggs, J.A.G. (2012). The structures of COPI-coated vesicles reveal alternate coatomer conformations and interactions. Science *336*, 1451-1454.

Fasshauer, D., Otto, H., Eliason, W.K., Jahn, R., and Brünger, A.T. (1997). Structural changes are associated with soluble N-ethylmaleimide-sensitive fusion protein attachment protein receptor complex formation. J Biol Chem *272*, 28036-28041.

Fath, S., Mancias, J.D., Bi, X., and Goldberg, J. (2007). Structure and organization of coat proteins in the COPII cage. Cell *129*, 1325-1336.

Feng, Y., He, D., Yao, Z., and Klionsky, D.J. (2014). The machinery of macroautophagy. Cell Res *24*, 24-41.

Finley, D. (2009). Recognition and processing of ubiquitin-protein conjugates by the proteasome. Annu Rev Biochem *78*, 477-513.

Förster, F., Unverdorben, P., Śledź, P., and Baumeister, W. (2013). Unveiling the long-held secrets of the 26S proteasome. Structure *21*, 1551-1562.

Fotin, A., Cheng, Y., Sliz, P., Grigorieff, N., Harrison, S.C., Kirchhausen, T., and Walz, T. (2004). Molecular model for a complete clathrin lattice from electron cryomicroscopy. Nature *432*, 573-579.

Fred Dice, J. (1990). Peptide sequences that target cytosolic proteins for lysosomal proteolysis. Trends Biochem Sci*15*, 305-309.

Fujioka, Y., Suzuki, S.W., Yamamoto, H., Kondo-Kakuta, C., Kimura, Y., Hirano, H., Akada, R., Inagaki, F., Ohsumi, Y., and Noda, N.N. (2014). Structural basis of starvation-induced assembly of the autophagy initiation complex. Nat Struct Mol Biol *21*, 513-521.

Ge, L., Melville, D., Zhang, M., and Schekman, R. (2013). The ER–Golgi intermediate compartment is a key membrane source for the LC3 lipidation step of autophagosome biogenesis. eLife *2*.

Graef, M., Friedman, J.R., Graham, C., Babu, M., and Nunnari, J. (2013). ER exit sites are physical and functional core autophagosome biogenesis components. Mol Biol Cell *24*, 2918 - 2931.

Griff, I.C., Schekman, R., Rothman, J.E., and Kaiser, C.A. (1992). The yeast SEC17 gene product is functionally equivalent to mammalian alpha-SNAP protein. J Biol Chem *267*, 12106-12115.

Groll, M., Ditzel, L., Lowe, J., Stock, D., Bochtler, M., Bartunik, H.D., and Huber, R. (1997). Structure of 20S proteasome from yeast at 2.4A resolution. Nature *386*, 463-471.

Guo, Jessie Y., Xia, B., and White, E. (2013). Autophagy-mediated tumor promotion. Cell *155*, 1216-1219.

Gurkar, A.U., Chu, K., Raj, L., Bouley, R., Lee, S.-H., Kim, Y.-B., Dunn, S.E., Mandinova, A., and Lee, S.W. (2013). Identification of ROCK1 kinase as a critical regulator of Beclin1-mediated autophagy during metabolic stress. Nat Commun *4*.

Gutierrez, M.G., Master, S.S., Singh, S.B., Taylor, G.A., Colombo, M.I., and Deretic, V. (2004). Autophagy is a defense mechanism inhibiting BCG and mycobacterium tuberculosis survival in infected macrophages. Cell *119*, 753-766.

Gwinn, D.M., Shackelford, D.B., Egan, D.F., Mihaylova, M.M., Mery, A., Vasquez, D.S., Turk, B.E., and Shaw, R.J. (2008). AMPK phosphorylation of Raptor mediates a metabolic checkpoint. Mol Cell *30*, 214-226.

Hamasaki, M., Furuta, N., Matsuda, A., Nezu, A., Yamamoto, A., Fujita, N., Oomori, H., Noda, T., Haraguchi, T., Hiraoka, Y.*, et al.* (2013). Autophagosomes form at ER-mitochondria contact sites. Nature *495*, 389-393.

Hanada, T., Noda, N.N., Satomi, Y., Ichimura, Y., Fujioka, Y., Takao, T., Inagaki, F., and Ohsumi, Y. (2007). The Atg12-Atg5 conjugate has a novel E3-like activity for protein lipidation in autophagy. J Biol Chem *282*, 37298-37302.

Hanson, P.I., and Whiteheart, S.W. (2005). AAA+ proteins: have engine, will work. Nat Rev Mol Cell Biol *6*, 519-529.

Hara-Kuge, S., Kuge, O., Orci, L., Amherdt, M., Ravazzola, M., Wieland, F., and Rothman, J. (1994). En bloc incorporation of coatomer subunits during the assembly of COP-coated vesicles. J Cell Biol *124*, 883-892.

He, C., Song, H., Yorimitsu, T., Monastyrska, I., Yen, W.-L., Legakis, J.E., and Klionsky, D.J. (2006). Recruitment of Atg9 to the preautophagosomal structure by Atg11 is essential for selective autophagy in budding yeast. J Cell Biol *175*, 925-935.

Hughson, F.M., and Reinisch, K.M. (2010). Structure and mechanism in membrane trafficking. Curr Opin Cell Biol *22*, 454-460.

Huotari, J., and Helenius, A. (2011). Endosome maturation. The EMBO Journal *30*, 3481-3500.

Ichimura, Y., Kirisako, T., Takao, T., Satomi, Y., Shimonishi, Y., Ishihara, N., Mizushima, N., Tanida, I., Kominami, E., Ohsumi, M.*, et al.* (2000). A ubiquitin-like system mediates protein lipidation. Nature *408*, 488-492.

Itakura, E., Kishi-Itakura, C., and Mizushima, N. (2012). The hairpin-type tail-anchored SNARE Syntaxin 17 targets to autophagosomes for fusion with endosomes/lysosomes. Cell *151*, 1256-1269.

Itakura, E., Kishi, C., Inoue, K., and Mizushima, N. (2008). Beclin 1 forms two distinct phosphatidylinositol 3-kinase complexes with mammalian Atg14 and UVRAG. Mol Biol Cell *19*, 5360-5372.

Jackson, L.P., Kümmel, D., Reinisch, K.M., and Owen, D.J. (2012). Structures and mechanisms of vesicle coat components and multisubunit tethering complexes. Curr Opin Cell Biol *24*, 475-483.

Jahn, R., and Scheller, R.H. (2006). SNAREs - engines for membrane fusion. Nat Rev Mol Cell Biol *7*, 631-643.

Janke, C., Magiera, M.M., Rathfelder, N., Taxis, C., Reber, S., Maekawa, H., Moreno-Borchart, A., Doenges, G., Schwob, E., Schiebel, E.*, et al.* (2004). A versatile toolbox for

PCR-based tagging of yeast genes: new fluorescent proteins, more markers and promoter substitution cassettes. Yeast *21*, 947-962.

Jao, C.C., Ragusa, M.J., Stanley, R.E., and Hurley, J.H. (2013). A HORMA domain in Atg13 mediates PI 3-kinase recruitment in autophagy. PNAS *110*, 5486–5491.

Jarvis, D.L. (2009). Chapter 14 Baculovirus–Insect Cell Expression Systems. In Methods in Enzymology, R.B. Richard, and P.D. Murray, eds. (Academic Press), pp. 191-222.

Jiang, P., Nishimura, T., Sakamaki, Y., Itakura, E., Hatta, T., Natsume, T., and Mizushima, N. (2014). The HOPS complex mediates autophagosome–lysosome fusion through interaction with syntaxin 17. Mol Biol Cell *25*, 1327-1337.

Jung, C.H., Jun, C.B., Ro, S.-H., Kim, Y.-M., Otto, N.M., Cao, J., Kundu, M., and Kim, D.-H. (2009). ULK-Atg13-FIP200 complexes mediate mTOR signaling to the autophagy machinery. Mol Biol Cell *20*, 1992-2003.

Kabeya, Y., Kamada, Y., Baba, M., Takikawa, H., Sasaki, M., and Ohsumi, Y. (2005). Atg17 functions in cooperation with Atg1 and Atg13 in yeast autophagy. Mol Biol Cell *16*, 2544-2553.

Kabeya, Y., Noda, N.N., Fujioka, Y., Suzuki, K., Inagaki, F., and Ohsumi, Y. (2009). Characterization of the Atg17-Atg29-Atg31 complex specifically required for starvation-induced autophagy in *Saccharomyces cerevisiae*. Biochem Biophys Res Commun *389*, 612-615.

Kakuta, S., Yamamoto, H., Negishi, L., Kondo-Kakuta, C., Hayashi, N., and Ohsumi, Y. (2012). Atg9 vesicles recruit vesicle-tethering proteins Trs85 and Ypt1 to the autophagosome formation site. J Biol Chem *287*, 44261-44269.

Kamada, Y. (2010). Prime-numbered Atg proteins act at the primary step in autophagy Unphosphorylatable Atg13 can induce autophagy without TOR inactivation. Autophagy *6*, 415-416.

Kamada, Y., Funakoshi, T., Shintani, T., Nagano, K., Ohsumi, M., and Ohsumi, Y. (2000). Tor-mediated induction of autophagy via an Apg1 protein kinase complex. J Cell Biol *150*, 1507-1513.

Kamada, Y., Yoshino, K., Kondo, C., Kawamata, T., Oshiro, N., Yonezawa, K., and Ohsumi, Y. (2010). Tor directly controls the Atg1 kinase complex to regulate autophagy. Mol Cell Biol *30*, 1049-1058.

Kanki, T., Wang, K., Cao, Y., Baba, M., and Klionsky, D.J. (2009). Atg32 Is a mitochondrial protein that confers selectivity during mitophagy. Dev Cell *17*, 98-109.

Kaufmann, A., Beier, V., Franquelim, Henri G., and Wollert, T. (2014). Molecular mechanism of autophagic membrane-scaffold assembly and disassembly. Cell *156*, 469-481.

Kaushik, S., and Cuervo, A.M. (2012). Chaperone-mediated autophagy: a unique way to enter the lysosome world. Trends Cell Biol *22*, 407-417.

Kawamata, T., Kamada, Y., Kabeya, Y., Sekito, T., and Ohsumi, Y. (2008). Organization of the pre-autophagosomal structure responsible for autophagosome formation. Mol Biol Cell *19*, 2039-2050.

Kihara, A., Noda, T., Ishihara, N., and Ohsumi, Y. (2001). Two distinct Vps34 phosphatidylinositol 3-kinase complexes function in autophagy and carboxypeptidase Y sorting in *Saccharomyces cerevisiae*. J Cell Biol *152*, 519-530.

Kijanska, M., Dohnal, I., Reiter, W., Kaspar, S., Stoffel, I., Ammerer, G., Kraft, C., and Peter, M. (2010). Activation of Atg1 kinase in autophagy by regulated phosphorylation. Autophagy *6*, 1168-1178.

Kijanska, M., and Peter, M. (2013). Atg1 kinase regulates early and late steps during autophagy. Autophagy *9*, 2-1.

Kim, J., Kundu, M., Viollet, B., and Guan, K.L. (2011). AMPK and mTOR regulate autophagy through direct phosphorylation of Ulk1. Nature Cell Biol *13*, 132-U171.

Kirisako, T., Ichimura, Y., Okada, H., Kabeya, Y., Mizushima, N., Yoshimori, T., Ohsumi, M., Takao, T., Noda, T., and Ohsumi, Y. (2000). The reversible modification regulates the membrane-binding state of Apg8/Aut7 essential for autophagy and the cytoplasm to vacuole targeting pathway. J Cell Biol *151*, 263-276.

Klionsky, D.J. (2007). Autophagy: from phenomenology to molecular understanding in less than a decade. Nature Rev Mol Cell Biol *8*, 931-937.

Komander, D., and Rape, M. (2012). The ubiquitin code. Annu Rev Biochem *81*, 203-229.

Komatsu, M., Waguri, S., Chiba, T., Murata, S., Iwata, J.-i., Tanida, I., Ueno, T., Koike, M., Uchiyama, Y., Kominami, E.*, et al.* (2006). Loss of autophagy in the central nervous system causes neurodegeneration in mice. Nature *441*, 880-884.

Kraft, C., Kijanska, M., Kalie, E., Siergiejuk, E., Lee, S.S., Semplicio, G., Stoffel, I., Brezovich, A., Verma, M., Hansmann, I.*, et al.* (2012). Binding of the Atg1/ULK1 kinase to the ubiquitin-like protein Atg8 regulates autophagy. EMBO J *31*, 3647 - 3784.

Kraft, C., Reggiori, F., and Peter, M. (2009). Selective types of autophagy in yeast. Mol Cell Res *1793*, 1404-1412.

Lamb, C.A., Dooley, H.C., and Tooze, S.A. (2013a). Endocytosis and autophagy: Shared machinery for degradation. BioEssays *35*, 34-45.

Lamb, C.A., Yoshimori, T., and Tooze, S.A. (2013b). The autophagosome: origins unknown, biogenesis complex. Nat Rev Mol Cell Biol *14*, 759–774.

Lang, T., Reiche, S., Straub, M., Bredschneider, M., and Thumm, M. (2000). Autophagy and the cvt pathway both depend on AUT9. J Bacteriol *182*, 2125-2133.

Lee, E.-J., and Tournier, C. (2011). The requirement of uncoordinated 51-like kinase 1 (ULK1) and ULK2 in the regulation of autophagy. Autophagy *7*, 689-695.

Lee, H.K., Mattei, L.M., Steinberg, B.E., Alberts, P., Lee, Y.H., Chervonsky, A., Mizushima, N., Grinstein, S., and Iwasaki, A. (2010). *In vivo* requirement for Atg5 in antigen presentation by dendritic cells. Immunity *32*, 227-239.

Legakis, J.E., Yen, W.-L., and Klionsky, D.J. (2007). A cycling protein complex required for selective autophagy. Autophagy *3*, 422-432.

Levine, B., Mizushima, N., and Virgin, H.W. (2011). Autophagy in immunity and inflammation. Nature *469*, 323-335.

Li, F., Kümmel, D., Coleman, J., Reinisch, K.M., Rothman, J.E., and Pincet, F. (2014). A half-zippered SNARE complex represents a functional intermediate in membrane fusion. J Am Chem Soc *136*, 3456-3464.

Li, W.-w., Li, J., and Bao, J.-k. (2012). Microautophagy: lesser-known self-eating. Cell Mol Life Sci *69*, 1125-1136.

Loewith, R., and Hall, M.N. (2011). Target of rapamycin (TOR) in nutrient signaling and growth control. Genetics *189*, 1177-1201.

Lv, L., Li, D., Zhao, D., Lin, R., Chu, Y., Zhang, H., Zha, Z., Liu, Y., Li, Z., Xu, Y.*, et al.* (2011). Acetylation targets the M2 isoform of pyruvate kinase for degradation through chaperone-mediated autophagy and promotes tumor growth. Mol Cell *42*, 719-730.

Lynch-Day, M.A., Bhandari, D., Menon, S., Huang, J., Cai, H., Bartholomew, C.R., Brumell, J.H., Ferro-Novick, S., and Klionsky, D.J. (2010). Trs85 directs a Ypt1 GEF, TRAPPIII, to the phagophore to promote autophagy. PNAS *107*, 7811-7816.

Lynch-Day, M.A., and Klionsky, D.J. (2010). The Cvt pathway as a model for selective autophagy. FEBS Lett *584*, 1359-1366.

Mao, K., Chew, L.H., Inoue-Aono, Y., Cheong, H., Nair, U., Popelka, H., Yip, C.K., and Klionsky, D.J. (2013). Atg29 phosphorylation regulates coordination of the Atg17-Atg31-Atg29 complex with the Atg11 scaffold during autophagy initiation. PNAS *110*, E2875 - E2884.

Mari, M., Griffith, J., Rieter, E., Krishnappa, L., Klionsky, D.J., and Reggiori, F. (2010). An Atg9-containing compartment that functions in the early steps of autophagosome biogenesis. J Cell Biol *190*, 1005-1022.

Matsunaga, K., Saitoh, T., Tabata, K., Omori, H., Satoh, T., Kurotori, N., Maejima, I., Shirahama-Noda, K., Ichimura, T., Isobe, T.*, et al.* (2009). Two Beclin 1-binding proteins, Atg14L and Rubicon, reciprocally regulate autophagy at different stages. Nat Cell Biol *11*, 385-396.

Matsuoka, K., Orci, L., Amherdt, M., Bednarek, S.Y., Hamamoto, S., Schekman, R., and Yeung, T. (1998). COPII-coated vesicle formation reconstituted with purified coat proteins and chemically defined liposomes. Cell *93*, 263-275.

Maxfield, F.R., and McGraw, T.E. (2004). Endocytic recycling. Nat Rev Mol Cell Biol *5*, 121-132.

McMahon, H.T., and Boucrot, E. (2011). Molecular mechanism and physiological functions of clathrin-mediated endocytosis. Nat Rev Mol Cell Biol *12*, 517-533.

McNew, J.A., Parlati, F., Fukuda, R., Johnston, R.J., Paz, K., Paumet, F., Sollner, T.H., and Rothman, J.E. (2000). Compartmental specificity of cellular membrane fusion encoded in SNARE proteins. Nature *407*, 153-159.

Mihaylova, M.M., and Shaw, R.J. (2011). The AMPK signalling pathway coordinates cell growth, autophagy and metabolism. Nat Cell Biol *13*, 1016-1023.

Miller, E., Antonny, B., Hamamoto, S., and Schekman, R. (2002). Cargo selection into COPII vesicles is driven by the Sec24p subunit. EMBO J *21*, 6105-6113.

Mizuno-Yamasaki, E., Rivera-Molina, F., and Novick, P. (2012). GTPase networks in membrane traffic. Annu Rev Biochem *81*, 637-659.

Mizushima, N. (2007). Autophagy: process and function. Genes Dev *21*, 2861-2873.

Mizushima, N., Noda, T., Yoshimori, T., Tanaka, Y., Ishii, T., George, M.D., Klionsky, D.J., Ohsumi, M., and Ohsumi, Y. (1998). A protein conjugation system essential for autophagy. Nature *395*, 395-398.

Mizushima, N., Yamamoto, A., Hatano, M., Kobayashi, Y., Kabeya, Y., Suzuki, K., Tokuhisa, T., Ohsumi, Y., and Yoshimori, T. (2001). Dissection of autophagosome formation using Apg5-deficient mouse embryonic stem cells. J Cell Biol *152*, 657-668.

Moreau, K., Ravikumar, B., Puri, C., and Rubinsztein, D.C. (2012). Arf6 promotes autophagosome formation via effects on phosphatidylinositol 4,5-bisphosphate and phospholipase D. J Cell Biol *196*, 483-496.

Moreau, K., Ravikumar, B., Renna, M., Puri, C., and Rubinsztein, David C. (2011). Autophagosome precursor maturation requires homotypic fusion. Cell *146*, 303-317.

Moreau, K., Renna, M., and Rubinsztein, D.C. (2013). Connections between SNAREs and autophagy. Trends Biochem Sci *38*, 57-63.

Müller, O., Sattler, T., Flötenmeyer, M., Schwarz, H., Plattner, H., and Mayer, A. (2000). Autophagic Tubes: Vacuolar Invaginations Involved in Lateral Membrane Sorting and Inverse Vesicle Budding. J Cell Biol *151*, 519-528.

Nair, U., Jotwani, A., Geng, J., Gammoh, N., Richerson, D., Yen, W.-L., Griffith, J., Nag, S., Wang, K., Moss, T.*, et al.* (2011). SNARE proteins are required for macroautophagy. Cell *146*, 290-302.

Nakagawa, I., Amano, A., Mizushima, N., Yamamoto, A., Yamaguchi, H., Kamimoto, T., Nara, A., Funao, J., Nakata, M., Tsuda, K.*, et al.* (2004). Autophagy defends cells against invading group A *Streptococcus*. Science *306*, 1037-1040.

Nakatogawa, H., Suzuki, K., Kamada, Y., and Ohsumi, Y. (2009). Dynamics and diversity in autophagy mechanisms: lessons from yeast. Nature Rev Mol Cell Biol *10*, 458-467.

Noda, T., Kim, J., Huang, W.-P., Baba, M., Tokunaga, C., Ohsumi, Y., and Klionsky, D.J. (2000). Apg9p/Cvt7p is an integral membrane protein required for transport vesicle formation in the cvt and autophagy pathways. J Cell Biol *148*, 465-480.

Noda, T., and Ohsumi, Y. (1998). Tor, a phosphatidylinositol kinase homologue, controls autophagy in yeast. J Biol Chem *273*, 3963-3966.

Obara, K., Noda, T., Niimi, K., and Ohsumi, Y. (2008). Transport of phosphatidylinositol 3-phosphate into the vacuole via autophagic membranes in *Saccharomyces cerevisiae*. Genes Cells *13*, 537-547.

Obara, K., Sekito, T., and Ohsumi, Y. (2006). Assortment of phosphatidylinositol 3-kinase complexes - Atg14p directs association of complex I to the pre-autophagosomal structure in *Saccharomyces cerevisiae*. Mol Biol Cell *17*, 1527-1539.

Orci, L., Ravazzola, M., Meda, P., Holcomb, C., Moore, H.P., Hicke, L., and Schekman, R. (1991). Mammalian Sec23p homologue is restricted to the endoplasmic reticulum transitional cytoplasm. PNAS *88*, 8611-8615.

Orsi, A., Razi, M., Dooley, H.C., Robinson, D., Weston, A.E., Collinson, L.M., and Tooze, S.A. (2012). Dynamic and transient interactions of Atg9 with autophagosomes, but not membrane integration, are required for autophagy. Mol Biol Cell *23*, 1860-1873.

Orvedahl, A., MacPherson, S., Sumpter Jr, R., Tallóczy, Z., Zou, Z., and Levine, B. (2010). Autophagy protects against Sindbis virus infection of the central nervous system. Cell Host Microbe *7*, 115-127.

Palade, G. (1975). Intracellular aspects of the process of protein synthesis. Science *189*, 867.

Papinski, D., Schuschnig, M., Reiter, W., Wilhelm, L., Barnes, Christopher A., Majolica, A., Hansmann, I., Pfaffenwimmer, T., Kijanska, M., Stoffel, I.*, et al.* (2014). Early steps in autophagy depend on direct phosphorylation of Atg9 by the Atg1 kinase. Mol Cell *53*. 515-521.

Peplowska, K., Markgraf, D.F., Ostrowicz, C.W., Bange, G., and Ungermann, C. (2007). The CORVET tethering complex interacts with the yeast Rab5 homolog Vps21 and is involved in endo-lysosomal biogenesis. Dev Cell *12*, 739-750.

Prakash, S., Tian, L., Ratliff, K.S., Lehotzky, R.E., and Matouschek, A. (2004). An unstructured initiation site is required for efficient proteasome-mediated degradation. Nat Struct Mol Biol *11*, 830-837.

Ragusa, M.J., Stanley, R.E., and Hurley, J.H. (2012). Architecture of the Atg17 complex as a scaffold for autophagosome biogenesis. Cell *151*, 1501–1512.

Ram, R.J., Li, B., and Kaiser, C.A. (2002). Identification of Sec36p, Sec37p, and Sec38p: components of yeast complex that contains Sec34p and Sec35p. Mol Biol Cell *13*, 1484-1500.

Ravikumar, B., Duden, R., and Rubinsztein, D.C. (2002). Aggregate-prone proteins with polyglutamine and polyalanine expansions are degraded by autophagy. Human Molecular Genetics *11*, 1107-1117.

Ravikumar, B., Moreau, K., Jahreiss, L., Puri, C., and Rubinsztein, D.C. (2010). Plasma membrane contributes to the formation of pre-autophagosomal structures. Nat Cell Biol *12*, 747-757.

Raymond, C.K., Howald-Stevenson, I., Vater, C.A., and Stevens, T.H. (1992). Morphological classification of the yeast vacuolar protein sorting mutants: evidence for a prevacuolar compartment in class E vps mutants. Mol Biol Cell *3*, 1389-1402.

Reggiori, F., and Klionsky, D.J. (2013). Autophagic processes in yeast: mechanism, machinery and regulation. Genetics *194*, 341-361.

Reggiori, F., Tucker, K.A., Stromhaug, P.E., and Klionsky, D.J. (2004). The Atg1-Atg13 complex regulates Atg9 and Atg23 retrieval transport from the pre-autophagosomal structure. Dev Cell *6*, 79-90.

Risselada, H.J., and Grubmüller, H. (2012). How SNARE molecules mediate membrane fusion: Recent insights from molecular simulations. Curr Opin Struct Biol *22*, 187-196.

Roberts, David J., Tan-Sah, Valerie P., Ding, Eric Y., Smith, Jeffery M., and Miyamoto, S. (2014). Hexokinase-II positively regulates glucose starvation-induced autophagy through TORC1 inhibition. Mol Cell *53*, 521–533.

Robinson, M.S. (2004). Adaptable adaptors for coated vesicles. Trends Cell Biol *14*, 167-174.

Romanov, J., Walczak, M., Ibiricu, I., Schuchner, S., Ogris, E., Kraft, C., and Martens, S. (2012). Mechanism and functions of membrane binding by the Atg5-Atg12/Atg16 complex during autophagosome formation. EMBO J *31*, 4249 - 4370.

Russell, R.C., Tian, Y., Yuan, H., Park, H.W., Chang, Y.-Y., Kim, J., Kim, H., Neufeld, T.P., Dillin, A., and Guan, K.-L. (2013). ULK1 induces autophagy by phosphorylating Beclin-1 and activating VPS34 lipid kinase. Nat Cell Biol *15*, 741–750.

Sacher, M., Barrowman, J., Wang, W., Horecka, J., Zhang, Y., Pypaert, M., and Ferro-Novick, S. (2001). TRAPP I implicated in the specificity of tethering in ER-to-Golgi transport. Mol Cell *7*, 433-442.

Sacher, M., Jiang, Y., Barrowman, J., Scarpa, A., Burston, J., Zhang, L., Schieltz, D., Yates, J.R., Abeliovich, H., and Ferro-Novick, S. (1998). TRAPP, a highly conserved novel complex on the cis-Golgi that mediates vesicle docking and fusion. EMBO J *17*, 2494-2503.

Sahu, R., Kaushik, S., Clement, C.C., Cannizzo, E.S., Scharf, B., Follenzi, A., Potolicchio, I., Nieves, E., Cuervo, A.M., and Santambrogio, L. (2011). Microautophagy of cytosolic proteins by late endosomes. Dev Cell *20*, 131-139.

Sarkar, S., Ravikumar, B., and Rubinsztein, D.C. (2009). Autophagic clearance of aggregate-prone proteins associated with neurodegeneration. Methods in Enzymology Vol 453: Autophagy in Disease and Clinical Applications, Pt C *453*, 83-87.

Sattler, T., and Mayer, A. (2000). Cell-free reconstitution of microautophagic vacuole invagination and vesicle formation. J Cell Biol *151*, 529-538.

Sawa-Makarska, J., Abert, C., Romanov, J., Zens, B., Ibiricu, I., and Martens, S. (2014). Cargo binding to Atg19 unmasks additional Atg8 binding sites to mediate membrane–cargo apposition during selective autophagy. Nat Cell Biol *16*, 425-433.

Schneider, C.A., Rasband, W.S., and Eliceiri, K.W. (2012). NIH Image to ImageJ: 25 years of image analysis. Nat Meth *9*, 671-675.

Scholz, J., Besir, H., Strasser, C., and Suppmann, S. (2013). A new method to customize protein expression vectors for fast, efficient and background free parallel cloning. BMC Biotechnology *13*.

SchrödingerLLC. The PyMOL molecular graphics system, Version 1.5.0.4 Schrödinger, LLC.

Schuck, P. (2000). Size-distribution analysis of macromolecules by sedimentation velocity ultracentrifugation and Lamm equation modeling. Biophys J *78*, 1606-1619.

Scott, C.C., Vacca, F., and Gruenberg, J. (2014). Endosome maturation, transport and functions. Sem Cell Dev Biol *31*, 2-10.

Sekito, T., Kawamata, T., Ichikawa, R., Suzuki, K., and Ohsumi, Y. (2009). Atg17 recruits Atg9 to organize the pre-autophagosomal structure. Genes Cells *14*, 525-538.

Sengupta, S., Peterson, T.R., and Sabatini, D.M. (2010). Regulation of the mTOR complex 1 pathway by nutrients, growth factors, and stress. Mol Cell *40*, 310-322.

Serafini, T., Orci, L., Amherdt, M., Brunner, M., Kahn, R.A., and Rothmant, J.E. (1991). ADP-Ribosylation factor is a subunit of the coat of Golgi-derived COP-coated vesicles: A novel role for a GTP-binding protein. Cell *67*, 239-253.

Shintani, T., and Klionsky, D.J. (2004). Cargo proteins facilitate the formation of transport vesicles in the cytoplasm to vacuole targeting pathway. J Biol Chem *279*, 29889-29894.

Shirahama-Noda, K., Kira, S., Yoshimori, T., and Noda, T. (2013). TRAPPIII is responsible for the vesicular transport from early endosomes to the Golgi apparatus that facilitates Atg9 cycling in autophagy. J Cell Sci *126*, 4963-4973.

Simonsen, A., and Stenmark, H. (2008). Self-eating from an ER-associated cup. J Cell Biol *182*, 621-622.

Stanley, R.E., Ragusa, M.J., and Hurley, J.H. (2013). The beginning of the end: how scaffolds nucleate autophagosome biogenesis. Trends Cell Biol *24*, 73–81.

Stenmark, H. (2009). Rab GTPases as coordinators of vesicle traffic. Nat Rev Mol Cell Biol *10*, 513-525.

Stephan, J.S., Yeh, Y.-Y., Ramachandran, V., Deminoff, S.J., and Herman, P.K. (2009). The Tor and PKA signaling pathways independently target the Atg1/Atg13 protein kinase complex to control autophagy. PNAS *106*, 17049-17054.

Stephens, D.J. (2003). *De novo* formation, fusion and fission of mammalian COPII-coated endoplasmic reticulum exit sites. EMBO reports *4*, 210-217.

Stroupe, C., Hickey, C.M., Mima, J., Burfeind, A.S., and Wickner, W. (2009). Minimal membrane docking requirements revealed by reconstitution of Rab GTPase-dependent membrane fusion from purified components. PNAS *106*, 17626-17633.

Suvorova, E.S., Duden, R., and Lupashin, V.V. (2002). The Sec34/Sec35p complex, a Ypt1p effector required for retrograde intra-Golgi trafficking, interacts with Golgi SNAREs and COPI vesicle coat proteins. J Cell Biol *157*, 631-643.

Suzuki, K., Akioka, M., Kondo-Kakuta, C., Yamamoto, H., and Ohsumi, Y. (2013). Fine mapping of autophagy-related proteins during autophagosome formation in *Saccharomyces cerevisiae*. J Cell Sci *126*, 2534-2544.

Suzuki, K., Kirisako, T., Kamada, Y., Mizushima, N., Noda, T., and Ohsumi, Y. (2001). The pre-autophagosomal structure organized by concerted functions of APG genes is essential for autophagosome formation. EMBO J *20*, 5971-5981.

Suzuki, K., Kubota, Y., Sekito, T., and Ohsumi, Y. (2007). Hierarchy of Atg proteins in pre-autophagosomal structure organization. Genes Cells *12*, 209-218.

Szul, T., and Sztul, E. (2011). COPII and COPI traffic at the ER-Golgi interface. Physiology *26*, 348-364.

Takáts, S., Pircs, K., Nagy, P., Varga, Á., Kárpáti, M., Hegedűs, K., Kramer, H., Kovács, A.L., Sass, M., and Juhász, G. (2014). Interaction of the HOPS complex with Syntaxin 17 mediates autophagosome clearance in Drosophila. Mol Biol Cell *25*, 1338-1354.

Tan, S. (2001). A modular polycistronic expression system for overexpressing protein complexes in *Escherichia coli*. Protein Express Purif *21*, 224-234.

Tang, H.-W., Wang, Y.-B., Wang, S.-L., Wu, M.-H., Lin, S.-Y., and Chen, G.-C. (2011). Atg1-mediated myosin II activation regulates autophagosome formation during starvation-induced autophagy. EMBO J *30*, 636-651.

Thumm, M., Egner, R., Koch, B., Schlumpberger, M., Straub, M., Veenhuis, M., and Wolf, D.H. (1994). Isolation of autophagocytosis mutants of *Saccharomyces cerevisiae*. FEBS Lett *349*, 275-280.

Tsukada, M., and Ohsumi, Y. (1993). Isolation and characterization of autophagy-defective mutants of *Saccharomyces cerevisiae*. FEBS Lett *333*, 169-174.

Ungar, D., Oka, T., Brittle, E.E., Vasile, E., Lupashin, V.V., Chatterton, J.E., Heuser, J.E., Krieger, M., and Waters, M.G. (2002). Characterization of a mammalian Golgi-localized protein complex, COG, that is required for normal Golgi morphology and function. J Cell Biol *157*, 405-415.

Unno, M., Mizushima, T., Morimoto, Y., Tomisugi, Y., Tanaka, K., Yasuoka, N., and Tsukihara, T. (2002). The structure of the mammalian 20S proteasome at 2.75 Å resolution. Structure *10*, 609-618.

Uttenweiler, A., Schwarz, H., Neumann, H., and Mayer, A. (2007). The Vacuolar Transporter Chaperone (VTC) Complex Is Required for Microautophagy. Mol Biol Cell *18*, 166-175.

van der Vaart, A., Griffith, J., and Reggiori, F. (2010). Exit from the Golgi is required for the expansion of the autophagosomal phagophore in yeast *Saccharomyces cerevisiae*. Mol Biol Cell *21*, 2270-2284.

Wada, Y., Ohsumi, Y., and Anraku, Y. (1992). Genes for directing vacuolar morphogenesis in *Saccharomyces cerevisiae*. I. Isolation and characterization of two classes of vam mutants. J Biol Chem *267*, 18665-18670.

Wang, J., Menon, S., Yamasaki, A., Chou, H.-T., Walz, T., Jiang, Y., and Ferro-Novick, S. (2013). Ypt1 recruits the Atg1 kinase to the preautophagosomal structure. PNAS *110*, 9800-9805.

Wang, Z., Wilson, W.A., Fujino, M.A., and Roach, P.J. (2001). Antagonistic controls of autophagy and glycogen accumulation by Snf1p, the yeast homolog of AMP-activated protein kinase, and the cyclin-dependent kinase Pho85p. Mol Cell Biol *21*, 5742-5752.

Wasilko, D.J., Edward Lee, S., Stutzman-Engwall, K.J., Reitz, B.A., Emmons, T.L., Mathis, K.J., Bienkowski, M.J., Tomasselli, A.G., and David Fischer, H. (2009). The titerless infected-cells preservation and scale-up (TIPS) method for large-scale production of NO-sensitive human soluble guanylate cyclase (sGC) from insect cells infected with recombinant baculovirus. Protein Express Purif *65*, 122-132.

Watanabe, Y., Kobayashi, T., Yamamoto, H., Hoshida, H., Akada, R., Inagaki, F., Ohsumi, Y., and Noda, N.N. (2012). Structure-based analyses reveal distinct binding sites for Atg2 and phosphoinositides in Atg18. J Biol Chem *287*, 31681-31690.

Webber, J.L., and Tooze, S.A. (2010). New insights into the function of Atg9. FEBS Lett *584*, 1319-1326.

Whyte, J.R.C., and Munro, S. (2002). Vesicle tethering complexes in membrane traffic. J Cell Sci *115*, 2627-2637.

Williams, A., Sarkar, S., Cuddon, P., Ttofi, E.K., Saiki, S., Siddiqi, F.H., Jahreiss, L., Fleming, A., Pask, D., Goldsmith, P.*, et al.* (2008). Novel targets for Huntington's disease in an mTOR-independent autophagy pathway. Nat Chem Biol *4*, 295-305.

Wollert, T., and Hurley, J.H. (2010). Molecular mechanism of multivesicular body biogenesis by ESCRT complexes. Nature *464*, 864-869.

Wong, E., and Cuervo, A.M. (2010). Autophagy gone awry in neurodegenerative diseases. Nat Neurosci *13*, 805-811.

Woodman, P.G., and Futter, C.E. (2008). Multivesicular bodies: co-ordinated progression to maturity. Curr Opin Cell Biol *20*, 408-414.

Wu, W.K.K., Coffelt, S.B., Cho, C.H., Wang, X.J., Lee, C.W., Chan, F.K.L., Yu, J., and Sung, J.J.Y. (2011). The autophagic paradox in cancer therapy. Oncogene *31*, 939–953.

Wurmser, A.E., Sato, T.K., and Emr, S.D. (2000). New component of the vacuolar class C-Vps complex couples nucleotide exchange on the Ypt7 Gtpase to SNARE-dependent docking and fusion. J Cell Biol *151*, 551-562.

Yamamoto, H., Kakuta, S., Watanabe, T.M., Kitamura, A., Sekito, T., Kondo-Kakuta, C., Ichikawa, R., Kinjo, M., and Ohsumi, Y. (2012). Atg9 vesicles are an important membrane source during early steps of autophagosome formation. J Cell Biol *198*, 219-233.

Yang, Z., and Klionsky, D.J. (2010). Mammalian autophagy: core molecular machinery and signaling regulation. Curr Opin Cell Biol *22*, 124-131.

Yeh, Y.-Y., Shah, K.H., and Herman, P.K. (2011). An Atg13-mediated self-association of the Atg1 protein kinase is important for the induction of autophagy. J Biol Chem *286*, 28931-28939.

Yeh, Y.Y., Wrasman, K., and Herman, P.K. (2010). Autophosphorylation within the Atg1 activation loop is required for both kinase activity and the induction of autophagy in *Saccharomyces cerevisiae*. Genetics *185*, 871-882.

Yen, W.-L., Legakis, J.E., Nair, U., and Klionsky, D.J. (2007). Atg27 is required for autophagy-dependent cycling of Atg9. Mol Biol Cell *18*, 581-593.

Yen, W.-L., Shintani, T., Nair, U., Cao, Y., Richardson, B.C., Li, Z., Hughson, F.M., Baba, M., and Klionsky, D.J. (2010). The conserved oligomeric Golgi complex is involved in double-membrane vesicle formation during autophagy. J Cell Biol *188*, 101-114.

Yorimitsu, T., and Klionsky, D.J. (2005). Atg11 links cargo to the vesicle-forming machinery in the cytoplasm to vacuole targeting pathway. Mol Biol Cell *16*, 1593-1605.

Yorimitsu, T., Zaman, S., Broach, J.R., and Klionsky, D.J. (2007). Protein kinase A and Sch9 cooperatively regulate induction of autophagy in *Saccharomyces cerevisiae*. Mol Biol Cell *18*, 4180-4189.

Young, A.R.J., Chan, E.Y.W., Hu, X.W., Köchl, R., Crawshaw, S.G., High, S., Hailey, D.W., Lippincott-Schwartz, J., and Tooze, S.A. (2006). Starvation and ULK1-dependent cycling of mammalian Atg9 between the TGN and endosomes. J Cell Sci *119*, 3888-3900.

Yu, I.-M., and Hughson, F.M. (2010). Tethering factors as organizers of intracellular vesicular traffic. Annu Rev Cell Dev Biol *26*, 137-156.

Yu, X., Breitman, M., and Goldberg, J. (2012). A Structure-Based Mechanism for Arf1-Dependent Recruitment of Coatomer to Membranes. Cell *148*, 530-542.

Zaman, S., Lippman, S.I., Zhao, X., and Broach, J.R. (2008). How *Saccharomyces* responds to nutrients. Annu Rev Genet *42*, 27-81.

Zhang, Y., Qi, H.Y., Taylor, R., Xu, W.H., Liu, L.F., and Jin, S.K. (2007). The role of autophagy in mitochondria maintenance - Characterization of mitochondrial functions in autophagy-deficient S-cerevisiae strains. Autophagy *3*, 337-346.

Zhao, C., Smith, E.C., and Whiteheart, S.W. (2012). Requirements for the catalytic cycle of the N-ethylmaleimide-Sensitive Factor (NSF). Mol Cell Res *1823*, 159-171.

Zhao, Z., Fux, B., Goodwin, M., Dunay, I.R., Strong, D., Miller, B.C., Cadwell, K., Delgado, M.A., Ponpuak, M., Green, K.G.*, et al.* (2008). Autophagosome-independent essential function for the autophagy protein Atg5 in cellular immunity to intracellular pathogens. Cell Host Microbe *4*, 458-469.

Zhong, Y., Wang, Q.J., Li, X., Yan, Y., Backer, J.M., Chait, B.T., Heintz, N., and Yue, Z. (2009). Distinct regulation of autophagic activity by Atg14L and Rubicon associated with Beclin 1-phosphatidylinositol-3-kinase complex. Nat Cell Biol *11*, 468-476.

Zimm, B.H. (1948). The dependence of the scattering of light on angle and concentration in linear polymer solutions. J Phys Colloid Chem *52*, 260-267.

Zimmermann, R., Eyrisch, S., Ahmad, M., and Helms, V. (2011). Protein translocation across the ER membrane. Biomembranes *1808*, 912-924.

Zinser, E., Sperka-Gottlieb, C.D., Fasch, E.V., Kohlwein, S.D., Paltauf, F., and Daum, G. (1991). Phospholipid synthesis and lipid composition of subcellular membranes in the unicellular eukaryote *Saccharomyces cerevisiae*. J Bacteriol *173*, 2026-2034.

Danksagung

Ich danke Dr. Thomas Wollert für die Möglichkeit diese Arbeit in seiner Arbeitsgruppe durchführen zu können und für seine intensive Betreuung. Darüber hinaus möchte ich mich für die Kommentare zu dieser Arbeit bedanken.

Prof. Dr. Johannes Buchner danke ich für die Bereitschaft die externe Betreuung dieser Arbeit zu übernehmen und für seine Ratschläge im Rahmen des Thesis Advisory Committee und darüber hinaus.

Dr. Stephan Gruber danke ich für die Teilnahme am Thesis Advisory Committee und spannende Diskussionen.

Prof. Dr. Tobias Gulder danke ich für die Übernahme des Prüfungsvorsitzes.

Prof. Dr. Sevil Weinkauf möchte ich für die Bereitschaft danken, sich als Zweitprüferin zur Verfügung zu stellen.

Dr. Yijian Rao danke ich für die enge und fruchtbare Zusammenarbeit bei unserem Projekt und für zahlreiche interessante Diskussionen.

Viola Beier danke ich für ihre Unterstützung und ihr Engagement für unser Projekt.

Meinen Kollegen Benjamin Hofmann, Anna Kaufmann, und Nena Matscheko danke ich für die gute Zusammenarbeit und die gegenseitige Unterstützung.

Dem gesamten Team der Core Facility danke ich für die Unterstützung bei verschiedenen Aufgaben und für das mit mir geteilte Wissen.

Ich danke darüber hinaus Dr. Gottfried Schroll, der meine Begeisterung für die Lebenswissenschaften bereits in jungen Jahren gefördert hat.

Ganz besonders danke ich meiner Familie. Ohne deren uneingeschränkte Unterstützung und deren Vertrauen in meine Fähigkeiten, wäre weder das Studium der Biochemie, noch der Abschluss dieser Arbeit möglich gewesen.